Tréhu, A.M., Bohrmann, G., Rack, F.R., Torres, M.E., et al., 2003
Proceedings of the Ocean Drilling Program, Initial Reports Volume 204

1. Leg 204 Summary[1]

Shipboard Scientific Party[2]

ABSTRACT

During Leg 204, we cored and logged nine sites on the Oregon continental margin to determine the distribution and concentration of gas hydrates in an accretionary ridge and adjacent slope basin, investigate the mechanisms that transport methane and other gases into the gas hydrate stability zone (GHSZ), and obtain constraints on physical properties of gas hydrates in situ. A three-dimensional seismic survey conducted from 19 June through 3 July 2000 provided images of potential subsurface fluid conduits and indicated the depth of the bottom-simulating reflector (BSR), a commonly used proxy for the base of the GHSZ. After coring at the first site, we acquired logging-while-drilling (LWD) data at all but one site to provide an overview of downhole physical properties prior to coring. The LWD data confirmed the general position of key seismic stratigraphic horizons and yielded an initial estimate of gas hydrate concentration through the proxy of in situ electrical resistivity. These records proved to be of great value in planning subsequent coring. We also tested the use of infrared (IR) thermal imaging of cores as a new and effective tool to identify gas hydrates as rapidly as possible after core retrieval. The thermal images were used to estimate the distribution and texture of hydrate within the cores. Geochemical analyses of interstitial waters and of headspace and void gases provided additional information on the distribution and concentration of gas hydrate within the GHSZ, the origin and pathway of fluids into and through the GHSZ, and the rates at which the process of gas hydrate formation is occurring. Biostratigraphic and lithostratigraphic descriptions of cores, measurement of physical properties, in situ pressure core sampling, and thermal measurements complement the data set, providing ground-truth tests of inferred physical and sedimentological properties.

Among the most interesting preliminary results are the following:

[1]Examples of how to reference the whole or part of this volume.
[2]Shipboard Scientific Party addresses.
Ms 204IR-101

1. Near the southern summit of Hydrate Ridge, very high concentrations of gas hydrate are present from the seafloor to ~30 meters below seafloor (mbsf), and they contain significant amounts of C_{2+} hydrocarbon gases in addition to methane.
2. High chloride concentrations near the summit indicate that hydrate formation is recent and rapid.
3. The lateral extent of the near-surface gas hydrate deposit at the summit can be mapped based on its backscatter and seismic signature.
4. Away from the summit, no gas hydrate is present in the upper ~45 mbsf.
5. Between ~45 mbsf and the base of the GHSZ, gas hydrates are distributed in lenses that are probably controlled by the physical properties of the sediments.
6. In a slope basin east of Hydrate Ridge, gas hydrate concentration is quite low, with the probable exception of a 12-m-thick zone of relatively high concentration near the base of the GHSZ.
7. Different physical and chemical proxies for gas hydrate distribution and concentration give generally consistent results.
8. Thermal anomalies recorded by systematically scanning cores with an IR thermal-imaging camera provide a robust record of gas hydrate distribution that can be calibrated using estimates of in situ gas hydrate concentration derived from pressure core samples and anomalies in chloride concentration.
9. An unprecedented number of cores retrieved at in situ pressure provide accurate estimates of subsurface methane concentration.
10. Density logs of cores retrieved at in situ pressure provide details of in situ gas hydrate distribution and direct evidence for free gas within the GHSZ and can be used to study the response of gas hydrate to depressurization.
11. The base of the GHSZ represents a discontinuity in C_1/C_2 and other chemical constituents of pore waters and gas voids, indicating that gas hydrate formation has profound geochemical effects.
12. Several different geochemical mixing and fractionation signals provide constraints on fluid flow and gas hydrate dynamics.
13. Ash-rich layers and thick turbidites serve as conduits for fluid flow.
14. Borehole breakouts provide constraints on tectonic forces and possibly on the in situ strength of gas hydrate–bearing sediments.

INTRODUCTION

Gas hydrate is an icelike compound that contains methane and/or other low molecular weight gases in a lattice of water molecules. Gas hydrates are stable under the temperature and pressure conditions generally found in the Arctic and near the seafloor at water depths >300 m. They are quite common beneath the slope of both active and passive continental margins where methane originates from the decomposition of organic matter by biogenic and/or thermogenic processes. International interest in gas hydrates has increased considerably in the past several years because of increasing recognition that the large volumes of gas stored in these structures represent a significant fraction of the global carbon budget (see review by Kvenvolden and Lorenson, 2001) and

may be a potential energy resource for the future (e.g., Milkov and Sassen, 2002). Several authors have also suggested that sudden widespread dissociation of subseafloor gas hydrates in response to changing environmental conditions may have had a significant effect on past climate (e.g., Revelle, 1983; Nisbet, 1990; Paull et al., 1991; Katz et al., 1999; Dickens, 2001). These effects remain speculative, as the volume of gas stored in the global gas hydrate reservoir and its behavior during changing environmental conditions are currently poorly constrained.

In order to evaluate the economic potential of hydrates, their role as a natural hazard, and their impact on climate, we need to know the following:

- How are hydrates and underlying free gas distributed vertically and horizontally in the sediment?
- What controls the distribution of gas hydrates and free gas (i.e., lithologic controls on fluid migration and on hydrate nucleation and growth)?
- What are the effects of the distribution of gas hydrate and free gas on the mechanical properties of the seafloor?
- How can gas hydrate and free gas distribution be regionally mapped using remote sensing geophysical techniques?
- How does gas hydrate respond to changes in pressure and temperature resulting from tectonic and oceanographic perturbation?
- How can we use the isotopic record preserved in microfossils and authigenic minerals as a proxy for past tectonic and climate changes?
- How does the sedimentary biosphere impact the formation and oxidation of methane?

These questions were the focus of Ocean Drilling Program (ODP) Leg 204, which was dedicated to understanding the biogeochemical factors controlling the distribution and concentration of gas hydrates in an accretionary margin setting. A three-dimensional (3-D) seismic site survey (Tréhu and Bangs, 2001; Tréhu et al., 2002) and logging-while-drilling (LWD) data acquired at the beginning of the leg provided "road maps" to guide coring and sampling. These data enabled us to anticipate the depths at which gas hydrates should be expected and select targets for special sampling tools. Accurate quantification of in situ gas hydrate and free gas concentrations is difficult because of hydrate dissociation and gas loss during core retrieval (Paull and Ussler, 2001). A major focus of Leg 204 was therefore to acquire samples under pressure using the ODP pressure core sampler (PCS) system and the recently developed Hydrate Autoclave Coring Equipment (HYACE) system, which includes a laboratory transfer chamber for maintaining pressure while making physical property measurements. Extensive use was made of infrared (IR) cameras immediately after core retrieval to rapidly identify potential hydrate-bearing samples and preserve them for careful study. Special attention was also given to making high-resolution measurements of the chemistry of interstitial waters (IWs), resulting in a large number of IW samples from this cruise. We also deployed tools to measure in situ temperature and pore pressure, especially in zones where LWD data indicated rapid changes in the physical properties of the sediments, and acquired downhole and two-ship seismic data.

GEOLOGIC AND BIOGEOCHEMICAL SETTING

Hydrate Ridge is a 25-km-long and 15-km-wide ridge in the Cascadia accretionary complex, formed as the Juan de Fuca plate subducts obliquely beneath North America at a rate of ~4.5 cm/yr (Fig. F1A). Sediment on the subducting plate contains large volumes of sandy and silty turbidites. At present, most of this sediment is accreted to the continental margin either by offscraping at the deformation front or by underplating beneath the accretionary complex some 10 km east of the deformation front (MacKay et al., 1992; MacKay, 1995) (Fig. F2).

Hydrate Ridge has been the site of many geological and geophysical cruises since cold seeps were first discovered on this part of the margin nearly 20 yr ago (Kulm et al., 1986). It is characterized by a northern summit at a water depth of ~600 m and a southern summit at a water depth of ~800 m (Fig. F1B). A nearly ubiquitous bottom-simulating reflector (BSR) (Tréhu et al., 1999) suggests that gas hydrate is present throughout Hydrate Ridge.

A regional two-dimensional multichannel seismic survey was acquired in 1989 as a site survey for ODP Leg 146, a drilling leg designed primarily to study dynamics of fluid flow in accretionary complexes. The location where an upward deflection of the BSR is cut by a fault on the northern summit of Hydrate Ridge was selected for ODP Site 892 (Westbrook et al., 1994). At this site, massive H_2S-rich hydrates were recovered from 2 to 19 meters below seafloor (mbsf) (Kastner et al., 1995). No hydrate was recovered near the BSR, but geochemical pore water and temperature anomalies suggested the presence of gas hydrate to 68 mbsf (Kastner et al., 1995; Hovland et al., 1995). Vertical seismic profiles (VSPs) indicated the presence of free gas for at least 20 m beneath the BSR (MacKay et al., 1994), and ocean-bottom seismometer (OBS) data suggest that free gas may extend for several 100 mbsf (Tréhu and Flueh, 2001). Methane at Site 892 is primarily of microbial origin (Kvenvolden, 1995), but C_{2+} hydrocarbon gases of thermogenic origin are also present (Hovland et al., 1995; Schlüter et al., 1998).

Since 1996, there have been several cruises per year to northern and southern Hydrate Ridge. These cruises have generated a comprehensive swath bathymetry and a deep-towed side-scan database as well as extensive seafloor observations and sample collections by submersibles and remotely operated vehicles (ROVs) (Suess and Bohrmann, 1997; Clague et al., 2001; Johnson et al., in press; Torres et al., 1998, 1999; Bohrmann et al., 2000; Linke et al., 2001). In addition, a high-resolution 3-D seismic survey was conducted from 19 June to 3 July 2000 as a site survey for Leg 204 (Tréhu and Bangs, 2001; Tréhu et al., 2002).

Seafloor Observations of Southern Hydrate Ridge

Side-scan data, seafloor camera tows, and diving with the manned submersible *Alvin* and various ROVs demonstrated the presence of extensive massive carbonate pavement on the northern summit of Hydrate Ridge (Carson et al., 1994; Clague et al., 2001; Sample and Kopf, 1995; Bohrmann et al., 1998; Greinert et al., 2001). Until recently, massive authigenic carbonate pavement was thought to be absent on the southern summit of Hydrate Ridge. During *Alvin* dives in 1999, however, a 50-m-high carbonate spire (the "Pinnacle") (Figs. F1C, F4A) was discovered ~250 m southwest of the summit (Torres et al., 1999). Deep-towed side-scan data indicate that the Pinnacle is located in the center

F1. Tectonic setting of Hydrate Ridge, p. 51.

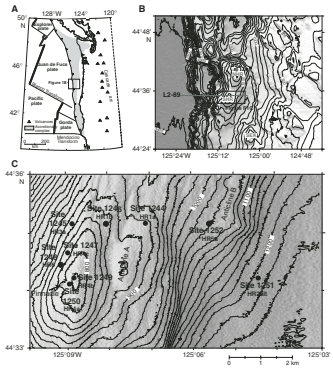

F2. Line drawing of the crustal structure across Hydrate Ridge, p. 52.

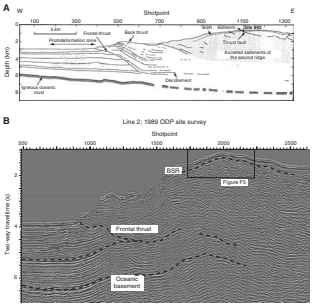

of a buried carbonate apron with a diameter of ~250 m (Johnson et al., in press). Authigenic carbonates on the Cascadia margin form within the sediments and at the seafloor as a result of oxidation of isotopically light methane. The relative absence of carbonate on the southern summit of Hydrate Ridge was interpreted to indicate that this gas hydrate system is younger than that on the northern summit, providing a spatial proxy for temporal evolution of hydrate-bearing accretionary ridges (Tréhu et al., 1999). This interpretation is supported by U-Th dating of recovered carbonates (Teichert et al., in press), which indicates that the Pinnacle is at least 11,400 yr old, whereas the carbonate chemoherms on northern Hydrate Ridge are up to 71,000 yr old.

One especially interesting feature of southern Hydrate Ridge is the abundance of massive hydrate at the seafloor near its summit. This was first discovered in 1996, when >50 kg of massive hydrate was recovered with a television-guided grab sample (Bohrmann et al., 1998). The samples show dense interfingering of gas hydrate with soft sediment (Fig. **F4B**). In most cases, pure white hydrate is present in layers several millimeters to several centimeters thick. Host sediment is often present as small clasts within the pure gas hydrate matrix. On a macroscopic scale, the gas hydrate fabric varies from highly porous, with pores of up to 5 cm in diameter, to massive (Suess et al., 2001). Thin sections show a structure in which gas bubbles have been filled with hydrate. Wet bulk densities of 80 hydrate samples measured on board the *Sonne* range from 0.35 to 0.75 g/cm^3 (Suess et al., 2002). Pore space was estimated from the change in sample volume before and after compression to ~160 kbar. The samples show high variability in pore volumes ranging from 10% to 70%, and the values are negatively correlated with sample density. From this correlation, the end-member density at zero porosity was estimated to be ~0.79 g/cm^3. This value is lower than the theoretical density of pure methane hydrate (0.91 g/cm^3). Field-emission scanning electron microscopy indicates that this is a result of submicrometer porosity of the massive hydrate (Suess et al., 2002). The low bulk density of the natural methane hydrates from Hydrate Ridge results in a strong positive buoyancy force, implying that the massive gas hydrate remains on the seafloor only because of the shear strength of the host sediment. The unusual seafloor topography observed on southern Hydrate Ridge during *Alvin* and *ROPOS* surveys, which is characterized by mounds and depressions with a wavelength of a few meters (Fig. **F4C**), may result from spontaneous breaking off of hydrate from the seafloor. This may be an important mechanism for transporting methane from the seafloor to the atmosphere (Suess et al., 2001). An important objective of Leg 204 was to determine the depth to which massive gas hydrate is present.

Vigorous streams of methane bubbles have been observed emanating from vents on the seafloor on the northern and summit regions of Hydrate Ridge (Suess and Borhmann, 1997; Suess et al., 1999; Torres et al., 1998, 1999, 2002; Heeschen et al., 2003) as well as from a similar, but smaller, reflective high in the accretionary complex known as Southeast Knoll (Figs. **F1B, F3B**). Because the seafloor at all three sites is well within the gas hydrate stability zone (GHSZ) (Fig. **F3A**), the presence of methane bubbles beneath and at the seafloor suggests rapid transport of methane to the seafloor from sediments beneath the GHSZ. Another objective of Leg 204 was to determine the mechanism whereby free gas migrates through the GHSZ to reach the water column.

F3. Water temperature profiles and echo sounder records from southern Hydrate Ridge, p. 53.

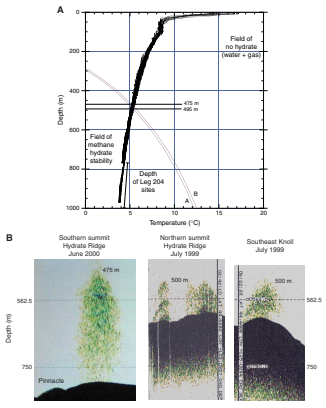

Biological Communities Associated with Hydrate and Geochemical Implications

Communities of tube worms, bacterial mats, clams, and other fauna are associated with seafloor hydrates and methane vents on Hydrate Ridge (Fig. F4D) and elsewhere (e.g., Kulm et al., 1986; MacDonald et al., 1989; Suess et al., 1999, 2001; Sassen et al., 2001). Chemosynthetic microorganisms, some of which are symbionts within larger fauna, are at the base of the food chain in these communities. Recent work suggests complex complementary relationships between sulfate-reducing, methanogenic, and methanotrophic microorganisms in hydrate-bearing sediments (e.g., Parkes et al., 2000; Boetius et al., 2000). These microorganisms are the kinetic controls on low-temperature methane formation and oxidation and are, therefore, a critical component of the hydrate system. Identification of these organisms and determination of their abundances, spatial variability, and activity are just beginning.

Particularly interesting are recently discovered organisms that play a critical role in anaerobic methane oxidation (AMO). Methane oxidation generates isotopically light dissolved inorganic carbon and results in the formation of authigenic carbonates. These carbonates remain in the geologic record as evidence of past fluid flow and hydrate formation and dissociation (e.g., Sample and Kopf, 1995; Bohrmann et al., 1998; Greinert et al., 2001). Very high rates of AMO have been measured in sediment overlying massive gas hydrates on southern Hydrate Ridge (Boetius et al., 2000) and attributed to structured aggregates consisting of a central cluster of methanotrophic Archaea surrounded by sulfate-reducing bacteria. That microbes oxidize methane by utilizing sulfate in the absence of oxygen was long suspected by geochemists based on interstitial sulfate and methane gradients (e.g., Claypool and Kaplan, 1974). Borowski et al. (1996) showed that steep sulfate gradients and shallow depths to the sulfate/methane interface (SMI) are a consequence of the increased influence of AMO, and Boetius et al. (2000) were the first to observe the microorganisms that presumably catalyze AMO. These microbial aggregates appear to be abundant in sediments of Hydrate Ridge and mediate AMO when enough sulfate is available.

Analysis of sulfide minerals provides a possible opportunity to reconstruct past biological activity because most of the reduced sulfide produced during microbial sulfate reduction is ultimately sequestered in various iron phases, which usually involves multiple steps terminating in the formation of sedimentary pyrite. The burial of these mineral phases contributes significantly to the oxygen level of the atmosphere, the sulfate concentration in seawater, and the pH of the oceans over geologic timescales (e.g., Garrels and Perry, 1974; Holland, 1978; Boudreau and Canfield, 1993). Anomalous intervals of high greigite content have been reported in intervals from which gas hydrates were recovered or were inferred to exist (Housen and Musgrave, 1996). Based on the rock magnetic properties at Site 889, Housen and Musgrave (1996) inferred the presence of a "fossil gas hydrate zone," which may have extended downward to 295 mbsf during the last glaciation. Data acquired during Leg 204 will be used in several shore-based studies to further understand the relationships between bacterial activity and sulfide mineralogy.

F4. Biogeochemical setting of Hydrate Ridge, p. 54.

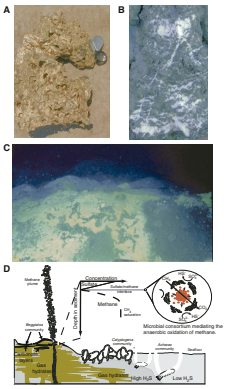

HIGH-RESOLUTION THREE-DIMENSIONAL SEISMIC DATA

Prior to acquisition of a 3-D high-resolution seismic site survey in 2000 (Tréhu and Bangs, 2001; Tréhu et al., 2002), the relationship between subsurface reflections and the summit vents was not known because no seismic profiles crossed the summit. The 3-D survey covers a 4 km × 10 km region that includes the southern summit and the slope basin to the east. Shots from two generator-injector guns fired simultaneously were recorded on the Lamont-Doherty Earth Observatory (LDEO) portable 600-m-long 48-channel towed streamer and on an array of 21 four-component OBSs (Institute for Geophysics, University of Texas). The locations of the ship and of the streamer were determined via the Differential Global Positioning System and four compasses, respectively, and data coverage was monitored during the cruise to identify locations where additional data were needed. Excellent data quality was obtained in spite of strong winds and high seas. The data contain frequencies up to ~250 Hz, providing considerable stratigraphic and structural resolution.

Figure F5 shows an east-west slice from the 3-D data. The profile is coincident with line 2 from the 1989 site survey (Fig. F2B). Locations of Sites 1244–1246 and 1252 are shown. Features in the data that were particular targets of Leg 204 are labeled. An upper facies of folded and uplifted sediments unconformably overlies a low-frequency incoherent facies interpreted to be highly deformed accretionary complex material. These two facies were sampled during Leg 204. Figure F6 shows seismic profiles that trend approximately north-south and illustrates the setting of Sites 1245, 1247, and 1248–1250, which form a transect from the flank to the summit.

The BSR is a negative polarity reflection generally believed to result from free gas underlying gas hydrate at the base of the GHSZ; a strong BSR is seen everywhere along the profiles of Figures F5 and F6, except for locally near Site 1252. The seismic data also show considerable stratigraphic and structural complexity both above and below the BSR. Certain reflective horizons are anomalously bright, and these amplitude anomalies are laterally continuous for hundreds of meters. Table T1 gives the depth to the BSR and other major reflections estimated prior to Leg 204 using seismic velocities obtained from inversion of first arrivals of data recorded on OBSs during the 3-D seismic survey (Arsenault et al., 2001). These estimated depths proved to be quite accurate. Some minor revisions to these depths, based on data from Leg 204, are also given.

Horizon A

The seismic reflection labeled "A" on Figure F5 has an amplitude that is ~10 times that of adjacent stratigraphic events and 10 times that of the BSR. Horizon A gets shallower and brighter toward the southern summit, as shown on relative true-amplitude seismic sections in Figure F6. Maps of the two-way traveltime (TWT) to this surface, of the time between this surface and the BSR, and of the amplitude of the seismic wavelet are also shown in Figure F6. These maps show that the amplitude of the Horizon A reflection is related to depth below sea level (or hydrostatic pressure) rather than depth below the seafloor. Speculation that this horizon is a major path transporting methane-rich fluids to

F5. East-west vertical slice through the 3-D seismic data, p. 55.

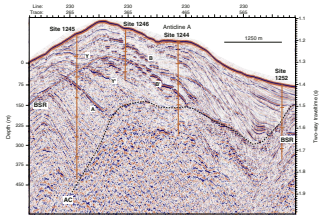

F6. North-south–trending vertical slices from the 3-D seismic data volume, p. 56.

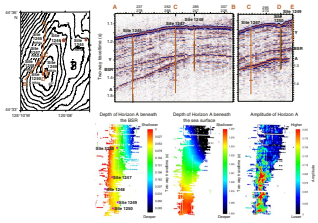

T1. Estimated depth to major seismic horizons, p. 71.

the summit of Hydrate Ridge and that the change in amplitude results from the onset of pressure-dependent exsolution of methane from fluids rising along Horizon A (Tréhu et al., 2002) were tested during Leg 204 by drilling at Sites 1245, 1247, 1248, and 1250. Sediments that lap onto Horizon A suggest that it is an uncomformity, as are the overlying Horizons Y and Y′.

Seismic Signature of the Southern Summit

Figure F7 shows the characteristics of Horizon A and of overlying actively venting features in the immediate vicinity of the southern summit of Hydrate Ridge. Locations of sections are shown on a map of seafloor reflectivity obtained by a deep-towed side scan (Johnson et al., in press) to illustrate the relationship between seafloor manifestations of venting and subsurface reflectivity. Chaotic bright reflectivity is observed just beneath the seafloor at the summit (line 300) (Fig. F7B). This reflectivity pattern is observed only at the summit and is almost exactly coincident with the "tongue" of intermediate strength seafloor reflectivity northeast of the Pinnacle observed in the deep-towed side-scan data. This pattern also underlies the acoustic bubble plume that was observed each time the southern summit was crossed during the seismic data acquisition cruise. We speculated that this pattern indicates the depth extent of surface massive hydrate (Tréhu et al., 2002) and tested this speculation by drilling at Site 1249.

Horizon A is probably a primary source of fluids for the summit vents. The mechanism whereby methane migrates from Horizon A to the seafloor, however, is not imaged in the seismic data. The region between Horizon A and the seafloor may be broken by small faults too small to be resolved in the seismic data. Site 1250 was planned to test this hypothesis.

F7. Seismic details near the summit of southern Hydrate Ridge, p. 57.

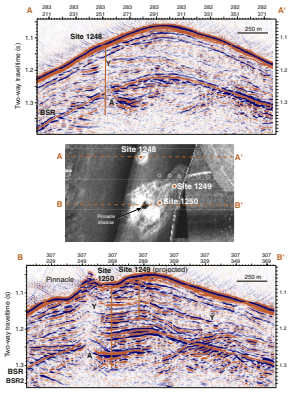

Horizons B and B′ on the Eastern Flank of Hydrate Ridge

A pair of strong reflections, referred to as Horizons B and B′, are also observed east of the southern axis of Hydrate Ridge and appear to be associated with an active secondary anticline (Anticline A) (Fig. F5). In contrast to Horizon A, Horizons B and B′ are pervasively faulted, with offsets consistent with tensional cracking in response to uplift and folding. These reflections seem to originate at Reflection AC (Fig. F5), interpreted to represent the top of the accretionary complex. Tréhu et al. (2002) speculated that Horizons B and B′ might be permeable stratigraphic horizons transporting fluids from the accretionary complex into the GHSZ. Sites 1244 and 1246 were designed to test this hypothesis by sampling Horizons B and B′ above and below the BSR.

Slope Basin East Of Hydrate Ridge

Site 1251 is located in the slope basin east of Hydrate Ridge. Sediments are accumulating rapidly in this basin, and the BSR is characterized by a change in amplitude of dipping stratigraphic horizons, with large amplitudes indicative of free gas below the BSR (Fig. F8). This site was chosen to provide a relative reference site where the processes controlling hydrate formation were hypothesized to be similar to those on the Blake Ridge of the Atlantic continental margin of the United States. Gas hydrates on the Blake Ridge were drilled during ODP Leg 164

F8. East-west–trending vertical slices through the seismic data around Sites 1251 and 1252, p. 58.

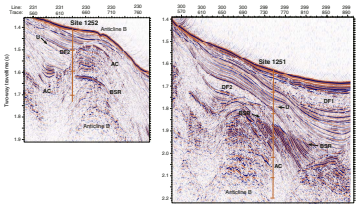

(Paull, Matsumoto, Wallace, et al., 1996). A secondary objective was to sample a layer in the center of the basin (labeled DF1 in Fig. F8), which was interpreted to represent a massive debris flow based on the absence of internal reflectivity. This horizon is one of two such thick events that can be traced through much of the 3-D data set.

Site 1252 was chosen to sample the sediments underlying Horizon AC where they are uplifted to form Anticline B. Here the sediments appear to be less deformed than beneath the crest of Hydrate Ridge and retain some coherent internal structure. Another objective at Site 1252 was to determine the reason for the absence of a BSR at Site 1252, in contrast to the very strong BSR observed only ~300 m to the east in the core of Anticline B. A third objective was to sample the lower inferred debris flow, which appears to have been blocked by Anticline B. Anticline B must have represented a topographic high when these sediments were deposited.

SUMMARY OF SCIENTIFIC OBJECTIVES

Stratigraphic and Structural Controls on Hydrate Development

The structural and stratigraphic setting of Hydrate Ridge contrasts with that of the adjacent slope basin to the east. Beneath the slope basin, the seismic indicators of gas hydrate and free gas are similar to those on the Blake Ridge, with an intermittent BSR and enhancement of stratigraphic reflectivity beneath the BSR (Holbrook et al., 1996). The sedimentation rate in this basin was expected to be very high. During Leg 204, we tested the hypothesis that the distribution, texture, and chemistry of hydrate and related pore fluids beneath Hydrate Ridge are different compared to the slope basin.

Formation of Massive Hydrate Near the Seafloor

The presence of massive hydrate near the seafloor is enigmatic, as most models for hydrate formation in a region of diffuse fluid flow predict a decreasing gradient in hydrate concentration above the BSR (e.g., Paull et al., 1994; Rempel and Buffett, 1998; Xu and Ruppel, 1999). Several explanations have been proposed including formation in the past when the stability boundary was near the seafloor, formation at depth and exposure by erosion (Bohrmann et al., 1998), and transport of methane through the hydrate stability field as free gas isolated from water (Suess et al., 2001). One objective of Leg 204 was to obtain constraints on the rate of hydrate formation, the depth extent of the massive hydrate, and mechanisms for transporting methane-rich fluids to the seafloor.

Methane Sources and Geochemical Effects of Hydrate Formation and Dissociation

It has been well established that fluids play a major role in many aspects of the geologic evolution of convergent margins. Changes in the chemical and isotopic composition of interstitial fluids with depth have been shown to be powerful tracers of fluid sources and migration patterns. Important objectives of Leg 204 were to document the fluid flow regime and evaluate its role in the formation of gas hydrates. Because

hydrate formation and destabilization modify the isotopic composition of the hydrogen and oxygen in pore water, a high-resolution set of pore water samples was collected during Leg 204, with the goal of using the dissolved chloride and the isotopic composition of these waters to constrain models of formation and dissociation of gas hydrates on this margin.

Geochemical Impact on the Geological Record

Changes in the isotopic composition of the dissolved carbonate resulting from oxidation of methane enriched in ^{12}C are thought to be incorporated into calcareous fossil tests (Wefer et al., 1994; Dickens et al., 1995, 1997; Kennett et al., 2003) and authigenic carbonate phases (e.g., Sample and Kopf, 1995; Bohrmann et al., 1998). An objective of Leg 204 was to determine the isotopic composition of the pore fluids and carbonates associated with gas hydrates to provide the framework needed to unravel the history of gas hydrate formation and dissociation recorded in benthic foraminifers and authigenic carbonate phases.

Calibration of Geophysical Estimates of Hydrate and Gas Volumes

Better calibration of regional estimates of gas hydrate and free gas volumes, based on geophysical mapping and modeling techniques, is of critical importance toward estimating the global abundance of hydrate and evaluating its role in climate change and its potential for economic exploitation. During Leg 204, we drilled through hydrates in a variety of settings with different seismic characteristics, measured in situ physical conditions, and conducted a series of nested seismic experiments to calibrate various techniques for remote sensing of hydrate distribution and concentration.

Hydrates and Slope Stability

The possible relationship between hydrates and slope failure is, at present, poorly understood. On the one hand, hydrates may stabilize slopes by cementing sediment grains. On the other hand, if hydrates impede fluid flow, they may weaken the underlying sediment by trapping fluids and free gas. Several investigators have noted the possible correlation between gas hydrates and slope instability (e.g., Booth et al., 1994; Tréhu et al., 1995; Paull, Matsumoto, Wallace, et al., 1996) and have discussed how such slope instability might release massive amounts of methane into the ocean (Paull, Matsumoto, Wallace, et al., 1996; Nisbet and Piper, 1998). One objective of Leg 204 was to determine the mechanical, hydrological, and dynamic properties of hydrate-bearing sediment to better constrain models of slope instability induced by earthquakes, changes in sea level, or changes in ocean temperature.

Biological Communities Associated with Hydrate and Underlying Free Gas Zones

Microorganisms play an important role in both methane formation and oxidation and are, therefore, a critical component of the hydrate system. Identification of these organisms and determination of their abundance, spatial variability, and rates of activities is just the begin-

ning. Important questions addressed during Leg 204 included the following:

What impact do the microorganisms have on the volume of methane produced and oxidized beneath Hydrate Ridge?
At what depths are they concentrated?
What effect do they have on sediment diagenesis and the development of magnetic minerals?
Does the hydrate-related biosphere differ between Hydrate Ridge and the adjacent slope basin?
How do microorganisms affect sediment texture and pore water chemistry and vice versa?

DRILLING STRATEGY

To test the hypotheses discussed above, we originally proposed three primary drill sites extending to depths of 400–700 mbsf. Preliminary analysis of the 3-D seismic data confirmed the rationale behind these three sites but led to minor modifications of site locations. It also led to the addition of seven shallow-penetration (<260 mbsf) sites to sample the massive hydrate at the summit and to determine changes along subsurface horizons that appeared to be fluid pathways feeding the summit vents. Four of these additional sites were primary sites and three were alternates as described in the Leg 204 Scientific Prospectus; all were approved for drilling by the Pollution Prevention and Safety Panel (PPSP). We drilled all sites except for alternate Site HR1c, for a total of nine sites. The locations of the sites drilled (see Table **T2**) are overlain on a map showing seafloor bathymetry in Figure **F1C.**

T2. Leg 204 site summary, p. 72.

Leg 204 started with 3 weeks dedicated to LWD. For safety reasons, Site 1244 (proposed Site HR1a) was cored to 350 mbsf prior to LWD, to sample all seismic facies that were to be drilled. We had approval from the PPSP to proceed with LWD prior to coring at all additional sites, or until the time allocated to LWD was expended, if no safety issues were encountered while drilling at Site 1244. Our objective was to use the LWD data to determine where to deploy time-consuming special downhole tools. The LWD data were of excellent quality, and this strategy proved to be very useful.

Another novel aspect of this leg was the use of IR thermal imaging to systematically scan each core (from within and near the GHSZ) as soon as it was brought on board. Because gas hydrate dissociation is a strongly endothermic process, cold spots thus detected permitted us to quickly confirm what portions of the core contained significant amounts of gas hydrate. Experiments were designed to calibrate the temperature record obtained with the IR camera relative to concentration estimates obtained from PCS and pore water chloride concentration sampling.

OPERATIONAL SUMMARY

Leg 204 was originally scheduled to begin in San Francisco, California, and end in San Diego, California. As a result of an impending West Coast dock strike, both port calls were ultimately moved to Victoria, British Columbia, Canada. Leg 204 officially began at 0655 hr on 7 July 2002 with the first line ashore at Westcan Terminal B.

In many ways, the leg turned out to be extraordinary. Almost all science objectives were successfully achieved during the course of drilling/coring the seven primary sites and two alternate sites. In addition, a series of holes geared specifically toward the rapid recovery and preservation of hydrate samples was cored at the end of the leg at Site 1249 as part of a gas hydrate geriatric study funded by the Department of Energy (DOE).

Some significant statistics of Leg 204 are listed below (see also Tables T2, T3, T4), followed by a more descriptive discussion:

Water depths ranged from 788.5 to 1228.0 meters below rig floor.
Eight of nine sites were drilled using LWD technology.
Overall, a total of 45 holes were drilled/cored at nine separate drill sites.
Eleven holes were drilled with a tricone bit for LWD/resistivity-at-the-bit (RAB)-8 or wireline logging.
Thirty-three holes were cored with the advanced piston corer (APC) and/or extended core barrel (XCB) coring systems, and one hole was rotary core barrel (RCB) cored.
A total of 3674.5 m was cored with 3068.3 m (83.5%) recovered.
Of a 57.1-day leg, 50.4 days (88.3% of the time) was spent on site operating and 6.7 days in port/transit.
Twenty-nine nautical miles (43.8 hr) were covered during 23 moves between sites, using dynamic positioning.
Seven helicopter and two supply boat rendezvous were conducted, resulting in 42 personnel exchanges.
Visitors included two journalists (*Dallas Morning News* and *American Geophysical Union/Eos*), two engineering observers (DOE and Chevron/Texaco), and a two-man German film crew (Context TV).
Whirl-Pak latex microbeads and perfluorocarbon tracer were used on 85 cores that were sampled for microbiology.
Fifty meters of hydrate-bearing core were recovered and stored under pressure in a methane environment; 35 m of additional samples was recovered and stored in six liquid nitrogen dewars.

Special tool deployments and successes during the leg included the following:

Sixteen of sixteen operationally successful runs with the Davis-Villinger Temperature-Pressure Probe (DVTPP);
Eight of eight operationally successful runs with the Davis-Villinger Temperature Probe (DVTP);
Sixty-one of sixty-one successful runs with the APC temperature (APCT) tool;
One hundred and seven of one hundred and ten successful runs with the APC-methane tool (APCM);
One of two successful deployments of the Fugro-McClelland piezoprobe;
Thirty of thirty-nine successful runs with PCS;
Two of ten cores successfully recovered under pressure using the Fugro Pressure Corer (FPC);
Five of eight cores successfully recovered under pressure using the HYACE Rotary Corer (HRC);

Twenty-eight runs with the Lamont-Doherty Earth Observatory (LDEO) drill string acceleration (DSA) tool; seventeen were all or partially successful; and
Eight of eight cores successfully recovered using the RAB-8 logging-while-coring (LWC) technology.

Operations on southern Hydrate Ridge also required coordination with other oceanographic research vessels. The *Sonne,* a German research vessel, operated in the same area, deploying and recovering instrumented seafloor landers. The *Ewing,* from LDEO, worked in conjunction with the *JOIDES Resolution* conducting two-ship seismic operations and independent research, including the setting of OBS packages on the seafloor. The *Atlantis,* from Woods Hole Oceanographic Institution, was on site for 4 days of *Alvin* diving at the southern summit. And finally, the *New Horizon,* a Scripps Institution of Oceanography vessel, was on location briefly doing independent oceanographic research work.

The leg included a two-ship seismic program conducted in conjunction with the *Ewing* to acquire vertical, constant-offset, and walkaway VSPs. A new Schlumberger tool called the Vertical Seismic Imager (VSI) was used for most of the VSP experiments, whereas the older Well Seismic Tool (WST) was used for the remaining seismic work. Deployment of the VSI tool was problematic because of its fragile construction and because the tool is not designed to have the electric line slacked off during the data-acquisition period. Nonetheless, the tool worked well enough to achieve most of the seismic objectives.

Eight of the sites were drilled using LWD technology. A developmental LWC system, jointly developed by LDEO, Anadrill, and Texas A&M University (TAMU), was also successfully tested using a RAB-8 LWD tool. This marked the first time that core samples have been recovered simultaneously with LWD data.

Several other specialized tools developed all or in part by TAMU were successfully deployed during the leg. These include the PCS, APCM, APCT tool, DVTP, and DVTPP.

Two new pressure coring systems developed by a European Union–funded consortium (deployment of HYACE tools in new tests on hydrates [HYACINTH]) were deployed. These systems were designed to allow transfer of a pressurized core from the downhole tools autoclave chamber to a pressurized logging or storage chamber. The FPC and HRC were deployed 10 times and 8 times, respectively. Two runs with the FPC and four runs with the HRC successfully recovered core at or near in situ pressure. Pressurized core transfer to the logging and storage chambers worked well, despite some tolerance variations with the FPC.

Prior to the leg, TAMU worked with Fugro-McClelland on the adaptation of their piezoprobe tool to the ODP/TAMU bottom-hole assembly (BHA). This tool was deployed twice at the first site, with the second attempt fully successful. Data from this electric line–deployed tool will be compared to DVTPP data. The DVTPP tool is much faster to deploy because it is deployed and recovered using the standard ODP coring line.

LDEO deployed its DSA tool to gather downhole data in support of the HYACINTH tool deployments and also as part of an experimental study using the APC as a seismic energy source. The APC impact energy was recorded using OBS stations placed on the seafloor earlier by the *Ewing*. Initial results indicated that this experiment was partially successful and that useful data were obtained.

The scientific and operational achievements were impressive; however, the leg was extremely demanding because all nine drill sites were

located within 3.6 nmi of each other. As a result of the close proximity of the sites, all moves between sites were done using the ship's dynamic positioning system. Because of the commonality of the coring BHAs used, most of these moves were made with the pipe suspended below the ship. When a BHA changed or bit replacement was required, the move was made simultaneously with the pipe trip to and from the surface. With no transit time, other than traveling to and from port and limited pipe trips between sites, the operating time available for drilling and coring was considerable. For the 57.1-day leg, 50.4 days (88.3% of available time) were spent on site. The remaining 6.7 days were spent in port (4.14 days) and under way (2.54 days).

Leg 204 operations were confined to an area located ~50 nmi off the coast of Oregon. The close proximity of land allowed for numerous changes of personnel and equipment. An initial supply boat rendezvous was planned to allow exchange of specialized and expensive LWD equipment and personnel for the VSP equipment. There were also numerous personnel changes via helicopter, and another supply boat brought out special pressure vessels and dewars of liquid nitrogen to support an add-on effort to recover and preserve the hydrate samples collected with additional funding from the DOE. There were a total of nine rendezvous completed with the *JOIDES Resolution,* including seven helicopters and two supply vessels.

Leg 204 officially ended at 0900 hr on 2 September 2002 with the first line ashore at Westcan Terminal Pier B in Victoria.

SITE SUMMARIES

In this section, we describe and discuss the primary results at each site. Relationships among sites are also discussed using figures that compare data from several sites. In general, sites fall into two primary groupings. Sites 1245 and 1247–1250 form a north-south transect that documents the evolution of the southern Hydrate Ridge gas hydrate system from the north flank to the summit and explores the role of Horizon A. Sites 1245, 1246, 1244, 1252, and 1251 form an east-west transect that compares the west and east flanks of southern Hydrate Ridge to the adjacent slope basin. Lithology at all sites is similar, with abundant turbidites, some debris flows, and several notable ash layers (Fig. **F9**). These ash layers are responsible for the largest-amplitude seismic reflections beneath the ridge and play a major role in focusing fluid flow and controlling hydrate distribution in this system.

F9. Examples of some of the characteristic lithologic features observed during Leg 204, p. 59.

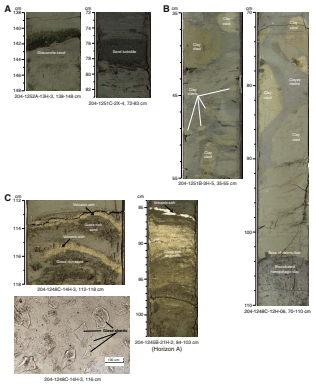

Site 1244

Site 1244 (proposed Site HR1a) is located in ~890 m of water on the eastern flank of Hydrate Ridge ~3 km northeast of the southern summit (Fig. **F1C**). The 3-D seismic data show that the BSR is present at a depth of ~124 mbsf at this site (Fig. **F5**). The temperature and pressure at the seafloor are well within the GHSZ (Fig. **F3**), indicating that gas hydrates can exist within the entire stratigraphic section above the BSR if hydrate-forming gases are available in concentrations that exceed their in situ solubility. The 3-D seismic data also image a zone of incoherent seismic reflections that forms the core of Hydrate Ridge (Fig. **F5**). At Site 1244, the top of this incoherent zone is located at a depth of ~300 mbsf. This facies has been interpreted to comprise fractured accretionary

complex material. Dipping, faulted, and strongly reflective strata, interpreted to be an uplifted and deformed slope basin, overlie this facies.

The primary drilling objectives at this site were to (1) determine the distribution and concentrations of gas hydrate within the GHSZ; (2) determine the nature of a pair of strong reflections (referred to as Horizons B and B′) that underlie much of the eastern flank of Hydrate Ridge; (3) determine the composition, structure, and fluid regime within the seismically incoherent unit underlying the stratified sediments; and (4) sample the subsurface biosphere associated with these features.

Operations

Five holes were cored at Site 1244, and an additional hole was drilled (Table T2). Hole 1244A was abandoned when the first core overshot and did not recover the mudline. Hole 1244B was abandoned at 53.1 mbsf after six cores were obtained because the BHA had to be brought to the surface to retrieve a downhole instrument (Fugro piezoprobe) that had become unscrewed from the Schlumberger conductor cable. One APCT tool measurement was taken at 35.1 mbsf in this hole. Hole 1244C, which comprises 39 cores (Table T3), began at the seafloor and continued to 334 mbsf. Special tools used in Hole 1244C (Table T4) included three APCT tool, one DVTP, one DVTPP, and three PCS runs. Hole 1244C was abandoned 17 m above the target depth of 350 mbsf when hole conditions suggested that a change from XCB to RCB coring would be appropriate. Examination of the core and the initial chemical data from this depth suggested that we had reached the deepest target (i.e., the accretionary complex) and therefore had fulfilled the PPSP requirement that we core the primary facies we expected to encounter during LWD prior to proceeding with LWD at all sites. We returned later in the leg to drill Hole 1244D, which was dedicated to wireline logging and seismic work, to 380 mbsf. This was followed by Hole 1244E, which was cored to 136 mbsf and extensively sampled for geochemistry, gas hydrates, and microbiology, and Hole 1244F, which was cored to 24 mbsf primarily for high-resolution microbiological sampling.

T3. Leg 204 coring summary, p. 73.

T4. Operations summary, p. 75.

Principal Scientific Results

On the basis of visual observations, smear slides, and correlation with physical property data (especially magnetic susceptibility [MS]), the sedimentary sequence can be divided into three primary lithostratigraphic units, with three subdivisions in the second unit. Lithostratigraphic Units I (from the seafloor to 69 mbsf) and II (69–245 mbsf) are both characterized by hemipelagic clay interlayered with turbidites. Thicker, coarser turbidites are common in lithostratigraphic Unit II. Individual turbidites are characterized by sand and silt layers that fine upward to bioturbated sulfide-rich silty clay and clay. The turbidites are particularly well developed in the interval from 160 to 230 mbsf. A 60-cm-thick layer at 216 mbsf that is especially rich in detrital volcanic ash shards corresponds to Horizon B′ (Fig. F5).

The lithology changes to more indurated and fractured claystone interbedded with glauconite-bearing to glauconite-rich silts and sands below 245 mbsf (Unit III). The boundary between lithostratigraphic Units II and III corresponds to the top of the seismically incoherent zone that underlies the slope basin sediments (Fig. F5) and was interpreted to represent highly deformed sediments of the accretionary complex.

Biogenic components vary downcore, with a predominance of siliceous microfossils. Biostratigraphic boundaries based on diatoms correlate fairly well with lithostratigraphic unit boundaries and with seismic stratigraphic boundaries identified in the 3-D seismic data, although there are some inconsistencies among these three data sets when comparisons are made among sites. Sediments immediately above Reflection AC yield diatoms that indicate the age to be younger than 1.6 Ma. Sediments immediately below this reflection yield nannofossils that indicate the age to be older than 1.7 Ma. This unconformity was also sampled at Site 1251 at 300 mbsf and at Site 1252 at 130 mbsf (Fig. **F10**). Lithostratigraphic Unit III is older than 1.7 Ma.

Physical property data are generally consistent with the lithostratigraphic, biostratigraphic, and seismic stratigraphic boundaries. The boundary between lithostratigraphic Units I and II is marked by a localized decrease in wet bulk density. As mentioned above, the turbidites of lithostratigraphic Unit II are particularly well developed in the interval from 160 to 230 mbsf. This interval is characterized by high values of whole-core MS (Fig. **F11**). The widest and strongest MS peak, at 168 mbsf, correlates with the seismic reflector known as Horizon B. This horizon is also coincident with an increase in wet bulk density. There is also excellent correlation between moisture and density (MAD) measurements on core samples and measurements of density and porosity obtained via LWD.

One novel aspect of Leg 204 was the regular use of both handheld and track-mounted IR cameras to image all cores. Cores from within the GHSZ were imaged several times by the physical property scientists. The handheld IR camera proved to be very effective for rapid identification of the location of hydrate specimens within the cores (Fig. **F12**). Gas hydrate samples were recovered as whole rounds in Cores 204-1244C-8H and 10H (samples from 63, 68, and 84 mbsf) and preserved in liquid nitrogen for detailed shore-based studies. A few pieces were dissociated for chemical analysis (discussed below). In all three cases, the hydrate was present as layers or nodules several millimeters to 1.5 cm thick, aligned at an angle of 45°–60° to the core liner, suggesting formation along steeply dipping fractures.

The track-mounted IR camera imaged the cores systematically, and these records were used to confirm the presence of hydrates spotted by the handheld cameras, to develop techniques for detecting more subtle signatures of disseminated hydrate, and to track the temporal evolution of the thermal signature of hydrate dissociation. The IR thermal imaging of the cores on the catwalk indicated the presence of numerous nodular and/or disseminated hydrates extending from ~45 mbsf to the BSR at 124 mbsf. The presence of these is shown in Figure **F13** as temperature anomalies in which local temperature along the core is 1°–7°C (ΔT in Fig **F13**) lower than in the adjacent sediments.

The LWD data obtained at this site are of excellent quality and provide spectacular images of electrical resistivity within the borehole (Fig. **F13**). High-amplitude variable resistivity from 40 to 130 mbsf (Fig. **F11**) suggests the presence of hydrate and correlates well with the depth range of the IR temperature anomalies and with geochemical indicators of hydrate presence discussed below. We note that this is the only site at which the LWD data were acquired after coring. At other sites, the pattern of high-amplitude variable resistivity was used to predict the presence of hydrate prior to coring. Sinusoidal patterns in the resistivity images of the borehole wall suggest that gas hydrate is concentrated in steeply dipping fractures as well as along bedding planes (Fig. **F14**). The

F10. Summary of biostratigraphic and lithologic observations, p. 60.

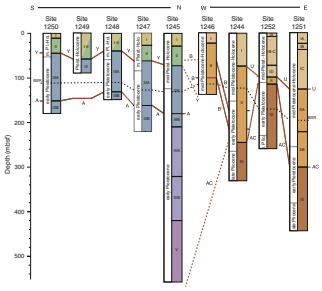

F11. Correlation between 3-D seismic data, density, and resistivity measured downhole, p. 61.

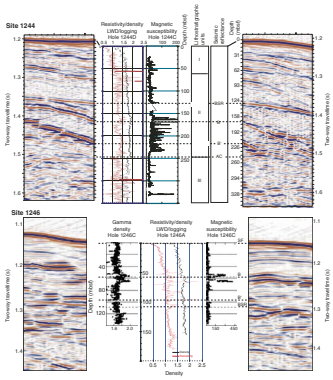

F12. Comparison of IR images and hydrate samples extracted from the core liner, p. 62.

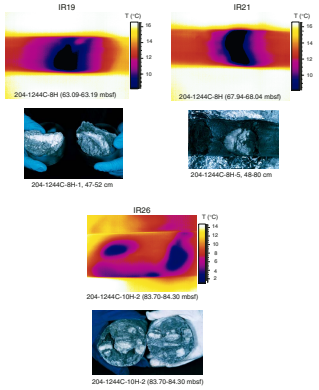

F13. Relative borehole resistivity compared to the presence of low temperature anomalies in recovered cores, p. 63.

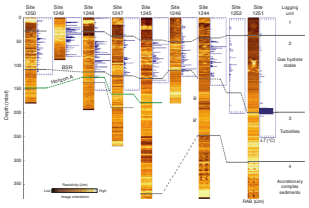

data also show strong borehole breakouts in Unit III, which are indicative of a northeast-southwest–oriented axis of least compressive stress (Fig. **F13**).

Geochemical analysis of IWs has revealed that depth variations in the concentration of several different chemical species correlate with the GHSZ. The most direct correlation is seen in Cl concentrations. Above the first occurrence of hydrate (from the seafloor to ~45 mbsf), Cl concentration in the pore water is similar to that in seawater (Fig. **F15**). Between 45 mbsf and the BSR at ~124 mbsf, there are numerous low Cl spikes that likely reflect the freshening effect of dissociated hydrate on the IWs. Correlation of Cl data with the IR camera data indicates that the IR thermal anomaly data can be used to interpolate between estimates of hydrate concentration based on sparsely sampled Cl anomalies. Considering uncertainties in the background concentration of Cl, we estimate that 2%–8% of the pore space is occupied by hydrate, with locally higher and lower concentrations.

Between the BSR and 300 mbsf, Cl concentrations decrease linearly at a rate of ~0.35 mM/m. This suggests a diffusive gradient between seawater and low-Cl fluids in the accretionary complex. The reduced chloride concentration at depth may reflect dehydration of clay minerals deeper in the accretionary complex. The Cl concentration profile within the deepest incoherent seismic facies is approximately constant, suggesting a zone of fluid advection and mixing consistent with LWD, physical properties, and core observations, all of which suggest a pervasively fractured medium.

The methane/ethane (C_1/C_2) ratio also shows a clear correlation with the presence of gas hydrate and the GHSZ (Fig. **F16**). Gases obtained by the headspace technique and by sampling void space in the cores show a sharp, often steplike, decrease in the C_1/C_2 ratio at the BSR. This was observed to a varying degree at all sites and will be discussed further in the site summary for Site 1251. Slightly lower C_1/C_2 ratios are observed in gas obtained by dissociating discrete hydrate samples, suggesting some fractionation of C_2 into hydrate.

After the first two cores, the cores were pervasively cracked and contained many voids, both of which are indications of degassing during recovery. In situ methane concentrations were measured directly using pressure cores. At Site 1244, in situ methane concentrations are below the solubility predicted for in situ conditions at depths of 24, 40, 120, and 131 mbsf and are above predicted solubility at 72 and 103 (Fig. **F17**) mbsf. These in situ gas concentrations corroborate the relatively low estimates of gas hydrate concentration at Site 1244 obtained from the chloride data.

The downhole temperature measurements (including the average of waterline temperatures) were used to define a linear temperature gradient of 0.061°C/m, very similar to the temperature gradient determined at northern Hydrate Ridge (ODP Site 892) during Leg 146 (Westbrook et al., 1994). This temperature gradient predicts that the base of the GHSZ should be at a depth of 133 mbsf, based on the pure methane and seawater stability curve.

Seismic data at this site include high-frequency sonic log data and lower-frequency vertical, offset, and walkaway seismic profiles. Preliminary picks of the VSP data and the V_p sonic logs indicate that the BSR depth is 127–129 mbsf, slightly deeper than the precruise estimate (Table **T1**). The data also indicate that positive velocity anomalies resulting

F14. Comparison of the resistivity structure between Sites 1244 and 1248, p. 64.

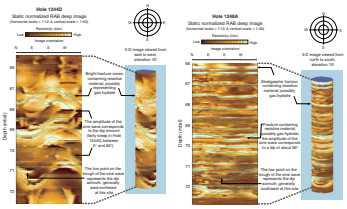

F15. Chloride concentration values measured at all sites, p. 65.

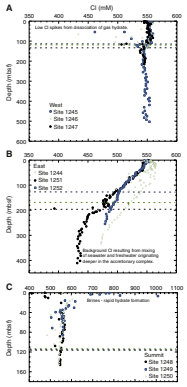

F16. C_1/C_2 values from vacutainer samples measured at all sites, p. 66.

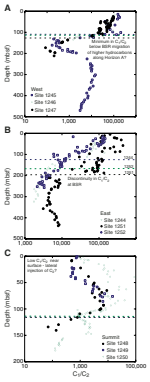

F17. Methane concentrations determined from PCS measurements, p. 67.

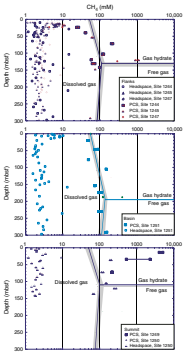

from hydrate presence above the BSR and low-velocity anomalies resulting from free gas below the BSR are small and local.

The pore pressure dissipation measurement made by the DVTPP follows the expected pattern, but detailed analyses to determine whether in situ pressure departs from hydrostatic pressure awaits postcruise study.

Samples were taken to support a range of shore-based microbiological studies. Measurements of sulfate concentration in the IWs, which indicate that the SMI is present at 8 mbsf at this site (Fig. F19), were used to guide high-resolution sampling for microbiological studies.

Summary

The recovery of several centimeter-thick veins of gas hydrate during the first week of Leg 204 drilling got the leg off to an exciting start by providing direct evidence for the presence of gas hydrate within the GHSZ. Multiple data sets, including images of borehole resistivity, IR thermal anomalies, and low chloride spikes in the IWs, indicate intermittent hydrate presence between ~45 mbsf and the BSR at 124 mbsf. A steplike decrease in C_1/C_2 beneath the GHSZ, the cause of which has not yet been determined, indicates that the presence of gas hydrate has a fundamental impact on the biogeochemical evolution of the margin. The data from this site also confirmed that 3-D reflection surveying, LWD-resistivity borehole images, and IR thermal scans are very useful for guiding subsequent sampling of sediments in gas hydrate provinces.

Site 1245

Site 1245 (proposed Site HR3a) is located in 870 m of water on the western flank of Hydrate Ridge ~3 km northwest of the southern summit (Fig. F1). The 3-D seismic data show that the BSR is at a depth of ~134 mbsf at this site. As at all sites drilled during Leg 204, the temperature and pressure at the seafloor at Site 1245 are well within the GHSZ, indicating that gas hydrates can exist within the entire stratigraphic section above the base of the GHSZ if hydrate-forming gases are available in concentrations that exceed their in situ solubility. Site 1245 intersects Horizon A, which can be mapped from the northern boundary of the seismic survey to the summit, where it appears as a "bright spot" beneath the BSR. On its downdip edge, it appears to lap onto the seismically incoherent facies interpreted to represent highly deformed sediments of the accretionary complex. Horizon A has been interpreted as a "conduit" that transports fluids from the accretionary complex to the summit. Several unconformities, referred to as Horizons Y and Y′, overlie Horizon A and appear to represent discontinuities in sediment accumulation in a slope basin that was formed during growth of an underlying accretionary anticline.

Primary objectives at Site 1245 were to (1) determine the distribution, composition, and concentration of gas hydrate in the sediments on the western flank of Hydrate Ridge and contrast these parameters with those on the eastern flank of the ridge and in the adjacent slope basin, where the sub-BSR fluid migration pathways inferred from seismic data are distinctly different; (2) sample sediments and fluids from seismic Horizon A; and (3) sample the sedimentary section of the western flank of Hydrate Ridge below the BSR to provide constraints for interpreting variations in BSR strength across the western flank. Site 1245

is also a reference site for a north-south–trending transect that extends from Site 1245 to the summit and includes Sites 1247–1250.

Operations

Four holes were cored and one was drilled without coring at Site 1245 (Table T2). Hole 1245A was drilled to a depth of 380 mbsf (without coring) to obtain the initial LWD data for this site. Hole 1245B was cored to 473.7 mbsf using the APC and XCB (Table T3). Holes 1245C and 1245D were cored to 201.7 and 24 mbsf, respectively, for extensive high-resolution geochemical and microbiological sampling. Hole 1245E was drilled to 473.7 mbsf and then cored to 540.3 mbsf using the RCB (Table T3). Coring in Hole 1245E stopped short of the originally planned depth of 700 mbsf because of deteriorating hole conditions. The hole began to collapse, trapping the BHA. Fortunately, it was not necessary to sever the pipe, although preparations were made to do so. The upper 300 mbsf of Hole 1245E was used for wireline logging. Plans for conventional, offset, and walkaway seismic lines were abandoned when the downhole seismometer would not clamp in Hole 1245E and the hole continued to collapse. The APCT tool was run eight times, the DVTP was run three times, and the PCS was run five times at this site (Table T4). There were also two runs each of the HYACINTH HRC and FPC. Eleven whole-round samples of sediment thought to contain gas hydrate were preserved in liquid nitrogen or in pressure vessels for post-cruise studies.

Principal Scientific Results

Biostratigraphic observations at Site 1245 indicate that the entire 540-m-thick sequence is younger than 1.65 Ma (Fig. F10). Distinct changes in sedimentation rate occurred at 55 and 150 mbsf. Sediments deeper than 150 mbsf were deposited from 1.0 to 1.65 Ma at a rate of ~62 cm/k.y., whereas the overlying strata were deposited at a slower rate of 10–23 cm/k.y. Lithostratigraphic analysis (Fig. F10) indicates that the dominant lithologies in the upper 0–31 mbsf are clay with carbonate concretions and foraminifer-rich interlayers. From 31.5 to 212.7 mbsf, the sediments are mainly diatom-bearing clay and silty clay with frequent sand-rich turbidites containing a few glass-rich layers. Included within this deeper sequence is seismic Horizon A, characterized by multiple ash-rich sandy layers between 176 and 183 mbsf. Between 212.7 and 419.3 mbsf, nannofossil-rich claystone and silty claystone with glauconite layers and turbidites are present, underlain by claystone containing thick turbidites and heterogeneous mud clasts.

The precruise 3-D seismic reflection site survey (Figs. F5, F6) and the LWD data (Fig. F13) obtained from Hole 1245A were used to guide the sampling and analysis strategy at this site. The logging data, which are of excellent quality, show a marked increase in the amplitude and variability of formation resistivity between 48 and 131 mbsf (logging Unit II). As discussed for Site 1244, this resistivity pattern is interpreted to indicate the zone within which gas hydrates are present. Some high-resistivity layers are subhorizontal, indicating accumulation of gas hydrate parallel to bedding; others are steeply dipping, indicating that hydrate fills fractures. Calculations of pore space saturation based on Archie's Relation (Collett and Ladd, 2000) predict a hydrate concentration of ~10%–30% of the pore volume in layers and veins distributed throughout this interval.

The estimated depth distribution of gas hydrate obtained from the LWD data was confirmed by several other chemical and physical proxies. Low chloride concentration anomalies (Fig. F14) were detected in IWs from 55 to 125 mbsf (Fig. F15) and are interpreted to reflect in situ hydrate concentrations that are generally below 3% of pore volume, with one anomaly suggesting a concentration of 15%. Low temperature anomalies were observed with the IR cameras between 50 and 129 mbsf (Fig. F13). Preliminary estimates of total in situ methane concentration obtained from a PCS core at 57 mbsf indicated a concentration very close to in situ saturation, and a PCS core located at 120 mbsf indicated that in situ methane concentration just above the BSR is an order of magnitude greater than saturation at in situ conditions (Fig. F17). Two PCS runs below the BSR yielded concentrations that are apparently slightly lower than saturation. The consistency between these multiple independent estimates of the depths where hydrate is present gives us considerable confidence in the validity of these estimates.

The IR camera was used to rapidly identify the potential location of hydrate samples in cores on the catwalk. In addition, the IR data were used to estimate the distribution and texture of gas hydrate downhole. Approximately 80 IR anomalies were identified and classified (Fig. F13). In Hole 1245B, 75% of the anomalies suggested disseminated hydrate and 25% suggested nodular hydrate; in Hole 1245C, 60% of the anomalies suggested disseminated hydrate and 17% suggested nodular hydrate.

The IR data were also used to select a section of core (Section 204-1245C-7H-5) for an experiment to investigate the relationship between IR imaging, chloride concentration anomalies in pore water, and hydrate distribution in the core. The core liner was split as soon as the IR anomaly was identified, and a 2-cm-thick steeply dipping layer of hydrate was found. After allowing the hydrate to dissociate for 90 min, closely spaced sediment samples were taken near the hydrate, including one sample from where the hydrate had been. The chloride concentration anomaly is strongly attenuated 5 cm away from the hydrate sample and has disappeared 10 cm from the hydrate. Since normally only two IW samples are taken in each 9.5-m-long core, the chloride concentration measurements are spatially aliased. Frequent low chloride concentration anomalies downcore probably indicate extensive distribution of hydrate. Additional comparison and calibration between data sets with different length scales and sensitivity to hydrate concentration should improve our ability to estimate in situ concentrations from such data.

A major objective at Site 1245 was to sample seismic Horizon A. At Site 1245, as well as at the other three sites where Horizon A was crossed during the LWD phase of Leg 204 (Sites 1247, 1248, and 1250), it is characterized by a very distinctive strong double-peaked low density anomaly that is 3–4 m thick (Fig. F18). At Site 1245, the density of sediments in Horizon A is <1.5 g/cm³ compared to 1.85 g/cm³ in adjacent sediments. Coincidence of this LWD density anomaly with the estimated depth of Horizon A in the seismic data provided confirmation that the velocities used for converting the seismic data to depth were accurate enough to predict the depth of target horizons to within a few meters. This was confirmed by sonic velocity measurements. The direct correlation between the low-density layers and the thick ash layers discussed above was confirmed by bulk density and MS measurements made on the cores.

F18. Density and RAB recorded through seismic Horizon A at Sites 1245 and 1247, p. 68.

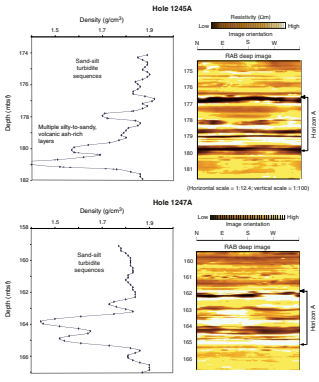

Another major result of drilling at Site 1245 was the discovery of significant concentrations of higher-order hydrocarbons beneath the BSR. Methane/ethane (C_1/C_2) ratios in headspace samples reach values <100 between 130 and 180 mbsf (Fig. F16). The C_1/C_2 anomaly is due entirely to an increase in ethane concentration, indicating that thermogenic hydrocarbons are migrating from deeper in the accretionary complex. Dissolved lithium anomalies observed in association with Horizon A support this interpretation. In addition to C_2, enrichments in C_3 and other higher-order hydrocarbons were also observed. At Site 1245, the minimum in the C_1/C_2 ratio was present at ~150 mbsf (~30 m above Horizon A). However, no thermal anomaly was detected associated with Horizon A, suggesting that the rate of fluid flow is relatively slow.

The SMI is well defined at a depth of ~7 mbsf at this Site (Fig. F19). Models to relate the depth of the SMI to the depth to the first occurrence of gas hydrate will be explored postcruise. The mismatch between the observed depth to the bottom of the GHSZ and that predicted by downhole temperature measurements for the measured in situ temperature gradient of 0.054°C/m is similar to that at Site 1244.

F19. Sulfate and methane concentration showing the SMI, p. 69.

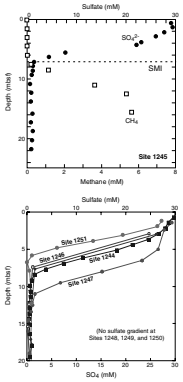

Summary

Site 1245 provided confirmation that multiple proxies for in situ hydrate presence (including electrical resistivity measured downhole, core temperatures measured on the catwalk, chloride anomalies measured in IWs, and direct measurements of gas concentration) are generally consistent in predicting the distribution and concentration of gas hydrates in the subsurface. Additional analysis is needed to more precisely understand and calibrate these different proxies. Drilling at this site also demonstrated that seismic Horizon A results from the presence of a pair of low-density ash-bearing sand layers that are likely to be conduits transporting fluids from the accretionary complex. Shipboard data provide evidence for migration of higher hydrocarbons beneath the GHSZ, although determining details of the role of seismic Horizon A in this migration will only be resolved through integration of data from several sites. Finally, this site provided important lithostratigraphic and biostratigraphic data for reconstructing the geologic history of this hydrate-bearing system, including the rate at which the system formed and lithologic controls on fluid migration and hydrate distribution.

Site 1246

Site 1246 (proposed Site HR1b) is located in ~850 m of water near the crest of Hydrate Ridge, ~3 km north of the southern summit (Fig. F1). The 3-D seismic data show that the BSR is at a depth of ~114 mbsf at this site. This site also intersects a pair of bright regional seismic reflectors, referred to as Horizons B and B′, at depths of ~60 and 100 mbsf, respectively. The temperature and pressure at the seafloor are well within the GHSZ, indicating that gas hydrates can exist within the entire stratigraphic section above the base of the GHSZ if hydrate-forming gases are available in concentrations that exceed their in situ solubility.

The primary objective at Site 1246 was to sample Horizons B and B′ where they are within the GHSZ. By comparing this site to Site 1244, where Horizons B and B′ are below the GHSZ, we hope to constrain lithologic and hydrologic explanations for the strong reflectivity of these seismic horizons, obtain insights into the processes that transport fluids

into and through the GHSZ, and develop more effective strategies to predict hydrate presence from seismic and other remote sensing data.

Operations

Hole 1246A was drilled to a depth of 180 mbsf without coring to obtain the initial LWD data for this site. In Hole 1246B, we obtained 16 APC cores, sampling to a depth of 136.7 mbsf with 99% recovery (Table T2). The APCT tool was run five times; no other special tools were deployed (Table T4). These cores were sampled for headspace and void gas analyses, chemical analysis of IW (two per core), basic physical property measurements, biostratigraphic analysis, and lithostratigraphic description.

Principal Scientific Results

The precruise 3-D seismic reflection site survey and the LWD data obtained in Hole 1246A were used to guide the sampling and analysis strategy at this site. As mentioned above, the seismic data define the link between Sites 1244 and 1246 and suggest approximate depths to Horizons B and B′ and the BSR of ~60, 100, and 114 mbsf, respectively (Table T1). The LWD data were processed and available for interpretation 3 weeks prior to coring. These logs provided a first look at the probable distribution of hydrate within the GHSZ. Based on Archie's Relation between electrical resistivity and porosity, we infer that hydrate should be present intermittently between 53 and 109 mbsf (Fig. F13). The LWD data also indicate that Horizon B is characterized by relatively high density and resistivity, as was found at Site 1244. Unlike at Site 1244, no prominent low density anomaly is found associated with Horizon B′ at Site 1246.

The IR camera was used to rapidly identify gas hydrate through the core liner, to investigate the distribution and texture of hydrate in the cores, and to visualize the process of dissociation. Temperature anomalies in the IR thermal images suggest the intermittent presence of hydrate from ~15 to 117 mbsf (Fig. F13), a somewhat more extensive depth range than is indicated by other hydrate proxies. In addition, several of the IR thermal anomalies are correlated with changes in the lithologic and physical properties of the sediments and with anomalies in chemistry of the pore waters. These changes are, in turn, correlated with seismic Horizon B. Whole rounds of core containing particularly strong IR temperature anomalies, and therefore suspected of containing gas hydrate veins or nodules, were recovered from 66.5, 96.6, and 105.0 mbsf and preserved in liquid nitrogen for detailed shore-based studies. A gas hydrate sample recovered from 109.5 mbsf was divided into two pieces; one piece was allowed to dissociate on board for chemical analysis (discussed below), and the other was preserved.

On the basis of visual sediment descriptions, examination of smear slides, and correlation with physical property data (especially MS), the sedimentary sequence can be divided into two primary lithostratigraphic units (Fig. F10). Lithostratigraphic Unit I (from the seafloor to 21.7 mbsf) is a late Pleistocene–Holocene unit characterized by dark greenish gray diatom and nannofossil-bearing hemipelagic clay. Lithostratigraphic Unit II, which extends to the base of Hole 1246B, is defined by the onset of graded silt and sand layers, which represents a series of turbidites of varying thicknesses bounded by erosional contacts and separated by periods of bioturbated hemipelagic sedimentation.

Layers composed of >50% sand are found at 62, 71, and 136 mbsf, respectively.

A silt turbidite layer at ~66 mbsf (found in Section 204-1246B-8H-3) can be correlated with the base of seismic Horizon B. The overlying graded sequence is ~2 m thick and gray colored, in sharp contrast to most of the sediment cored during this leg. The gray color results from a high percentage of quartz grains. This zone contains fewer biogenic components than adjacent strata, suggesting rapid deposition. A similar sequence is found at 56 mbsf in Section 204-1246B-7H-3. Detailed analysis of physical property data reveals that these two turbidite sequences are characterized by high density and high MS anomalies (Fig. **F11**). Preliminary synthetic seismograms, calculated based on the density log, confirm that the resulting double-peaked density anomaly extending from 54 to 67 mbsf explains the complicated waveform of seismic Horizon B at this site. The relatively high density probably results from the grain size and packing of the sediments. The source of the high MS has not yet been identified. A thin (<50 cm thick) high resistivity anomaly also appears near the base of each of these turbidites in the LWD resistivity logs, suggesting the presence of gas hydrate. Low temperatures measured on the catwalk with the IR camera are additional indirect indicators for the presence of gas hydrate in the lowermost coarse-grained portion of each turbidite sequence. A sample with anomalously low temperatures was recovered from the base of the lower turbidite (Sample 204-1246B-8H-4, 25–30 cm) and preserved in liquid nitrogen for postcruise analysis. Samples of this coarse-grained layer were also taken for IW studies.

The correlation between physical properties, lithology, and seismic Horizon B′ at Site 1246, where it is present a few meters above the BSR, is not clear. A thin (<1 cm thick) volcanic ash–rich layer is observed at ~95 mbsf in Section 204-1246B-11H-4, 96 cm. Narrow (<1 m) layers of high resistivity observed in the LWD resistivity data and thermal anomalies indicative of the presence of gas hydrate are observed at 96–97 mbsf. A sample thought to contain hydrate was recovered in Section 204-1246B-11H-5 at this depth. Recovery in Core 204-1246B-11H was 80%, and the primary lithologic source of Horizon B′ may not have been recovered. Shore-based studies are planned to determine the age and provenance of this ~95-mbsf ash and compare it to the ash recovered from Site 1244. The ash data will complement the biostratigraphic ages, which suggest an age of ~0.3 Ma at Horizon B′. Seismic modeling will also provide constraints on the nature of fluids in this horizon. At Site 1244, where Horizon B′ is found at 216 mbsf (well below the GHSZ), it is associated with a 60-cm-thick layer that is rich in detrital shards of volcanic glass and corresponds to a distinctive low density anomaly in the LWD and shipboard physical property data. We will test the model that Horizon B′ contains free gas at Site 1244 and that the disappearance of the density anomaly at Site 1246 results from the replacement of free gas by gas hydrate.

Geochemical analyses of IWs made during Leg 204 revealed variations in the concentration of several different chemical species with depth that correlate with the presence of gas hydrate in the GHSZ. At Site 1246, the most direct correlation is based on chloride concentrations, which show a pattern similar to those observed at most other sites, with the exception of those at the southern summit of Hydrate Ridge (Fig. **F14**). From the seafloor to ~40 mbsf, the chloride concentrations are similar to that of seawater, suggesting that no hydrate is present. Between 40 mbsf and the BSR at ~114 mbsf, there are

numerous low-chloride spikes that probably reflect the dilution of pore water by freshwater from dissociated hydrate. The lowest chloride value at this site (~430 mM) is from an IW sample that fortuitously coincided with the coarse-grained basal zone of the Horizon B turbidite discussed above. Assuming an in situ "no hydrate" background chloride concentration, the amplitude of this chloride anomaly suggests that 23% of the pore space was filled by hydrate. Ba, Li, and Na are depleted in this interval, and Ca, Mg, and Sr are depleted in the overlying sample, located ~3 m higher in the section. The correlation of IW chemistry with specific horizons defined by lithologic and physical properties suggests that isotopic analysis and modeling of these chemical data may provide constraints on the origin, evolution, and flow rate of fluids that transport methane into and through the GHSZ.

Analyses of hydrocarbon gases at Site 1246 indicate that processes here are similar to those at Site 1244. The ratio of methane to ethane (C_1/C_2) shows a steplike decrease at the BSR (Fig. **F16**), which reflects an increase in C_2 beneath the BSR rather than a change in methane concentration. The presence of propane (C_3) below the BSR suggests that heavier hydrocarbons migrate upward from deeper unsampled sediment, and the absence of C_3 within the GHSZ (with one exception at ~22 mbsf) indicates that gas above solubility in this zone should be in the form of Structure I rather than Structure II hydrate. The apparent fractionation of C_2 into gas hydrate, which was reported at Site 1244, is not apparent here. However, this may be an artifact of sampling because only one hydrate sample was available for gas analysis at Site 1246. Because no PCS runs were made at this site, no in situ gas concentration estimates are possible.

The SMI at Site 1246 falls between 4 and 7 mbsf but is poorly defined as a result of sparse sampling; it is slightly shallower than at Site 1244, where it is identified at 9 mbsf (Fig. **F19**). Variations in the depth of the SMI among Leg 204 sites will be compared to variations in depth to the first occurrence of hydrate as part of a postcruise study.

Summary

There are multiple correlations between geological and geophysical parameters and the presence of gas hydrate at Site 1246. The primary preliminary result is that seismic Horizon B is caused by a pair of high-MS, high-density, and low-porosity layers ~2.5 m thick and spaced 10 m apart. Sedimentological analysis indicates that each layer is formed by a turbidite sequence with a complicated internal structure indicating deposition, erosion, and redeposition. Electrical resistivity, IR temperature, and geochemical anomalies are associated with the basal coarser-grained layers of each of the two turbidites that constitute Horizon B, indicating that hydrates preferentially form here. Indirect and direct indicators of hydrate were also found associated with Horizon B′. Postcruise work is planned to determine the source of the MS anomaly and to correlate lithologic and physical properties of these horizons between Site 1244 and Site 1246. Additional efforts will be focused on modeling the seismic response of this horizon as it changes from a fluid-rich layer beneath the BSR to a hydrate-bearing layer above it and to constrain the source and evolution of the fluids using the geochemical data.

Site 1247

Site 1247 (proposed Site HR4c) is located in ~845 m of water on the western flank of Hydrate Ridge, ~800 m northwest of the southern summit and approximately halfway between Site 1245 and the summit (Fig. F1). The 3-D seismic data indicate that the seismic stratigraphic setting is similar to that of Site 1245 (Fig. F5). The BSR is at a depth of ~121–124 mbsf at this site. Horizon A is brighter and shallower (~160 mbsf) at Site 1247 than at Site 1245; Horizon Y is also shallower (~60 mbsf) at this site.

The primary objective at Site 1247 was to sample sediments and fluids from Horizon A approximately halfway between Site 1245 and the summit (Site 1249) in order to determine lateral variations in the physical and chemical characteristics of this horizon and thus understand the role it plays in fluid migration and formation of hydrate on the seafloor at the summit. Although they are only 75 m apart, the two holes drilled at this site sample parts of Horizon A with distinctly different seismic characteristics.

Operations

Hole 1247A was drilled without coring to a depth of 270 mbsf to obtain LWD data for this site. We returned to core Hole 1247B, which was offset from Hole 1247A, ~75 m to the east (Table T2). Hole 1247B was cored to 220 mbsf using the APC and XCB (Table T3). The APCT tool was run six times (including a mudline run to obtain seafloor temperature), the DVTP was run twice, and the PCS was run three times in this hole (Table T4). Hole 1247B was then logged using the triple combination (triple combo) and Formation MicroScanner (FMS)-sonic tool strings. After wireline logging, vertical and offset VSPs covering the interval of 104–214 mbsf were acquired by alternately shooting from the *JOIDES Resolution* and the *Ewing,* which held station ~700 m away. Plans to conduct walkaway VSPs were abandoned when the Schlumberger VSI tool string would no longer clamp in the hole.

Principal Scientific Results

Biostratigraphic observations from the 220 m of core recovered in Hole 1247B indicate that the entire sequence is younger than 1.65 Ma (Fig. F10). Sediments deeper than ~165 mbsf were deposited at a rapid but poorly constrained rate. These deep strata can be correlated with strata yielding a linear sedimentation rate of 62 cm/k.y. at Site 1245. The interval from ~150 to 165 mbsf, which contains Horizon A, yields a relatively slow sedimentation rate of 4 cm/k.y., based on nannofossils. The overlying sediments were deposited at a rate of 9–22 cm/k.y., similar to what was observed at Site 1245.

Lithostratigraphic analysis (Fig. F10) indicates that the dominant lithologies are clay with authigenic carbonates and foraminifer-rich interlayers in the upper 0–27 mbsf (lithostratigraphic Unit I). This unit is underlain by diatom-bearing clay and silty clay with frequent sand-rich turbidites containing a few glass-rich layers from 27 to 212.7 mbsf (Unit II). Lithostratigraphic Unit III (60–220 mbsf) is distinguished from Unit II by an increase in turbidites and biogenic components. Included in lithostratigraphic Unit II is seismic Horizon A. Unlike at the other sites where Horizon A was sampled and found to correspond with volcanic ash–rich layers, at Site 1247B Horizon A appeared to be a soft-

sediment debris flow bounded by turbidites. Because the signature of Horizon A in the LWD resistivity data from Hole 1247A (located only 75 m from Hole 1247B) is very similar to that observed at Sites 1245, 1248, and 1250, we conclude that the change in seismic amplitude of Horizon A between the two holes at Site 1247 results from a dramatic local change in lithology rather than from processes related to gas hydrates.

As at other sites, the different hydrate proxies are in agreement and together indicate the apparent top of the zone where hydrate is present. The onset of high and variable electrical resistivity and of thermal anomalies observed with the IR camera on the catwalk are both at ~45 mbsf (Fig. **F13**). High-resistivity layers are subhorizontal, indicating accumulation of gas hydrate parallel to bedding, and steeply dipping, indicating that hydrate fills fractures. The onset of low chloride concentration anomalies is at ~55 mbsf (Fig. **F15**). The onset of in situ methane oversaturation as projected from headspace and PCS measurements is at ~38 mbsf (Fig. **F17**).

Samples suspected of containing hydrate based on IR temperature anomalies were recovered from 93 to 113 mbsf and were stored in liquid nitrogen. However, on later inspection, no hydrate was actually preserved in these samples.

The above proxies are consistent with similar depths for the base of the GHSZ. The deepest IR thermal anomaly is at 118 mbsf (Fig. **F13**). The deepest chloride concentration anomaly is at 114 mbsf (Fig. **F15**). A PCS core, indicating a volume of methane greater than in situ concentration, was taken at 123 mbsf (Fig. **F17**). Seismic velocities from the sonic log and the VSP clearly resolve a velocity decrease indicative of the presence of free gas beneath the BSR that occurs at 129–134 mbsf.

The significant concentrations of C_{2+} hydrocarbons gases found beneath the BSR at Site 1245 were also observed at Site 1247 (Fig. **F16**). Here, low values of the methane/ethane ratio ($C_1/C_2 < 100$) persist to a slightly deeper depth than at Site 1245 (~220 mbsf compared to ~180 mbsf at Site 1245). Hole 1247B did not extend deep enough to resolve whether the C_1/C_2 ratio returns to normal at greater depth, as it did at Site 1245.

One of the notable results from this site was identification of a new hydrate proxy that has the potential to provide valuable constraints on the dynamics of hydrate formation. It was found that many samples collected from the depth range in which other proxies indicate the presence of hydrate showed ethane enrichment and propane depletion. This was attributed to preferential incorporation of ethane and exclusion of propane (C_3) during the formation of Structure I hydrate. The observed pattern of C_1/C_2 and C_1/C_3 anomalies, relative to baseline ratios defined by the majority of samples, can be explained by invoking the presence of dissociated gas hydrates. The C_1/C_2–C_1/C_3 anomaly hydrate proxy is, therefore, similar to the chloride anomaly hydrate proxy.

At Site 1247, Horizon A shows a low-amplitude chloride concentration low and methane high. Considering that Horizon A should be more permeable where it is characterized by coarse-grained ash-rich layers than where it consists of a clay-rich debris flow, these observations are surprising and have not yet been explained. At this horizon, there is also Li enrichment similar in magnitude to that observed at other sites, supporting the interpretation of a stratigraphic horizon that transports fluids from greater depth.

The depth of the SMI at this site is well constrained by high-resolution samples and is determined to be at 11 mbsf (Fig. F19). Assuming that this depth is entirely controlled by AMO (using sulfate as the oxidant), a methane flux of 2.5×10^{-3} mM/cm^2/yr is inferred, which is ~1.4 times greater than at the Blake Ridge and ~30% less than at Site 1251. However, the assumptions on which this estimate is based may not be valid for the entire interval above the SMI, leading to considerable uncertainty in this estimate.

The in situ temperature measurements in Hole 1247B yielded a very precisely defined slope of 0.053°C/m (correlation coefficient = 0.999) and did not reveal any sign of a positive temperature anomaly at Horizon A. This observation will be used to place an upper boundary on the rate of fluid transport from depth along this horizon, which can be compared to rates obtained from the chemical anomalies.

Summary

Site 1247 provided further confirmation that multiple proxies for the presence of in situ hydrate are consistent with direct measurements of gas concentration in predicting the distribution and concentration of gas hydrates in the subsurface. These include electrical resistivity and porosity measured downhole via LWD, core temperatures measured on the catwalk, and chloride anomalies measured in IWs extracted from sediment samples. A new hydrate proxy, ethane enrichment and propane depletion, was discovered and holds promise for constraining hydrate dynamics. Results from this site also indicate that lateral changes in the amplitude of Horizon A between Holes 1247A and 1247B probably result from lithologic changes rather than from the presence of more stable hydrates of higher-order hydrocarbons, as had been speculated (Tréhu et al., 2002). Finally, the small chloride concentration depletion and methane enhancement associated with Horizon A, which is not observed at Sites 1245, 1248, and 1250, leads to the apparently contradictory conclusion that Horizon A is a more active conduit for deeper fluids where it is composed of a clay-rich debris flow rather than where it is composed of coarse-grained ash-rich sandy silt.

Site 1248

Site 1248 (proposed Site HR6) was drilled in ~830 m of water, ~300 m northwest of the southern Hydrate Ridge summit (Fig. F1). This site is located in the middle of a small (~150-m diameter) high-reflectivity spot on the seafloor imaged by a deep-towed side-scan sonar survey (Fig. F7). The small spot is located 300 m north of a larger circular high-reflectivity patch around the Pinnacle, a well-known active carbonate chemoherm. These are the only two locations on southern Hydrate Ridge where high backscatter reflectivity is observed. It is interpreted to indicate authigenic carbonate resulting from fluid venting at the seafloor. Television-sled surveys revealed some evidence for the presence of scattered authigenic carbonate fragments within the small high-reflectivity patch, which might be responsible for the higher backscatter signal observed in the side-scan sonar data. The 3-D seismic data show attenuation of the underlying stratigraphic reflectivity, similar to what is observed beneath the Pinnacle (Fig. F7). Both areas of high backscatter overlie the intersection of seismic Horizon A and the BSR.

The principal objectives at Site 1248 were to (1) investigate whether the sediments below the high-reflectivity seafloor spot contain evi-

dence of active fluid advection and (2) determine whether these fluids are supplied by Horizon A.

Operations

Three holes were drilled at Site 1248 (Table T2). LWD measurements were made in Hole 1248A down to 194 mbsf. Hole 1248B was abandoned at 17 mbsf after three cores. Coring disturbance because of massive near-seafloor gas hydrate presence and a shattered liner during retrieval of Core 204-1248B-3H resulted in poor core recovery (44%). Of the 17 cores from Hole 1248C, 5 XCB cores were drilled to 48 mbsf, followed by 11 APC cores and 1 XCB core to 149 mbsf (Table T3). After poor core recovery (23%) in Cores 204-128C-1X through 5X, recovery increased to 90%. Six temperature measurements were made using the DVTP, APCT tool, and DVTPP (Table T4).

Principal Scientific Results

Three lithostratigraphic units were recognized at Site 1248 (Fig. F10). The uppermost sediments that comprise Units I and II (late Pleistocene–Holocene age) are characterized by dark greenish gray diatom-bearing clay and silty clay and extend from the seafloor to 39 mbsf. These fine-grained lithologies are commonly structureless except for sulfide mottles. Lithostratigraphic Unit III (39–149 mbsf), of middle–early Pleistocene age, is dominated by homogenous silty clays with varying amounts of biogenic components. Sand- and silt-sized turbidites are intercalated as minor lithologies throughout this unit.

High concentrations of beige to white volcanic glass shards were observed in the tail of a few turbidites near 130 mbsf in Core 204-1248C-14H (Fig. F9). These glass-rich layers are the lithologic signature of seismic Horizon A, which appears in the LWD data as a 2-m-thick interval characterized by high-resistivity and low-density values within the depth interval from 126 to 128 mbsf. Physical property measurements on discrete samples of the cores from Site 1248 confirm the low-density character of Horizon A sediments, which is interpreted to be a result of the reduced grain density of the ash. The presence of volcanic ash in Horizon A reduces the grain density because amorphous silica particles in the ash have distinctly lower grain densities than other sedimentary components like quartz, feldspar, and clay minerals. Sediments from the interval of Horizon A do not show higher porosity values than the surrounding sediments. The distinctly larger grain size of the ash-rich sediments, however, implies a different packing structure and possibly higher permeability in these intervals, supporting the idea that Horizon A is a potential fluid migration conduit.

Organic geochemistry measurements on gases from Site 1248 reveal high methane contents throughout. In addition to the high methane levels, there is a surprising variation in ethane content with depth. C_1/C_2 is <1000 near the seafloor, increasing to 10,000 near the base of the GHSZ, and decreases sharply below the BSR (Fig. F16). In addition to ethane, propane (C_3) is present in relatively high concentrations in the upper 120 mbsf and is even more abundant in headspace gas below that depth. The gas analyses at Site 1248 reflect the complex mixing of gases from two hydrocarbon sources (Fig. F16). Mixed microbial and thermogenic gases are present in the uppermost 40 mbsf followed downhole by an intermediate interval (40–100 mbsf) dominated by microbial gas. Mixed microbial and thermogenic gas is also present in the deepest sed-

iments at Site 1248 (below 100 mbsf), with thermogenic gas possibly being injected at Horizon A at ~130 mbsf. The data suggest rapid advection of deeper gas to the seafloor, bypassing the lower part of the GHSZ.

Analyses of gases from dissociated hydrate samples collected from the shallow zone above 40 mbsf showed that even though methane occupies most of the water cages of the hydrate structure, higher-order hydrocarbons are also present. Gas hydrates at Site 1248 are probably primarily Structure I hydrate that incorporates ethane molecules within the cage structure. However, in Sample 204-1248C-2H-2, 0–10 cm (7.37 mbsf), a higher concentration of propane than ethane suggests that Structure II hydrate is present. Although thermogenic Structure II gas hydrates are common in petroleum provinces such as the Gulf of Mexico and the Caspian Sea (Sassen et al., 2001; Ginsburg and Soloviev, 1998), this hydrate type was not known to be at Hydrate Ridge prior to Leg 204.

IW geochemistry results clearly show the influence of gas hydrate formation at Site 1248 (Fig. **F15**). Based on the chloride distribution in the pore water, the presence of hydrate is suggested from the seafloor to the BSR at 115 mbsf. The data indicate 25% gas hydrate content in the pore space of the uppermost 20 mbsf, whereas LWD resistivity data indicate up to 50% occupancy of pore space by gas hydrates. Below 20 mbsf, gas hydrate content calculated from chloride concentration anomalies ranges from 2% to 5% of pore volume.

Soupy and mousselike textures present in silty clay and diatom-bearing silty clay, interpreted to result from dissociation of hydrates, provide additional evidence for the presence of hydrate in situ. These textures were particularly common in the uppermost 20 mbsf, where massive gas hydrate samples were recovered. In contrast, farther downcore, only small nuggets and thin veins of hydrate were sampled. The samples were identified by thermal IR imaging of cores on the catwalk using a handheld IR camera. Postacquisition processing of the IR data shows a good correlation with the pore volume saturation derived by LWD resistivity logs, the chloride pore water data, and the sedimentological observations of the presence of dissociated hydrate layers.

High advective flow rates in the uppermost 20 mbsf of the sediments drilled at Site 1248 are indicated by several findings. Sulfate concentrations were near zero even in the shallowest pore water sample, implying a high methane flux from below that feeds microbial AMO. Microbial reduction of near-seafloor sulfate during AMO produces millimolar quantities of dissolved sulfide within the uppermost core. In addition, the authigenic carbonates described in the cores are probably a result of increased carbon dioxide production, reflected in the high pore water alkalinities.

Temperature measurements from downhole tools (three APCT tool, one DVTP, and two DVTPP runs) indicate a temperature gradient of 0.057C°/m and predict the base of the GHSZ at 127 mbsf. This is 12 m deeper than indicated by the seismic and LWD data and is consistent with a general pattern of greater mismatch between measured in situ temperature and BSR depth near the summit of Hydrate Ridge, the cause of which has not yet been determined.

Summary

Gas hydrate is present throughout the sediment column from the seafloor to the BSR at Site 1248, as documented by IR imaging, LWD resistivity and gamma density, chloride anomalies in the pore water,

analyses of sedimentary fabric, and direct sampling of gas hydrates. The Pleistocene–Holocene sediments drilled here indicate strong advection of water and/or gas near the summit of southern Hydrate Ridge. There is abundant hydrate in near-surface sediments and no sulfate in the shallowest IW samples collected at Site 1248, clearly indicating active flow of methane-bearing fluids. Authigenic carbonates form close to the seafloor, probably induced by AMO. The presence of authigenic carbonate as well as gas hydrate near the seafloor probably causes the high reflectivity that was mapped during the deep-towed side-scan sonar survey of the seafloor. Lateral advection is also indicated by the shallow presence of thermogenic hydrocarbons mixed with microbial gases. Gases obtained from dissociation of a shallow gas hydrate sample revealed a higher concentration of propane than ethane ($C_3 > C_2$) in addition to methane. Such a gas composition should form Structure II hydrate, although we were not able to confirm this on board. Structure II gas hydrate is well known from petroleum basins like the Gulf of Mexico (Sassen et al., 2001), and this is the first indication of Structure II hydrate along an accretionary margin.

Site 1249

Site 1249 (proposed Site HR4b) was drilled in 778 m of water on the summit of southern Hydrate Ridge (Fig. F1). This area is characterized by massive gas hydrate deposits at the seafloor (Suess et al., 2002). Vigorous streams of bubbles are known to emanate from the seafloor, as documented by submersible observations and high-frequency echo sounding surveys, which have repeatedly imaged bubble plumes in the water column (Heeschen et al., 2003) (Fig. F3). These observations are interpreted to indicate that whereas some of the methane rising through the sediment column is trapped as hydrate near the seafloor, some escapes into the water column (Suess et al., 2001).

The seafloor in this area is anomalously reflective (Johnson et al., in press), and the seafloor reflectivity is spatially correlated with strong subsurface seismic reflectivity that extends to ~30 mbsf (Fig. F7). These geophysical observations have been interpreted to indicate the spatial extent of lenses of massive hydrate intercalated with sediment (Tréhu et al., 2002). Seismic data also indicate that the BSR at this site is at ~115 mbsf. However, coring was only permitted to 90 mbsf because of the possibility of trapped gas beneath the BSR at this structural high.

The objectives at Site 1249 were to (1) determine the distribution and concentration of gas hydrate with depth at the southern summit of Hydrate Ridge, (2) investigate processes that allow methane gas bubbles to coexist with gas hydrate and pore water within the hydrate stability field, and (3) test whether the pattern of chaotic reflectivity accurately predicts the spatial extent of massive hydrate lenses.

Operations

Twelve holes were drilled at Site 1249 (Table T2). LWD measurements were made during drilling in Hole 1249A. Hole 1249B was drilled using the new RAB-8 LWD and coring system, which permits simultaneous acquisition of core and logging data. For this test, we washed down to 30 mbsf before beginning RAB coring operations; eight cores (4.5 m long) were taken with liners followed by 9-m-long cores without liners until we reached the permitted penetration depth of 90 mbsf. Following this test, the 90-m sediment sequence was APC sampled in Holes

1249C through 1249F, with core recoveries of <30% in the uppermost 20 mbsf and increased core recovery (up to 70%) deeper in the holes (Table T3). Six holes (Holes 1249G–1249L) were APC/XCB cored for a special shore-based "geriatrics" study, in which several means of preserving gas hydrates for future study will be compared. During this effort, 244 m of gas hydrate–bearing sediments were cored with 35% core recovery. The samples were either stored in liquid nitrogen or steel pressure vessels, which were repressurized using methane gas and water.

All pressure coring systems available (PCS, HRC, and FPC) were used at Site 1249 (Table T4). The PCS was deployed seven times in Holes 1249C, 1249E, and 1249F. The FPC was used in Holes 1249D, 1249H, and 1249G. The HRC was deployed in Holes 1249F and 1249G. Temperature measurements were made using the DVTP and the APCT tool.

Principal Scientific Results

Based on visual observations, smear slide analyses, physical property measurements, seismic stratigraphy, and logging data, the sediments at Site 1249 were divided into three lithostratigraphic units. Each of the three units correlates well with lithostratigraphy of other sites on the western flank of Hydrate Ridge (Fig. F10). Because of poor core recovery resulting, in part, from the presence of massive hydrate, lithostratigraphic Units I and II at Site 1249 were combined into a single unit referred to as Unit I-II. This unit, of early Pleistocene–Holocene age, is composed of clay and silty clay; the biogenic component changes from nannofossil bearing to diatom bearing and diatom rich. Lithostratographic Unit III, of early Pleistocene age, has similar lithologies to Unit I-II. The boundary between Unit III and Unit I-II is defined by the presence of visible turbidites in the cores, an increase in grain size, a slight increase in calcareous components, and a slight decrease in biogenic opal. This boundary varies in depth among the holes (from 51 to 59 mbsf) and is coincident with seismic Horizon Y (Figs. F5, F7, F10), which is interpreted to be a regional angular unconformity.

During Leg 204, the highest concentration of gas hydrates was encountered at Site 1249, leading to considerable whole-round sampling. Massive gas hydrate pieces were recovered in the uppermost two cores. Layers of apparently pure gas hydrate up to several centimeters thick were interbedded with soft sediment. Temperature anomaly profiles from the IR camera support this generalized model for gas hydrate distribution (Fig. F13). Downhole gas hydrate presence can also be inferred from LWD resistivity data, and Archie's Relation between resistivity and porosity implies gas hydrate saturations in the pore space at Site 1249 that locally range from 10% to 92% of the pore space. However, the application of Archie's Relation in highly heterogeneous media (e.g., sediments containing massive hydrates, free gas, and laterally discontinuous hydrate layers) is likely to result in significant errors.

As a result of dissociation of gas hydrate during core recovery, cores were highly disturbed and most of the original gas hydrate fabric was probably not preserved. Soupy and mousselike textures, probably related to gas hydrate presence, were commonly observed. Soupy textures are thought to result from the dissociation of massive gas hydrate, a process that releases a considerable amount of water. Mousselike textures result from the dissociation of disseminated gas hydrates in fine-grained sediments.

Pore fluids recovered from the upper 20 mbsf show pronounced enrichment in dissolved chloride concentration. The highest chloride

concentration measured was 1368 mM in a sample with a dry-looking coherent fabric specifically selected (after the core was split) to represent the in situ pore fluid with minimal addition of water from hydrate dissociation. The observed enrichment in dissolved chloride is only possible in a system in which the rate of gas hydrate formation exceeds the rate at which excess salts can be removed by diffusion and/or advection. The presence of brines in the upper 20 mbsf is also reflected by the concentration of other dissolved ions such as Na^+, K^+, Ba^{2+}, Sr^{2+}, and Mg^{2+}, which are excluded from the hydrate structure and enriched in the residual pore water. The IW chemistry also reflects the effect of rapid advection of deeply sourced fluids and diagenetic processes occurring in near-surface sediments superimposed on the dissolved ion enrichment resulting from brine formation. Below 20 mbsf, small negative chloride anomalies have been attributed to hydrate dissociation during core recovery.

In comparison to other sites, headspace samples at Site 1249 showed extremely high methane contents consistent with the presence of gas hydrate in the headspace samples. Ethane and propane are also present in high concentrations, indicating migration of thermogenic hydrocarbons. Gases from decomposed hydrate samples show that some of the gas hydrates contain propane and butane, suggesting the presence of Structure II hydrate.

In order to determine in situ methane concentration, PCS cores were successfully obtained at 14, 34, and 72 mbsf (Fig. **F17**). The degassing experiments document methane concentrations that may range from 200 to 6000 mM, which are above saturation at in situ temperature and pressure conditions.

One of the highlights of Site 1249 was the successful recovery of gas hydrate at in situ pressure using the new HYACINTH pressure sampling tools. Two cores, an HRC and an FPC, from above 15 mbsf all contained high concentrations of gas hydrate. Gamma density logs show a spectacular interlayering of sediments and hydrate. Because some layers have densities slightly lower than 1 g/cm^3, we interpret these low-density layers to be relatively pure hydrate layers. In addition, a very low-density spike (0.75 g/cm^3) in a 8-cm-thick gas hydrate layer reveals the presence of free gas within a massive gas hydrate layer. One HRC core was frozen under pressure and transferred to liquid nitrogen; this transfer was accompanied by small explosions that may also indicate free gas within the hydrate structure.

Downhole temperatures derived from the APCT tool define a temperature gradient of 0.047°–0.051°C/m and predict a depth to the base of the GHSZ that is 20 m deeper than the BSR. The data at this site show more scatter than is observed at other sites, where a comparable number of measurements were made. Some possible explanations for this scatter are that dissociation of hydrate resulting from frictional heating when the temperature probe is inserted affects the measurements. Alternatively, thermal conductivities measured on core samples may not be representative of in situ thermal conductivity when large concentrations of hydrate are present. This will be investigated further as part of shore-based recalibration and reanalysis of the downhole temperature data.

Summary

Early Pleistocene–Holocene sediments of lithostratigraphic Units I-II and II at Site 1249 are well correlated with other sites along the western

flank of southern Hydrate Ridge. Site 1249 was cored to a depth of 90 mbsf; thus, this entire sequence lies within the GHSZ, and large quantities of gas hydrates were sampled. Core recovery at this site was limited by the presence of massive gas hydrate close to the seafloor. Rapid formation of massive hydrates in the uppermost 20 mbsf at this site induces brine formation, with pore water chloride values of up to 1368 mM. This is the greatest chloride enrichment as a result of gas hydrate reported to date. Degassing of PCS Core 204-1249F-4P produced 95 L of gas at atmospheric pressure, which is the largest amount of gas ever collected by the PCS. At this site, we obtained the first density measurements from gas hydrates under in situ conditions using the HYACINTH pressure coring and laboratory transfer systems. One HYACINTH core showed direct evidence for free gas within gas hydrate layers at 13 mbsf.

Site 1250

Site 1250 (proposed Site HR4a) was drilled in 792 m of water ~100 m west of the southern summit of Hydrate Ridge and ~100 m east of the Pinnacle (Fig. F1). On southern Hydrate Ridge, the Pinnacle is the only carbonate mound, whereas at northern Hydrate Ridge several major chemoherms are known. The Pinnacle has near-vertical flanks rising ~40 m above the seafloor and a diameter of ~50 m. The carbon source for the Pinnacle is oxidized biogenic methane based on very low $\delta^{13}C$ values of samples recovered by the *Alvin* or ROV (Teichert et al., in press). $^{230}Th/^{234}U$ data indicate that the Pinnacle probably formed during the last 12 k.y. (Teichert et al., in press). It is located in the middle of a high-reflectivity patch (Fig. F7) (Johnson et al., in press), which might be created by scattered carbonates close to the seafloor and/or the presence of shallow gas hydrates. Site 1250 lies close to the eastern rim of the high-reflectivity patch (Fig. F7). The precruise 3-D seismic reflection survey data show that seismic Horizon A (~150 mbsf at Site 1250) meets the BSR (~114 mbsf at Site 1250) just below the Pinnacle (Fig. F7).

The primary objective at Site 1250 was to sample the sediments, fluids, gases, and gas hydrates under the high-backscatter seafloor flanking the Pinnacle. The sediments at Site 1250 were expected to be strongly affected by the upward fluid migration that has resulted in the formation of the Pinnacle chemoherm. In this context, understanding the role of Horizon A as a conduit for fluid flow and its interaction with the BSR was of special interest.

Operations

Five holes were drilled at Site 1250 (Table T2). Recording of the LWD RAB tool failed during the first run in Hole 1250A because of depleted batteries; therefore, the LWD operation was repeated in Hole 1250B, which was drilled to 180 mbsf. Holes 1250C and 1250D were APC/XCB cored down to 145 mbsf (Table T3). In Holes 1250C and 1250D, 19 cores were recovered, with average recovery of 82% of the total penetration. Two cores were recovered in Hole 1250E, which was dedicated to biogeochemical sampling, with 92% core recovery. Because of relatively high levels of higher-order hydrocarbons encountered near Horizon A at Site 1248, we decided not to penetrate Horizon A until a better understanding of possible hazards associated with this horizon had been obtained from drilling through it further downdip. After coring through Horizon A at Sites 1245 and 1247, we returned to Site 1250 to APC/XCB core Hole 1250F from 100 to 180 mbsf.

The PCS was deployed twice in Hole 1250C, three times in Hole 1250D, and three times in Hole 1250F (Table T4). HYACINTH autoclave pressure coring tools were deployed in Holes 1250C and 1250D. Special tools were used for temperature measurements in Hole 1250C, including five APCT tool runs and two DVTP runs. Temperature measurements in Hole 1250D included four APCT tool runs and two DVTP runs. Wireline logging was performed in Hole 1250F using separate runs of the triple combo and FMS-sonic tool strings down to 180 mbsf. Vertical and offset VSPs were acquired with the *JOIDES Resolution* and the *Ewing* (located at an offset of ~700 m) alternating shots. This was followed by walkaway VSPs shot by the *Ewing* to downhole seismometers clamped at 91, 138, and 172 mbsf.

Principal Scientific Results

On the basis of visual sediment descriptions, physical property measurements, LWD data, and seismic correlation, the sedimentary sequence at Site 1250 was divided into three lithostratigraphic units. Lithostratigraphic Unit I, late Pleistocene–Holocene in age, extends from the seafloor to 9.5 mbsf and is mainly composed of dark greenish gray clay or silty clay, which is generally diatom bearing or diatom rich. Lithostratigraphic Unit II (9.5–14 mbsf), of late Pleistocene age, is principally composed of lithologies similar to those in Unit I. However, lithostratigraphic Unit II also contains graded silt and sand layers, interpreted as turbidites, which are not present in lithostratigraphic Unit I. Lithostratigraphic Unit III (14–181 mbsf) consists of silty clay that is nannofossil rich or diatom rich, with an age range of early–late Pleistocene.

The boundary between lithostratigraphic Units II and III is correlated with Horizon Y (Fig. F10), a seismic reflector that corresponds to a regional stratigraphic unconformity (Figs. F5, F7). This boundary is well defined by a 6-m-thick sequence of coarse-grained high-frequency thin turbidite layers, which includes individual sand layers up to 20 cm thick. LWD recorded a high-density peak around seismic Horizon Y, which was confirmed by shipboard physical property measurements of core samples. In addition, shipboard multisensor track (MST) data reveal a large positive excursion of MS caused by a higher content of magnetic minerals within the sand layers at the boundary between lithostratigraphic Units II and III.

Lithostratigraphic Unit III at Site 1250 is divided in two subunits. Subunit IIIA includes several mass-wasting deposits, of which a debris flow layer between 86.5 and 100 mbsf is the most pronounced example. This deposit is characterized by the presence of mud clasts up to 5 cm in diameter, similar to those observed at other sites (Fig. F9) and several soft sediment deformation features. Subunit IIIB has a distinctly higher abundance of calcareous nannofossils and foraminifers than Subunit IIIA. The boundary between the stratigraphic Subunits IIIA and IIIB is marked by several light-colored ash-rich layers that are composed of volcanic glass–rich silt to silty volcanic ash, typically a few centimeters thick. This ash-rich interval is well defined in the LWD data by a low density anomaly and corresponds to the regional seismic reflector known as Horizon A. Physical property measurements on discrete samples at Site 1250 revealed low grain densities in this depth interval, which are partly explained by the low grain density of the amorphous silicate components of the ash. Free gas in this interval may also con-

tribute to the low densities and high resistivities recorded in the LWD data and to the low seismic velocities recorded by the sonic logs and VSPs.

IR imaging of the cores on the catwalk using a handheld camera enabled us to identify 20 whole-round samples likely to contain gas hydrates. The hydrate samples show a wide range of morphologies, ranging from massive to nodular, and are often embedded in soupy sediments, which are interpreted to result from decomposition of disseminated hydrate and fluidization of the sediment by hydrate water.

In addition, IR imaging with the track-mounted camera revealed 40 temperature anomalies between 14 and 109 mbsf in Hole 1250C and 57 anomalies between 6 and 113 mbsf in Hole 1250D. The depth range of the low-temperature anomalies correlates well with the depth distribution of moussey and soupy textures observed by the sedimentologists during core description. The lowermost gas hydrate piece was sampled in Hole 1250F at 100.23 mbsf, which is slightly above the base of the GHSZ at 114 mbsf as defined in the *P*-wave sonic log.

Chloride concentrations in the pore water at Site 1250 document the different geochemical processes linked to the presence of gas hydrates. As observed at Site 1249, an enrichment in dissolved chloride in the upper 20–30 mbsf at Site 1250 shows the effect of rapid and recent gas hydrate formation. Below 20–30 mbsf, the chloride shows a gently sloping baseline toward fresher chloride values. Using this curve as the baseline, the negative chloride anomalies were used to calculate the amount of gas hydrate responsible for the dilution of each sample. Average hydrate concentrations were calculated to be 0%–6% of pore space, with a maximum concentration of 15%

IW chemistry documents upward fluid advection and near-surface diagenetic processes. Sulfate is depleted even in the shallowest sample because of the upward methane flux and methane oxidation. Alkalinity is anomalously high in the upper tens of meters, reflecting fluid advection. Authigenic carbonate formation is documented by very low Ca concentration in the pore fluids and discrete carbonate samples close to the seafloor. The IW chemistry also reflects migration of fluids from a deep source. A downhole linear increase in lithium concentration with depth is believed to reflect the diagenetic remobilization of lithium at depth in the accretionary wedge, where the temperature exceeds 80°C. Superimposed on this downhole lithium increase is a peak in the pore fluid concentration around seismic Horizon A, indicating focused fluid transport along this high-permeability pathway.

Gas samples from Site 1250 show high methane content throughout the sediment sequence, and there is no decrease in the shallow samples. This is in agreement with the lack of sulfate in the pore water and the inferred high advection rates. Void gas samples show that the ethane content is relatively high. The observed enrichment of higher hydrocarbons (C_3–C_5) close to the seafloor indicates lateral migration of wet gas hydrocarbons that must have originally been derived from a deep source. A distinct increase in ethane observed near the BSR could be a result of ethane release from decomposed gas hydrate. An increase in propane and *n*-butane probably reflects migration of hydrocarbons from deeper depths.

In order to obtain in situ gas concentrations, the PCS was deployed successfully five times. Three PCS deployments above the BSR show concentrations clearly above methane saturation (Fig. **F17**), which predict gas hydrate concentrations of 0.6%–2.2% within the pore volume of the cores. One PCS sample (Core 204-1250F-4P), recovered ~5 m be-

low the BSR, also contains methane concentration above saturation. Another sample (Core 204-1250D-18P) collected ~24 m below the BSR, indicates a gas concentration below saturation at in situ conditions.

Nine APC temperature measurements were made at this site, and they yielded a thermal gradient of 0.049°C/m, which is lower than expected and predicts the base of the GHSZ at 130 mbsf. This is 18 m deeper than the level of the GHSZ indicated by the seismic and LWD data and is consistent with a general pattern of greater mismatch between measured in situ temperature and BSR depth near the summit of Hydrate Ridge. The cause of this discrepancy is yet not known.

Summary

At Site 1250, hemipelagic fine-grained sediments interbedded with turbidites are Quaternary in age (younger than 1.6 Ma) and contain gas hydrate in varying amounts. Positive chloride anomalies in the pore water in the upper 20–30 mbsf reveal rapid and active formation of gas hydrate during recent times, consistent with LWD resistivity data and direct sampling. High methane concentration, no sulfate, high alkalinity, and carbonate diagenesis in the uppermost sediments document high advection rates of water and/or gas, similar to what was observed at the other seep-related sites (Sites 1248 and 1249). Below 30 mbsf, chloride anomalies in IW samples and direct measurement of in situ gas concentrations using the PCS indicates that gas hydrates occupy <1% to a few percent of the pore space. The presence of free gas just below the BSR is documented by the concentrations of methane well above in situ solubility found in a PCS core from below the BSR and from *P*-wave data obtained by sonic logs and VSPs.

Site 1251

Site 1251 (proposed Site HR2alt) was drilled at a water depth of ~1210 m ~5.5 km east of the southern summit of Hydrate Ridge (Fig. F1). The site is located in a slope basin where well-stratified sediments were apparently deposited at a rapid rate. Seismic data record a history of deposition, tilting, folding, and depositional hiatuses in the basin that is probably related to the evolution of Hydrate Ridge. A strong BSR suggests that the base of the GHSZ is at ~200 mbsf at this site.

The principal objectives at Site 1251 were to (1) determine the source of water and gases forming gas hydrates in a setting that is characterized by rapid deposition of hemipelagic sediments and mass-wasting deposits, in contrast to the uplifted sediments of the accretionary complex; (2) determine the distribution of gas hydrates in relation to the typical lithologic parameters for the basin; (3) test general models for hydrate formation in regions of rapid sediment accumulation that were developed in the Blake Ridge area from results of ODP Leg 164; and (4) provide age constraints on the geological history recorded by seismic stratigraphy.

Operations

Eight holes were drilled at Site 1251 (Table T2). In Hole 1251A, LWD measurements were made using a variable, but generally low, rate of penetration (ROP) in the upper 30 mbsf followed by an increased ROP of ~50 m/hr from 30 mbsf to the bottom of the hole (at 380 mbsf). Hole 1251B was APC cored (including PCS deployments at 105 and 154 mbsf

and an FPC deployment at 172 mbsf), with an average core recovery of 80.6% down to 194.6 mbsf, where more lithified sediments significantly reduced the penetration of the bit (Table T3). Coring continued using the XCB down to 445.1 mbsf with an average recovery of 85.5%. In addition to the XCB coring, the three pressure coring tools (PCS, FPC, and HRC) were used at 291, 330, and 397 mbsf, respectively. Special tools in Hole 1251B included four APCT tool and two DVTPP runs (Table T4). Hole 1251C was terminated after two cores. In Hole 1251D, 3 XCB cores were drilled to 26.9 mbsf followed by 15 APC cores to 173.4 mbsf and 6 XCB cores to 226.5 mbsf. Special tools in Hole 1251D included one APCT tool, two DVTPP, four PCS, one FPC, and one HRC runs. Holes 1251E and 1251F were each cored with the APC to 9.5 mbsf for high-density coupled geochemical and microbiological sampling. Hole 1251G was washed to 2.5 mbsf before one APC core was taken for special sampling of turbidite layers. The hole was then washed down to 20 mbsf before an additional PCS (at 21 mbsf) was deployed.

Principal Scientific Results

Based on the major and minor lithologies and additional criteria like sediment fabric, physical properties, microscopic, chemical, and X-ray diffraction (XRD) analysis, the hemipelagic strata and turbidite sequences recovered at Site 1251 were divided in three lithostratigraphic units (Fig. F10). Lithostratigraphic Unit I, subdivided into three subunits, extends from the seafloor to 130 mbsf and is characterized dominantly by dark greenish gray clay to silty clay ranging from Pleistocene to Holocene age (0–~0.3 Ma). The sediments of Subunit IA (0–23 mbsf) are characterized by clay and silty clay, some of which is diatom bearing, interlayered with several coarse-grained turbidites. Subunit IB (23–34 mbsf) is characterized by unsorted pebble-sized mudclasts in a clay matrix and a series of soft sediment deformation fabrics representing a debris flow unit. This unit can be traced regionally based on its chaotic character in seismic reflection records (Fig. F8) and reaches a maximum thickness of ~70 m in the center of the slope basin. Stratified diatom-bearing silty clays comprise Subunit IC (34–130 mbsf), which shows clear seismic stratification. The base of Subunit IC is defined to correspond to a prominent angular unconformity imaged in the seismic data, although there is no apparent lithologic discontinuity at that boundary.

Hemipelagic clays of middle Pleistocene age, partly enriched in siliceous and calcareous biogenic components, form lithostratigraphic Unit II (130–300 mbsf). Unit III (300–443 mbsf) consists of partly lithified clays that show a downcore transition to claystones. A distinct enrichment of green glauconite grains in a 120-cm-thick interval on top of lithostratigraphic Unit III is probably associated with a major unconformity or period of very low sedimentation rate that lasted from 1.6 to 1.0 Ma, as defined by biostratigraphic data. Between 320 and 370 mbsf, the sediments contain a higher amount of biogenic opal, which is well documented by smear slide estimates and XRD analyses. Authigenic carbonates of various morphologies and mineralogical compositions as well as glauconite grains are scattered throughout this unit. Biostratigraphic investigations using diatoms and calcareous nannofossils indicate an early Pleistocene and late Pliocene age for these sediments. The Pleistocene/Pliocene boundary is at ~375 mbsf.

Major downcore changes in sedimentary physical properties are generally in agreement with seismic stratigraphy and lithostratigraphic

boundaries. The uppermost sediments of lithostratigraphic Units I and II are characterized by increasing bulk density values that follow a standard compaction curve. A generally increasing trend in bulk densities measured with the MST and in density measurements on discrete samples (MAD) is interrupted by a 50-m-thick sediment sequence between 320 and 370 mbsf in which the bulk densities drop significantly and porosity values increase. This change in physical properties is caused by higher amounts of biogenic opal-A, an amorphous silica phase having low grain density and high skeleton porosity. MS values at Site 1251 are characterized by generally uniformly low values. Various high-amplitude MS peaks are correlated with either turbidites, enrichments of magnetic minerals resulting from low sedimentation rates, or diagenetic iron sulfide minerals.

Thermal imaging of cores using the IR cameras was used to detect intervals of disseminated gas hydrate between 40 and 200 mbsf. Discrete samples of hydrate were not seen in Hole 1251B, although several cold anomalies were observed. The sediments hosting the BSR were not sampled in Hole 1251B because of low recovery in this interval. The IR temperature anomalies observed in Hole 1251B were relatively small (ΔT = ~1°–1.5°C) compared to an IR temperature anomaly (ΔT = ~6°C) encountered in Hole 1251D between 190 and 197 mbsf (Fig. **F20**), which corresponds to the interval just above the BSR.

IW geochemistry at Site 1251 focused on hydrate-related changes in chloride concentration pattern, changes in fluid composition in relation to dewatering of the sediments, and biogeochemical processes within the sediments. As observed at Sites 1244 and 1252 as well as in other accretionary wedges, the profile of dissolved chloride at Site 1251 decreases downcore from present seawater values close to the seafloor. At Site 1251, the chloride decrease in the IWs corresponds to an increase in dissolved lithium, revealing a fluid source from deeper sediments of the accretionary complex. The dissolved chloride distribution at Site 1251 shows only one distinct negative anomaly, seen in several samples taken just above the BSR from ~190 to 200 mbsf (Fig. **F20**). This is consistent with the IR temperature and visual observations, which indicate the presence of disseminated hydrate just above the BSR. Based on the lowest chloride value measured relative to an estimated background concentration, gas hydrate occupies up to 20% of the pore space in this zone. This finding is in contrast to other sites drilled during the leg, where repeated excursions to low chloride concentration values record the presence of gas hydrate over much larger depth intervals above the BSR. We note that this low chloride anomaly was missed completely in Hole 1215B because of poor recovery of this interval. Special care was taken to sample this interval in Hole 1251C.

As at other sites on Hydrate Ridge, a number of processes control whether methane reaches levels above saturation within the GHSZ. An important process controlling the methane distribution in the sediments at Site 1251 is methane consumption by AMO using sulfate as an oxidant. Methane flux at the SMI can be estimated from the sulfate and methane concentration gradients. At Site 1251, over half the sulfate being reduced is a result of AMO. Sulfate depletion at the SMI at 4.5 mbsf (Fig. **F19**) also leads to high dissolved barium concentrations below the SMI.

Methane concentrations obtained from headspace analyses increased rapidly below the level of sulfate depletion. Eight PCS deployments revealed methane concentrations from 46.4 to 158.4 mM at depths ranging from 20 to 290 mbsf (Fig. **F17**). The methane concentration at 20

F20. IR thermal anomalies and comparison between chloride anomalies, p. 70.

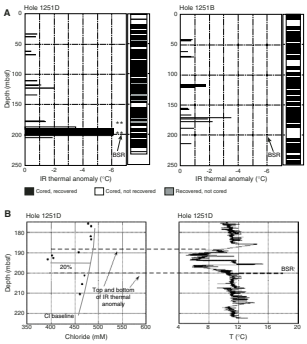

mbsf is compatible with the shallower headspace methane estimates and provides the gradient from which the methane flux is calculated. Based on measured methane concentrations slightly above solubility, two PCS deployments within the GHSZ (at 45 and 104 mbsf) show methane concentrations with values above saturation, implying the presence of methane hydrate. Observations below the BSR are ambiguous. A PCS sample from 32 m below the BSR did not show methane concentration above solubility, whereas one from 100 m below the BSR did.

In addition to methane (C_1), traces of higher molecular weight hydrocarbons such as ethane (C_2), ethylene ($C_{2=}$), and propane (C_3) were also detected throughout the sequence cored at Site 1251. As at Sites 1244 and 1246, the composition of gas samples recovered from both expansion voids in the core liner and headspace measurements show a systematic in decrease in C_1/C_2 ratios below the BSR (Fig. **F16**). This order of magnitude decrease in the C_1/C_2 ratio is caused by an abrupt increase of ethane rather than by a change in methane concentration. Two possible mechanisms have been considered to explain this observation. In the first mechanism, ethane is preferentially stored in hydrates and then released when the ethane-enriched gas hydrates at the base of the GHSZ dissociate in response to subsidence of the slope basin and the resulting upward migration of the GHSZ through the sediment column. In the second mechanism, the GHSZ is a barrier to C_2 migration. Additional analysis of the gas composition in hydrate samples from Leg 204 should permit us to distinguish between these two mechanisms.

Temperature measurements obtained with five APCT tool and three DVTPP deployments were used to calculate a linear temperature gradient of 0.0575°C/m at Site 1251, which is very similar to temperature profiles from other sites on Hydrate Ridge. Extrapolating laboratory measurements of gas hydrate stability for pure methane in water of 3.5% salinity, this temperature gradient predicts the base of the GHSZ to be at ~196 mbsf, which is in excellent agreement with the BSR depth determined from 3-D seismic reflection data and from other data acquired during Leg 204.

LWD data in the basin sediments in Hole 1251A are of high quality even though data were collected at a faster ROP than at other sites. There is minimal loss of vertical resolution. Resistivity and density log variations indicate thin-bedded changes in lithologies throughout the hole below 130 mbsf, which most likely reflect the downhole presence of interbedded turbidites that were observed during core description. There is little direct evidence for the presence of gas hydrate in the LWD data, except for the depth interval from 90 to 110 mbsf and again immediately above the BSR. Archie's Relation for estimating water saturation from the resistivity log data (Collett and Ladd, 2000) implies as much as 18% gas hydrate saturation in the sediments just above the BSR, in excellent agreement with the estimate based on the maximum chloride anomaly. The resistivity data also indicate the presence of free gas extending for ~100 m below the BSR. Borehole breakouts are well developed below 300 mbsf and indicate a north-south axis of least compressive stress.

Summary

Drilling at Site 1251 recovered a sequence of well-stratified hemipelagic sediments in the slope basin adjacent to Hydrate Ridge.

Major lithostratigraphic units were characterized and are, in most cases, separated by clearly defined unconformities in the seismic record. Thermal, sedimentological, geophysical, and geochemical proxies for the presence of hydrate, as well as direct sampling, were used to document the presence of gas hydrates in host sediments younger than 500,000 yr old. At this site, significant hydrate accumulations seem to be limited to two intervals, 90–110 mbsf and just above the BSR at 190–200 mbsf. This is in sharp contrast to the hydrate distribution at the other sites cored during Leg 204, where hydrate is found throughout most of the hydrate stability zone.

Site 1252

Site 1252 (proposed Site HR5a) was drilled in 1039 m of water ~4.5 km northeast of the southern summit of Hydrate Ridge. The site is located on the western flank of a secondary anticline east of the crest of Hydrate Ridge. The sediments in the core of the anticline appear to be continuous with the accretionary complex sediments sampled near the base of Site 1244 (~1.5 km to the west). Although there is an anomalously bright BSR at a depth of ~170 mbsf within the core of the anticline, the BSR disappears abruptly at an apparent stratigraphic boundary within the accretionary complex sequence and does not extend beneath Site 1252 (Fig. F8). Sediments onlapping the anticline from the west can be correlated with sediments sampled at Site 1251.

The principal objectives at Site 1252 were to (1) sample the sediments in the core of the anticline to determine whether they are compositionally and biostratigraphically similar to those at the base of Site 1244, (2) determine the structure of these sediments in order to constrain the mode of growth of the anticline/diapir, (3) determine whether hydrates are present at a site near a very strong BSR but where no BSR is present, and (4) provide age constraints on the geological history recorded by seismic stratigraphy.

Operations

One hole was drilled at Site 1252, comprising 28 cores (14 APC and 14 XCB) and sampling sediments to a depth of 260 mbsf (Tables T2, T3). The APCT tool, which was deployed six times to measure in situ temperature, was the only special downhole tool used at this site (Table T4). This is the only site where we did not acquire LWD data. Wireline logging data were acquired, including one run with the triple combo tool string and one run with the FMS-sonic tool string. This was an alternate site and was the last site drilled during Leg 204.

Principal Scientific Results

Drilling at Site 1252 showed evidence for only very limited presence of gas hydrate. Nonetheless, it is a very interesting site in that it showed clear correlations between lithostratigraphic observations, physical property measurements, and wireline logging results throughout the entire cored sequence. It is the only site to show significant authigenic carbonate formation beneath the upper tens of meters.

Based on the major and minor lithologies and additional criteria like fabric, physical properties, and microscopic analysis, the sediments recovered at Site 1252 were divided in three lithostratigraphic units (Fig. F10). Lithostratigraphic Unit I, subdivided into four subunits, extends

from the seafloor to 96.5 mbsf and is dominated by dark greenish gray clay to silty clay ranging in age from 0 to ~0.3 Ma. Subunit IA is characterized by a strong negative density gradient in the MST data, which probably results from the onset of gas exsolution at ~7 mbsf. The lower boundary of Unit I is defined by the same unconformity that was sampled at a depth of 130 mbsf at Site 1251. At both sites, this unconformity is clearly seen in seismic data ("U") (Fig. F8) and is compatible with biostratigraphic data but does not have a striking lithologic signature. At Site 1252, the U unconformity is overlain by an apparent debris flow called Subunit ID, the top of which corresponds to a strong anomaly in MS. Subunit ID (Fig. F10) pinches out just west of Site 1251 and was not sampled there. In contrast, the debris flow that comprises Subunit IB at Site 1251 is not present at Site 1252 (Fig. F8). Subunit IC at both sites is strikingly similar in its lithologic description and its seismic reflection character.

Unit II at Site 1252 is a dark green foraminifer-rich silty clay that is intercalated with lighter-colored fine sand and coarse silt turbidite layers. These thin turbidites result in a nearly continuous zone of high MS. In contrast to Site 1251, where Unit II is ~180 m thick, Unit II at Site 1252 is only ~20 m thick. This is primarily due to the location of this site, where Unit II laps onto the west flank of uplifted accretionary complex sediments. Subunits IB and IC through Unit II are characterized by a normal increase in density and decrease in porosity with depth that is probably caused by sediment compaction.

The boundary between Unit II and Unit III is marked by a 5-m-thick series of glauconite-rich sands, including a 2-cm-thick layer of almost pure glauconite. This is underlain by a layer of authigenic carbonate that required a transition from APC to XCB coring at 125 mbsf. Wireline density, resistivity, and chemical (uranium and potassium) logs all show very high values in a 6-m-thick interval at this depth, consistent with extensive carbonate precipitation forming concretions and cement. The top of Unit III corresponds closely with the top of the uplifted accretionary complex sediments in the core of the anticline/diapir and is referred to as Subunit IIIA (131–210 mbsf). It is underlain by Subunit IIIB (210–260 mbsf), which is distinguished from Subunit IIIA by an increase in biogenic opal and a decrease in silt. The biostratigraphic age of Unit III is 1.6 to >2 Ma.

The density profile of Unit III is unusual. Physical property measurements (MST gamma ray attenuation [GRA] logs and MAD bulk density) indicate that the density decreases by 0.2 g/cm^3 (from 1.8 to 1.6 g/cm^3) over a distance of ~25 m below the carbonate-rich zone and is then variable, with an average value of ~1.7 g/cm^3. No systematic increase in density is observed until the base of the hole at 260 mbsf. The wireline density logs show similar behavior, with a local increase to nearly 2.0 g/cm^3 in the carbonate layers underlain by a nearly constant density of 1.7 g/cm^3 with occasional thin (~2 m thick) low-density (~1.5 g/cm^3) excursions. This anomalous density profile, similar to but better defined than what was observed in the lower part of the section at Sites 1244 and 1251, suggests that density-driven diapirism may be a mechanism contributing to the tectonic evolution of the accretionary prism.

Thermal imaging of cores using the IR cameras indicated only very limited hydrate presence at Site 1252. Two possible hydrate samples were preserved from depths of 83 mbsf (in Subunit ID) and 99 mbsf (in Unit II). The chloride concentration in the pore water and the C_1/C_2 ratios in void-space gas samples did not show anomalies indicative of

dissociated hydrate, unlike what was observed at other sites (see, for example, discussion of Site 1247). In contrast, Subunit IIIA showed several examples of classic moussey and soupy texture in cores recovered from above the base of the GHSZ. A sample of the soupy sediment was taken for postcruise chloride analysis.

The chloride profile shows a general decrease with depth similar to those observed at Sites 1244 and 1251 (Fig. F15). This decrease has been attributed to diffusion or slow advection of low chloride concentration pore waters generated by dewatering of aluminosilicates deeper in the accretionary complex. A closer look at the chloride profile suggests breaks in slope that can be roughly correlated with lithologic boundaries, suggesting lithologic control on permeability.

The thermal gradient of 0.063°C/m measured at Site 1252 is relatively high. This is the only site at which the BSR depth predicted based on the measured thermal gradient is shallower than the seismic BSR, although interpretation of the significance of this observation requires more detailed analysis of measurement uncertainty.

Summary

Site 1252 provided the best sampling of the older (>1.65 Ma) sediments that comprise the uppermost part of the seismically incoherent facies referred to as the accretionary complex. This zone is characterized by a density inversion relative to the base of the overlying slope basin sediments and an anomalous density vs. depth profile. This observation suggests that gravitational instability should be considered as a possible driving force contributing to the evolution of forearc structure here. The data from this site also reinforce previous observations that the accretionary complex is characterized by low chloride concentration IWs and is relatively permeable. Although this site yielded little direct evidence of gas hydrate, sediment textures and limited IR thermal anomalies indicate that some hydrate was present even though no BSR is observed at this site.

CONCLUSIONS

In this section, we summarize some of the general conclusions that emerge from the above discussions of the preliminary results at each site. We also point out additional questions that are the focus of ongoing postcruise data integration and modeling efforts.

Multiple proxies for hydrate presence and concentration are consistent and complementary. They indicate that gas hydrate is present and concentrated in relatively coarse-grained layers over a broad depth range between the seafloor and the BSR. One of the main conclusions to emerge from the shipboard analysis of the data collected during Leg 204 is that gas hydrates are distributed through a broad depth range within the GHSZ. Electrical resistivity anomalies measured downhole with LWD and wireline logging, low-temperature anomalies measured with IR camera scans immediately after cores came on deck, low chloride concentration measured in IWs, anomalously low C_1/C_2 ratios measured in vacutainer samples, and gas volumes measured from pressure core samples are all proxies for the presence of gas hydrate in the subsurface. All are consistently observed to start at a similar depth at a given site (~30–50 mbsf at sites away from the summit and at the seafloor at sites near the

summit) and lead to consistent conclusions about the distribution and concentration of gas hydrate beneath Hydrate Ridge.

The various proxies for the presence of gas hydrate measure different length scales and have different sensitivity to hydrate concentration. Downhole electrical resistivity, seismic velocity and attenuation, and temperature anomalies in recovered cores can be continuously measured at high resolution and indicate that hydrate concentration probably varies considerably on scales of millimeters to tens of centimeters. These data provide continuous profiles of relative hydrate concentration and indicate that hydrate is distributed over a broad depth range. Exceptions are Site 1251 in the eastern slope basin, where hydrate is concentrated in a 12-m-thick zone just above the BSR, and sites near the summit, where it is concentrated near the seafloor. These geophysical parameters, however, do not give a direct measurement of concentration, although concentration can be estimated through physical models (e.g., through Archie's Relation in the case of resistivity) (see Collett and Ladd, 2001).

The PCS data give a direct measurement of gas concentration in situ. The concentration of gas hydrate or free gas may be estimated by comparing the in situ gas concentration to the predicted in situ solubility. These measurements, however, are restricted to only a handful at each site because of logistical constraints. The ODP PCS provides measurements of concentration averaged >1 m, whereas the newer HYACE tools demonstrated the potential to provide additional information about centimeter-scale hydrate distribution and the presence of free gas in sediments.

Chloride concentration measurements provide robust estimates of hydrate concentration if the background chloride concentration profile can be constrained. However, they are spatially aliased because it is not practical to routinely obtain measurements less than several meters apart. Leg 204 has demonstrated that background chloride concentration can be well defined, except near the summit where the background chloride concentration cannot be determined because of very rapid hydrate formation (see **"Site 1249,"** p. 30). The Leg 204 chloride data also demonstrate that it is essential to extend chloride measurements well below the base of the GHSZ. In the Hydrate Ridge chloride data, there is a clear freshening of the IWs as a result of diffusion from a low chloride concentration source at depth (probably water derived from dehydration of subducted minerals). Estimates that do not take this into account will incorrectly estimate the in situ hydrate concentration.

C_1/C_2 ratios have the potential to become a new proxy for hydrate concentration. Leg 204 data suggest preferential incorporation of ethane into hydrate. Decomposition of hydrate then results in a signal that can be detected in routine headspace and vacutainer measurements.

Additional analysis of the data from Leg 204 is under way to better calibrate quasicontinuous geophysical data using robust geochemical estimates of in situ hydrate concentration. This will result in greatly improved estimates of the total amount of methane and other hydrocarbon gases sequestered in the gas hydrate system on the Oregon continental margin. The calibrated downhole geophysical results will, in turn, be used to calibrate surface and seafloor seismic reflection and refraction data, which will then have the potential to robustly estimate hydrate distribution and concentration over large areas of the seafloor.

Horizon A is an ash-rich layer that serves as a fluid pathway transporting methane and other hydrocarbons from the accretionary complex to the sum-

mit of Hydrate Ridge. Determining the origin and significance of a strong seismic reflection (Horizon A), which underlies the BSR and shallows toward the southern summit of Hydrate Ridge, was an important objective of Leg 204. This reflection was crossed at Sites 1245, 1247, 1248, and 1250. In the LWD data, it is characterized by a strong 2- to 4-m-wide double-peaked low density and low-resistivity anomaly.

Cores at Sites 1245, 1248, and 1250 reveal several coarse-grained layers at this depth. Microscopic analysis of these sediments reveals that the sediment is composed primarily of relatively fresh glass shards indicating volcanic ash. The number and thickness of the ash layers could not be determined precisely because of core disruption during recovery, which was probably due to high fluid content and possible overpressure. Grain density is low, possibly because of vesicles within the glass shards. The age and provenance of the ash will be determined postcruise.

Although the physical properties of Horizon A are remarkably similar from site to site, interpretation of hydraulic properties from chemical analysis of gases and IWs is more complicated. Increased lithium concentrations are clearly associated with this horizon, supporting the interpretation that it is a conduit for fluids coming from greater depth. However, no thermal anomaly is detected, placing an upper limit on flow rate. Relatively high levels of heavier hydrocarbons are observed in a 30- to 50-m-thick zone below the BSR at all sites, but the maximum level of heavier hydrocarbons does not generally coincide with Horizon A (Fig. **F16**). A qualitative explanation for these observations is that diffusion away from Horizon A is superimposed on accumulation of C_{2+} gases beneath the BSR. Postcruise modeling is needed to quantitatively test this hypothesis.

Massive hydrate lenses extend to a depth of ~30 mbsf near the summit of southern Hydrate Ridge, and hydrate formation here is very rapid. Prior to Leg 204, it was known that methane bubbles were venting from the southern summit of Hydrate Ridge and that massive hydrate was present at the seafloor; however, the rate of hydrate formation and the depth to which massive hydrate is present were unknown. Seismic reflection data suggested that this zone extends to ~30 mbsf (Tréhu et al., 2002) (Fig. **F7**). Electrical resistivity anomalies recorded in LWD data indicate extremely high resistivities (approximately two orders of magnitude greater than observed at other sites) from 0 to 40 mbsf. The resistivity is higher than at other sites logged during Leg 204 to a depth of ~70 mbsf.

In the upper 10–20 mbsf near the summit at Sites 1249 and 1250, interstitial fluids are high in chloride, cores contain pervasive gas hydrate veins and nodules, and pressure core samples indicate the presence of massive hydrate. Moreover, core recovery from this interval was poor, probably because of the presence of massive hydrate. Below 15–30 mbsf, high-chloride brines give way to the low-chloride anomalies characteristic of dissociation of hydrate relative to background IWs. The background pore fluids in this zone do not retain the signature of hydrate-driven brine, presumably because of much slower rates of hydrate formation. At these depths, core recovery improved significantly. Both of these observations indicate a change from a shallow zone in which methane is provided through vigorous advection of water or gas and hydrate forms rapidly to a zone in which methane flux and hydrate formation rate are slower. Below ~20–30 mbsf, lenses of massive hydrate containing significant pockets of free gas are not likely to form, although gas hydrate and free gas in disseminated form may be present

in relatively large concentrations. The cause of the very high resistivity from 30 to 70 mbsf remains poorly understood and is a focus of post-cruise research as is estimation of hydrate formation rate from the positive chloride concentration measurements.

Free gas is trapped in gas hydrates tens of meters beneath the seafloor at the southern summit of Hydrate Ridge. Gamma density logging of a HYACE FPC core from 14 mbsf at Site 1249 indicated the presence of several layers of massive hydrate, one of which contained material with very low density, indicating the presence of free gas. This is the first direct evidence for free gas in the GHSZ, although the presence of free gas had previously been hypothesized based on observations of gas bubbles emanating from the seafloor (Suess et al., 2001; Torres et al., 2002; Tréhu and Bangs, 2001; Heeschen et al., 2003). However, it is not clear from the available data if free gas is present inside gas hydrate specimens or within sediments. Modeling of elastic wave velocities and attenuation should further constrain the presence and distribution of free gas within the GHSZ.

Lithology can be a major factor influencing hydrate concentration. Integrated analysis of Horizon B provides an excellent example of the potential impact of lithology on hydrate distribution (see discussions in **"Site 1244,"** p. 14, and **"Site 1246,"** p. 21). Detailed analysis of physical properties and IR thermal anomalies combined with lithologic description demonstrates that gas hydrates are concentrated in the coarse-grained layers in this ash-rich turbidite section.

Ethane is enriched beneath the BSR. All sites show an abrupt decrease in C_1/C_2 at the BSR except for Site 1252 (where there is no BSR). This effect results from an increase in ethane rather than a decrease in methane. It is most evident at Sites 1244 and 1251, where this signal is not obscured by additional effects of Horizon A. There are at least two possible mechanisms to explain this observation. In one model, the BSR serves as a barrier to upward flow of ethane. In the other model, ethane is preferentially incorporated into hydrate; dissociation of the hydrate at a later time in response to tectonic uplift recycles ethane into the free gas zone beneath the hydrate. Relative enrichment of ethane observed in gases from several dissociated hydrate samples support the second mechanism. Discontinuities at the BSR in several other chemical species support the first mechanism. It is possible that both mechanisms operate simultaneously.

There is less free gas beneath the BSR at southern Hydrate Ridge than beneath northern Hydrate Ridge and the Blake Ridge. One of the more surprising results of Leg 146 on north Hydrate Ridge and Leg 164 on the Blake Ridge was the depth to which free gas is present beneath the BSR. Seismic experiments at both of these sites indicated that free gas is present in the sediments for several hundred meters below the BSR (MacKay et al., 1994; Holbrook et al., 1996; Tréhu and Flueh, 2001). In contrast, PCS measurements of gas concentration and seismic measurements during Leg 204 indicate that free gas is present beneath the BSR but only in thin layers.

The accretionary complex is permeable and is a source of freshwater, which must be accounted for when estimating hydrate concentration from chloride concentration anomalies. Data acquired during Leg 204 confirm the interpretation that the boundary in the 3-D seismic reflection data between stratified sediments and seismically incoherent material represents an unconformity between slope basin material and older indurated and fractured sediments, presumably composing the accretionary complex. In addition, IWs from sites on the eastern flank of Hydrate

Ridge (Sites 1244, 1251, and 1252) show a decrease in chloride concentration and an increase in lithium with depth, which indicates that freshwater migrates from deeper in the accretionary complex where it probably originates from dehydration of subducted oceanic crust and sediment. The slope of the mixing curve between seawater and water from this deep source changes at the top of the accretionary complex, implying that the accretionary complex is more permeable than the overlying deformed slope basin and that diffuse vertical migration of fluids through this material is significant. Although this freshening effect has been documented previously from the Cascadia margin (Kastner et al., 1995), implications for estimation of hydrate concentration from salinity have not been fully appreciated. Leg 204 provides a systematic transect across the margin that can be integrated with structural information to constrain depth and volume of dewatering and the mechanism of fluid expulsion.

REFERENCES

Arsenault, M.A., Tréhu, A.M., Bangs, N., and Nakamura, Y., 2001. *P*-wave tomography of Hydrate Ridge, Oregon continental margin. *Eos, Trans.*, 82:604. (Abstract)

Boetius, A., Ravenschlag, K., Schubert, C.J., Rickert, D., Widdel, F., Gieseke, A., Amann, R., Jorgensen, B.B., Witte, U., and Pfannkuche, O., 2000. Microscopic identification of a microbial consortium apparently mediating anaerobic methane oxidation above marine gas hydrate. *Nature,* 407:623–626.

Bohrmann, G., Greinert, J., Suess, E., and Torres, M., 1998. Authigenic carbonates from the Cascadia subduction zone and their relation to gas hydrate stability. *Geology,* 26:647–650.

Bohrmann, G., Linke, P., Suess, E., Pfannkuche, O., and Scientific Party, 2000. R/V *SONNE* cruise report, SO143 TECFLUX-I-1999. *GEOMAR Rpt.,* 93.

Bohrmann, G., Suess, E., Greinert, J., Teichert, B., and Naehr, T., 2002. Gas hydrate carbonates from Hydrate Ridge, Cascadia convergent margin: indicators of near-seafloor clathrate deposits. *Fourth Int. Conf. Gas Hydrates,* Yokohama, Japan, 102–107.

Booth, J.S., Winters, W.J., and Dillon, W.P., 1994. Circumstantial evidence of gas hydrate and slope failure associations on the United States Atlantic continental margin. *In* Sloan, E.D., Happel, J., and Hantow, M.A. (Eds.), *Int. Conf. Nat. Gas Hydrates,* 7:487–489.

Borowski, W.S., Paull, C.K., and Ussler, W., III, 1996. Marine pore-water sulfate profiles indicate in situ methane flux from underlying gas hydrate. *Geology,* 24:655–658.

Boudreau, B.P., and Canfield, D.E., 1993. A comparison of closed and open system models for porewater and calcite saturation state. *Geochim. Cosmochim. Acta,* 57:317–334.

Carson, B., Seke, E., Paskevich, V., and Holmes, M.L., 1994. Fluid expulsion sites on the Cascadia accretionary prism: mapping diagenetic deposits with processed GLORIA imagery. *J. Geophys. Res.,* 99:11959–11969.

Clague, D., Maher, N., and Paull, C.K., 2001. High-resolution multibeam survey of Hydrate Ridge, offshore Oregon. *In* Paull, C.K., and Dillon, W.P. (Eds.), *Natural Gas Hydrates: Occurrence, Distribution, and Detection.* Am. Geophys. Union, Geophys. Monogr. Ser., 124:297–306.

Claypool, G.E., and Kaplan, I.R., 1974. The origin and distribution of methane in marine sediments. *In* Kaplan, I.R. (Ed.), *Natural Gases in Marine Sediments:* New York (Plenum), 99–139.

Collett, T.S., and Ladd, J., 2000. Detection of gas hydrate with downhole logs and assessment of gas hydrate concentrations (saturations) and gas volumes on the Blake Ridge with electrical resistivity log data. *In* Paull, C.K., Matsumoto, R., Wallace, P.J., and Dillon, W.P. (Eds.), *Proc. ODP, Sci. Results,* 164: College Station, TX (Ocean Drilling Program), 179–191.

Dickens, G.R., 2001. Modeling the global carbon cycle with a gas hydrate capacitor: significance for the latest Paleocene thermal maximum. *In* Paull, C.K., and Dillon, W.P. (Eds.), *Natural Gas Hydrates: Occurrence, Distribution, and Detection.* Am. Geophys Union, Geophys. Monogr. Ser., 124:19–40.

Dickens, G.R., Castillo, M.M., and Walker, J.G.C., 1997. A blast of gas in the latest Paleocene: simulating first-order effects of massive dissociation of oceanic methane hydrate. *Geology,* 25:259–262.

Dickens, G.R., O'Neil, J.R., Rea, D.K., and Owen, R.M., 1995. Dissociation of oceanic methane hydrate as a cause of the carbon isotope excursion at the end of the Paleocene. *Paleoceanography,* 10:965–971.

Garrels, R.M., and Perry, E.A., 1974. Cycling of carbon, sulfur, and oxygen through geologic time. *In* Goldberg, E.D. (Ed.), *The Sea* (Vol. 5): *Marine Chemistry: The Sedimentary Cycle:* New York (Wiley), 569–655.

Ginsburg, G.D., and Soloviev, V.A., 1998. Submarine gas hydrates. *VNIIOkeangeologia,* St. Petersburg, 216.

Greinert, J., Bohrmann, G., and Suess, E., 2001. Gas hydrate-associated carbonates and methane-venting at Hydrate Ridge: classification, distribution and origin of authigenic lithologies. *In* Paull, C.K., and Dillon, W.P. (Eds.), *Natural Gas Hydrates: Occurrence, Distribution, and Detection*. Am. Geophy. Union, Geophys. Monogr. Ser., 124:99–114.

Heeschen, K.U., Tréhu, A.M., Collier, R.W., Suess, E. and Rehder, G., 2003. Distribution and height of methane bubble plumes on the Cascadia margin characterized by acoustic imaging. *Geophys. Res. Lett.,* 30:1643.

Holbrook, W.S., Hoskins, H., Wood, W.T., Stephen, R.A., Lizzarralde, D., and the Leg 164 Science Party, 1996. Methane gas-hydrate and free gas on the Blake Ridge from vertical seismic profiling. *Science,* 273:1840–1843.

Holland, H.D., 1978. *The Chemistry of the Atmosphere and Oceans:* New York (Wiley).

Housen, B.A., and Musgrave, R.J., 1996. Rock-magnetic signature of gas hydrates in accretionary prism sediments. *Earth Planet. Sci. Lett.,* 139:509–519.

Hovland, M., Lysne, D., and Whiticar, M., 1995. Gas hydrate and sediment gas composition, Hole 892A. *In* Carson, B., Westbrook, G.K., Musgrave, R.J., and Suess, E. (Eds.), *Proc. ODP, Sci. Results,* 146 (Pt 1): College Station, TX (Ocean Drilling Program), 151–161.

Johnson, J.E., Goldfinger, C., and Suess, E., in press. Geophysical constraints on the surface distribution of authigenic carbonates across the Hydrate Ridge region, Cascadia margin. *Mar. Geol.*

Kastner, M., Sample, J.C., Whiticar, M.J., Hovland, M., Cragg, B.A., and Parkes, J.R., 1995. Geochemical evidence for fluid flow and diagenesis at the Cascadia convergent margin. *In* Carson, B., Westbrook, G.K., Musgrave, R.J., and Suess, E. (Eds.), *Proc. ODP, Sci. Results,* 146 (Pt. 1): College Station, TX (Ocean Drilling Program), 375–384.

Katz, M.E., Pak, D.K., Dickens, G.R., and Miller, K.G., 1999. The source and fate of massive carbon input during the latest Paleocene thermal maximum. *Science,* 286:1531–1533.

Kennett, J.P., Cannariato, K.G., Hendy, I.L., and Behl, R.J., 1996. *Methane Hydrates in Quaternary Climate Change: The Clathrate Gun Hypothesis*. Spec. Publ.—Am. Geophys. Union.

Kulm, L.D., Suess, E., Moore, J.C., Carson, B., Lewis, B.T., Ritger, S.D., Kadko, D.C., Thornburg, T.M., Embley, R.W., Rugh, W.D., Massoth, G.J., Langseth, M.G., Cochrane, G.R., and Scamman, R.L., 1986. Oregon subduction zone: venting, fauna, and carbonates. *Science,* 231:561–566.

Kvenvolden, K.A., 1995. A review of the geochemistry of methane in natural gas hydrate. *Org. Geochem.,* 23:997–1008.

Kvenvolden, K.A., and Lorenson, T.D., 2001. The global occurrence of natural gas hydrate. *In* Paull, C.K., and Dillon, W.P. (Eds.), *Natural Gas Hydrates: Occurrence, Distribution, and Detection*. Am. Geophys. Union, Geophys. Monogr. Ser., 124:3–18.

Linke, P., Suess, E., and Scientific Party, 2001. R/V *SONNE* cruise report, SO148 TECFLUX-II-2000. *GEOMAR Rpt.,* 98.

MacDonald, I.R., Boland, G.S., Baker, J.S., Brooks, J.M., Kennicutt, M.C., II, and Bidigare, R.R., 1989. Gulf of Mexico hydrocarbon seep communities II. Spatial distribution of seep organisms and hydrocarbons at Bush Hill. *Mar. Biol.,* 101:235–247.

MacKay, M.E., 1995. Structural variation and landward vergence at the toe of the Oregon accretionary prism. *Tectonics,* 14:1309–1320.

MacKay, M.E., Jarrad, R.D., Westbrook, G.K., Hyndman, R.D., and Shipboard Scientific Party, 1994. ODP Leg 146, origin of BSRs: geophysical evidence from the Cascadia accretionary prism. *Geology,* 22:459–462.

MacKay, M.E., Moore, G.F., Cochrane, G.R., Moore, J.C., and Kulm, L.D., 1992. Landward vergence and oblique structural trends in the Oregon margin accretionary prism: implications and effect on fluid flow. *Earth Planet. Sci. Lett.,* 109:477–491.

Milkov, A.V., and Sassen, R., 2002. Economic geology of offshore gas hydrate accumulations and provinces. *Mar. Petr. Geol.,* 19:1–11.

Nisbet, E.G., 1990. The end of the ice age. *Can. J. Earth Sci.,* 27:148–157.

Nisbet, E.G., and Piper, D.J., 1998. Giant submarine landslides. *Nature,* 392:329–330.

Parkes, R.J., Cragg, B.A., and Wellsbury, P., 2000. Recent studies on bacterial populations and processes in marine sediments: a review. *Hydrogeol. Rev.,* 8:11–28.

Paull, C.K., Matsumoto, R., Wallace, P.J., et al., 1996. *Proc. ODP, Init. Repts.,* 164: College Station, TX (Ocean Drilling Program).

Paull, C.K., and Ussler, W., III, 2001. History and significance of gas sampling during the DSDP and ODP. *In* Paull, C.K., and Dillon, W.P. (Eds.), *Natural Gas Hydrates: Occurrence, Distribution, and Detection.* Am. Geophys. Union, Geophys. Monogr. Ser., 124:53–66.

Paull, C.K., Ussler, W., III, and Borowski, W.A., 1994. Sources of biogenic methane to form marine gas-hydrates: in situ production or upward migration? *Ann. N.Y. Acad. Sci.,* 715:392–409.

Paull, C.K., Ussler, W., III, and Dillon, W.P., 1991. Is the extent of glaciation limited by marine gas-hydrates? *Geophys. Res. Lett.,* 18:432–434.

Rempel, A.W., and Buffett, B.A., 1998. Mathematical models of gas hydrate accumulation. *In* Henriet, J.P., and Mienert, J. (Eds.), *Gas Hydrates: Relevance to World Margin Stability and Climate Change.* Spec. Publ.—Geol. Soc. London, 137:63–74.

Revelle, R., 1983. Methane hydrates in continental slope sediments and increasing atmospheric carbon dioxide. In *Changing Climate:* Washington (National Academy Press), 252–261.

Sample, J.C., and Kopf, A., 1995. Isotope geochemistry of syntectonic carbonate cements and veins from the Oregon margin: implications for the hydrogeologic evolution of the accretionary wedge. *In* Carson, B., Westbrook, G.K., Musgrave, R.J., and Suess, E. (Eds.), *Proc. ODP, Sci. Results,* 146 (Pt. 1): College Station, TX (Ocean Drilling Program), 137–148.

Sassen, R., Sweet, S.T., Milkov, A.V., Defreitas, D.A., Kennicutt, M.C., and Roberts, H.H., 2001. Stability of thermogenic gas hydrate in the Gulf of Mexico: constraints on models of climate change. *In* Paull, C.K., and Dillon, W.P. (Eds.), *Natural Gas Hydrates: Occurrence, Distribution, and Detection.* Am. Geophys. Union, Geophys. Monogr. Ser., 124:131–144.

Schlüter, M., Linke, P., and Suess, E., 1998. Geochemistry of a sealed deep-sea borehole on the Cascadia margin. *Mar. Geol.,* 148:9–20.

Shipboard Scientific Party, 1994. Leg 146 introduction: Cascadia margin. *In* Westbrook, G.K., Carson, B., Musgrave, R.J., et al., *Proc. ODP, Init. Repts.,* 146 (Pt. 1): College Station, TX (Ocean Drilling Program), 5–14.

Suess, E., and Bohrmann, G., 1997. FS *SONNE* cruise report, SO110:SO-RO (*SONNE-ROPOS*), Victoria-Kodiak-Victoria, July 9–Aug. 19, 1996. *GEOMAR Rpt.,* 59:181.

Suess, E., Bohrmann, G., Rickert, D., Kuhs, W., Torres, M., Tréhu, A., and Link, P., 2002. Properties and fabric of near-surface hydrates at Hydrate Ridge, Cascadia margin. *Fourth Int. Conf. Gas Hydrates:* Yokohama, Japan, 740–744.

Suess, E., Torres, M.E., Bohrmann, G., Collier, R.W., Rickert, D., Goldfinger, C., Linke, P., Heuser, A., Sahling, H., Heeschen, K., Jung, C., Nakamura, K., Greinert, J., Pfannkuche, O., Tréhu, A., Klinkhammer, G., Whiticar, M.J., Eisenhauer, A., Teichert, B., and Elvert, M., 2001. Sea floor methane hydrates at Hydrate Ridge, Cascadia margin. *In* Paull, C.K., and Dillon, W.P. (Eds.), *Natural Gas Hydrates: Occurrence, Distribution, and Detection.* Am. Geophysical Union, Geophys. Monogr. Ser., 124:87–98.

Suess, E.M., Torres, M.E., Bohrmann, G., Collier, R.W., Greinter, J., Linke, P., Rehter, G., Tréhu, A.M., Wallmann, K., Winckler, G., and Zulegger, E., 1999. Gas hydrate destabilization: enhanced dewatering, benthic material turnover, and large methane plumes at the Cascadia convergent margin. *Earth Planet. Sci. Lett.,* 170:1–15.

Teichert, B.M.A., Eisenhauer, A., and Bohrmann, G., 2001. Chemoherm buildups at the Cascadia margin (Hydrate Ridge)—evidence for long-term fluid flow. *2001 MARGINS Meet.,* Kiel, 208.

Teichert, B.M.A., Eisenhauer, A., Bohrmann, G., Haase-Schramm, A., Bock, B., and Linke, P., in press. U/Th systematics and ages of authigenic carbonates from Hydrate Ridge, Cascadia margin: recorders of fluid flow variations. *Geochim. Cosmochim. Acta.*

Torres, M.E., Bohrmann, G., Brown, K., deAngelis, M., Hammond, D., Klinkhammer, G., McManus, J., Suess, E., and Tréhu, A.M., 1999. Geochemical observations on Hydrate Ridge, Cascadia margin. *Oregon State Univ. Data Rpt.,* 174:99–3.

Torres, M.E., Colbert, S., Collier, R.W., deAngelis, M., Hammond, D., Heeschen, K., Hubbard, D., McManus, J., Moyer, C., Rehder, G., Tréhu, A.M., Tyron, M., and Whaling, P., 1998. Active gas discharge resulting from decomposition of gas hydrates on Hydrate Ridge, Cascadia margin. *Eos, Trans.,* 79:461.

Torres, M.E., McManus, D.E., Hammond, M.A., de Angelis, K.U., Heeschen, S.L., Colbert, M.D., Tryon, K.M., Brown, K., and Suess, E., 2002. Fluid and chemical fluxes in and out of sediments hosting methane hydrate deposits on Hydrate Ridge, OR: I. hydrological provinces. *Earth Planet. Sci. Lett.,* 201:525–540.

Tréhu, A.M., and Bangs, N., 2001. 3-D seismic imaging of an active margin hydrate system, Oregon continental margin, report of cruise TTN112. *Oregon State Univ. Data Rpt., 182.*

Tréhu, A.M., Bangs, N.L., Arsenault, M.A., Bohrmann, G., Goldfinger, C., Johnson, J.E., Nakamura, Y., and Torres, M.E., 2002. Complex subsurface plumbing beneath southern Hydrate Ridge, Oregon continental margin, from high-resolution 3-D seismic reflection and OBS data. *Fourth Int. Conf. Gas Hydrates:* Yokohama, Japan, 19023:90–96.

Tréhu, A.M., and Flueh, E., 2001. Estimating the thickness of the free gas zone beneath Hydrate Ridge, Oregon continental margin, from seismic velocities and attenuation. *J. Geophys. Res.,* 106:2035–2045.

Tréhu, A.M., Lin, G., Maxwell, E., and Goldfinger, C., 1995. A seismic reflection profile across the Cascadia subduction zone offshore central Oregon: new constraints on methane distribution and crustal structure. *J. Geophys. Res.,* 100:15101–15116.

Tréhu, A.M., Torres, M.E., Moore, G.F., Suess, E., and Bohrmann, G., 1999. Temporal and spatial evolution of a gas-hydrate-bearing accretionary ridge on the Oregon continental margin. *Geology,* 27:939–942.

Wefer, G.P., Heinze, M., and Berger, W.H., 1994. Clues to ancient methane release. *Nature,* 369:282.

Xu, W., and Ruppel, C., 1999. Predicting the occurrence, distribution, and evolution of methane gas hydrate in porous marine sediments. *J. Geophys. Res,* 104:5081–5096.

Figure F1. A. Tectonic setting of Hydrate Ridge in the accretionary complex of the Cascadia subduction zone. The box shows region of (B). **B.** Bathymetric map of the Hydrate Ridge vicinity. The box shows location of (C). Locations of ODP Site 892, seismic line L2-89 (shown in Fig. F2, p. 52), north Hydrate Ridge (NHR), south Hydrate Ridge (SHR), and Southeast Knoll (SEK) are also shown. **C.** Detailed bathymetric map of the region south of Hydrate Ridge. Leg 204 sites are shown along with their site numbers (e.g., Site 1244) and precruise designation (e.g., proposed Site HR1a). Bathymetry from Clague et al. (2001).

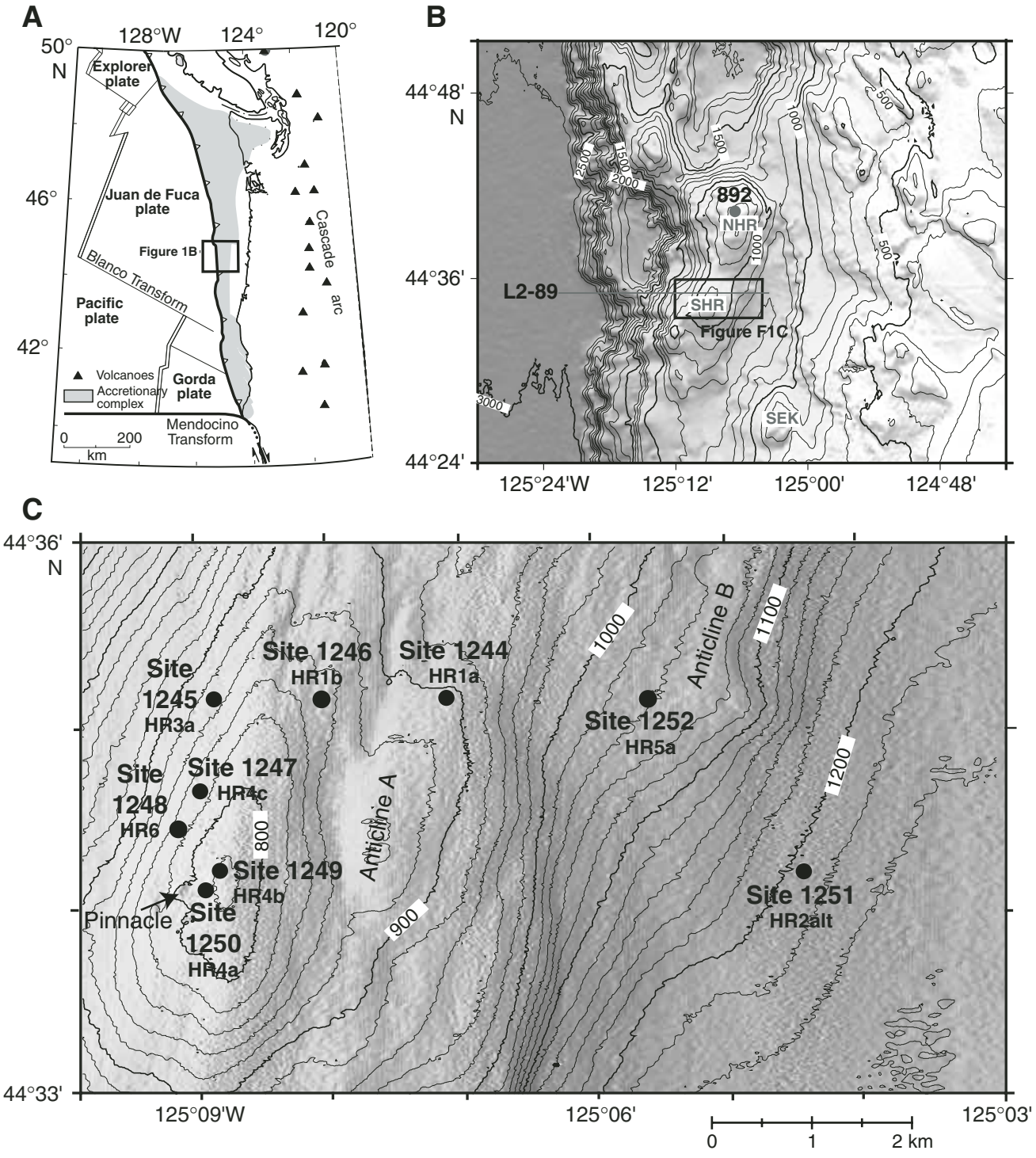

Figure F2. A. Schematic line drawing of the crustal structure across Hydrate Ridge based on depth-converted migrated seismic reflection data (from Shipboard Scientific Party, 1994). Interpretation is based on line 9 from the 1989 ODP site survey (MacKay et al., 1992), along which ODP Site 892 was located. On the scale shown here, primary structural features are the same as those along line 2, which is shown in (B). **B.** Line 2 from the 1989 ODP site survey showing primary structural features of the deformation front and the location of data shown in Figure F5, p. 55. BSR = bottom-simulating reflector, ODP = Ocean Drilling Program.

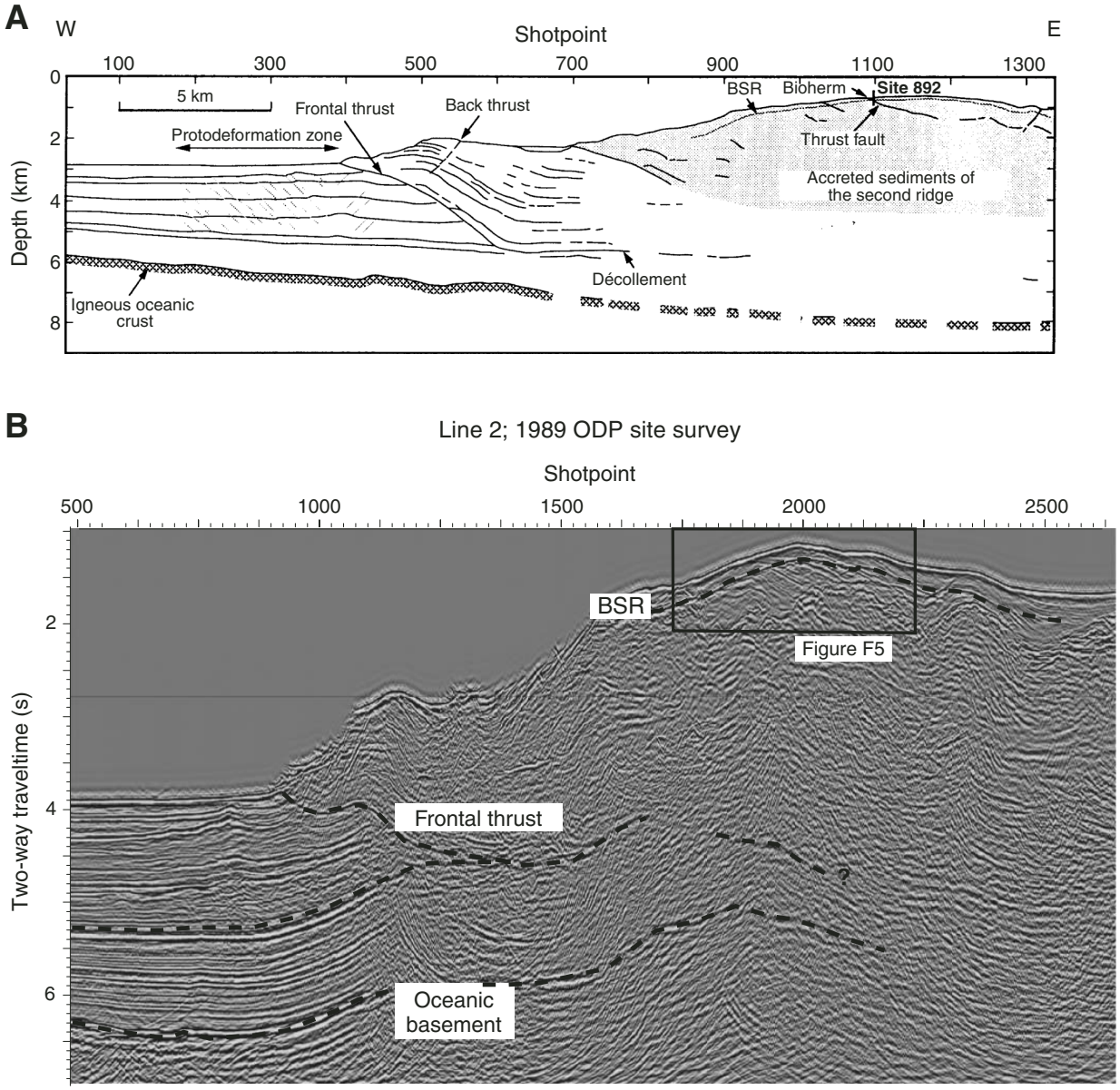

Figure F3. A. Water temperature profiles from conductivity/temperature/depth recorder profiles of the water column over southern Hydrate Ridge. The stability boundaries for (A) pure methane hydrate and (B) a mixture of 97.5% methane and 2.5% hydrogen sulfide are shown, as are the water depths of Leg 204 sites. **B.** Echo sounder records (12 kHz) from the Hydrate Ridge region showing bubbles in the water column (Torres et al., 1999; Tréhu and Bangs, 2001).

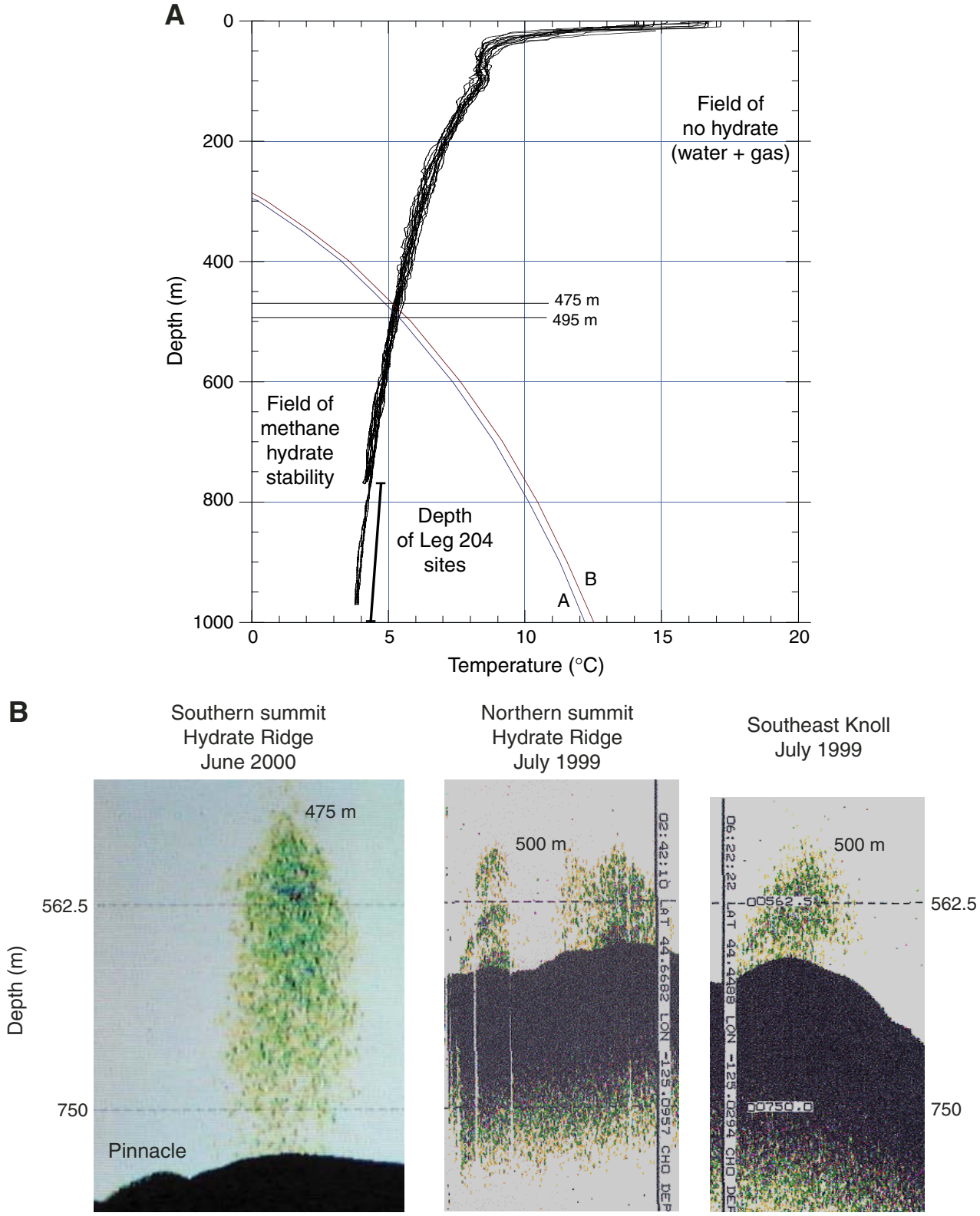

Figure F4. A. Carbonate sample from the top of the Pinnacle showing the porous nature of carbonates from this environment. **B.** Sample of sediment from near the seafloor at southern Hydrate Ridge showing hydrate lenses parallel to bedding connected to hydrate veins perpendicular to bedding (Suess et al., 2002). **C.** Landscape at southern Hydrate Ridge showing mounds covered by bacterial mats. A chemosynthetic clam colony is seen in the right edge of this picture taken during an *Alvin* dive (Torres et al., 1999). **D.** Illustration of the complex biogeochemical relationships expected near the southern summit of Hydrate Ridge (Bohrmann et al., 2002). BSR = bottom-simulating reflector.

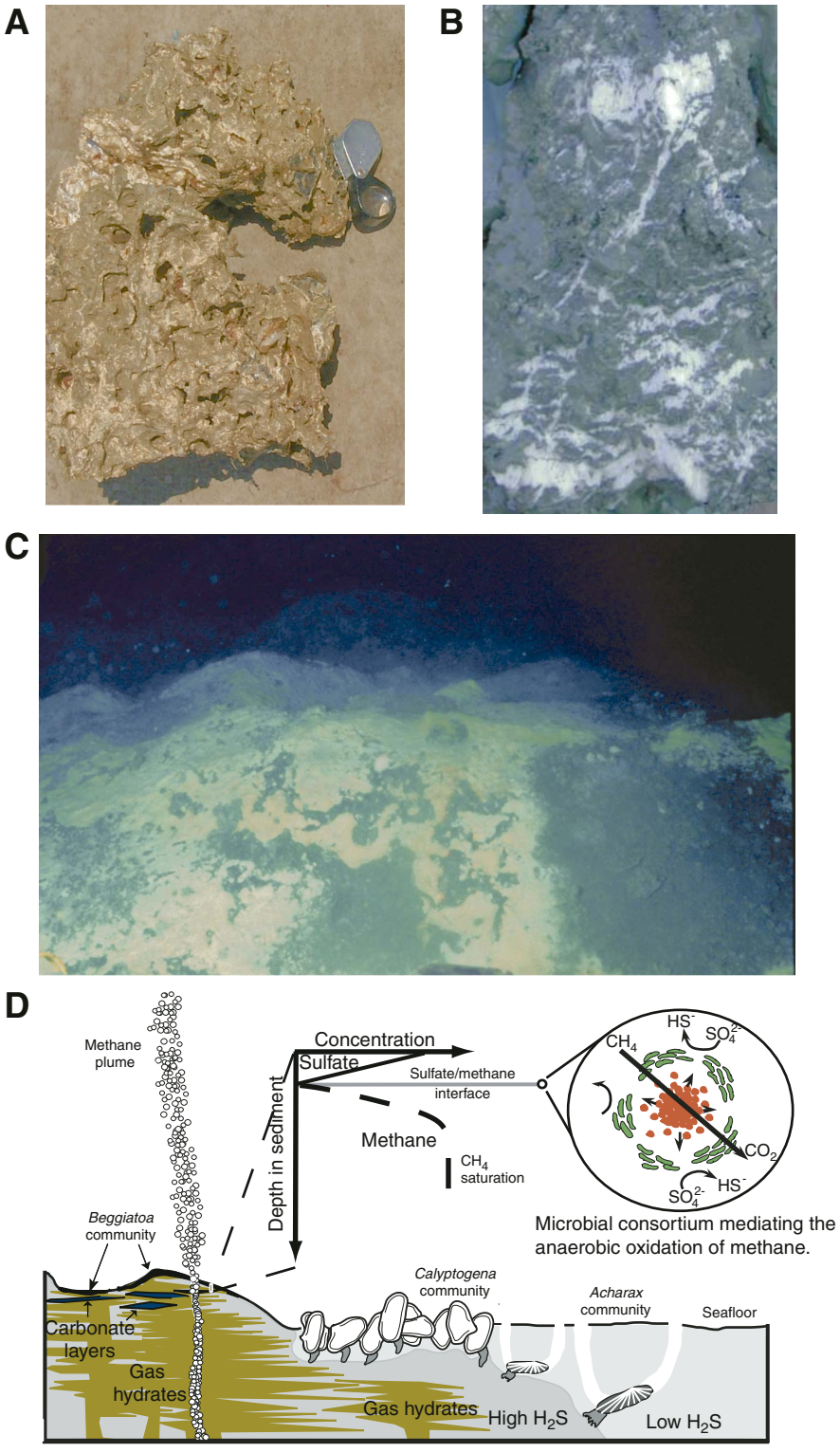

Figure F5. East-west vertical slice through the 3-D seismic data (Tréhu and Bangs, 2001) showing the stratigraphic and structural setting of Sites 1244–1246 and 1252. Seismic Reflections A, B, B′, Y, and Y′ are anomalously bright stratigraphic events and are discussed further in the text. Seismic reflection AC is the top of the seismically incoherent core of Hydrate Ridge, interpreted to represent older, highly deformed sediments of the accretionary complex. The depth scale in meters is shown on the left, assuming a velocity of 1550 m/s above 150 mbsf and 1650 m/s below 150 mbsf. The length of the lines representing sites indicates maximum depth of penetration at that site, and horizontal ticks are located 75 m apart.

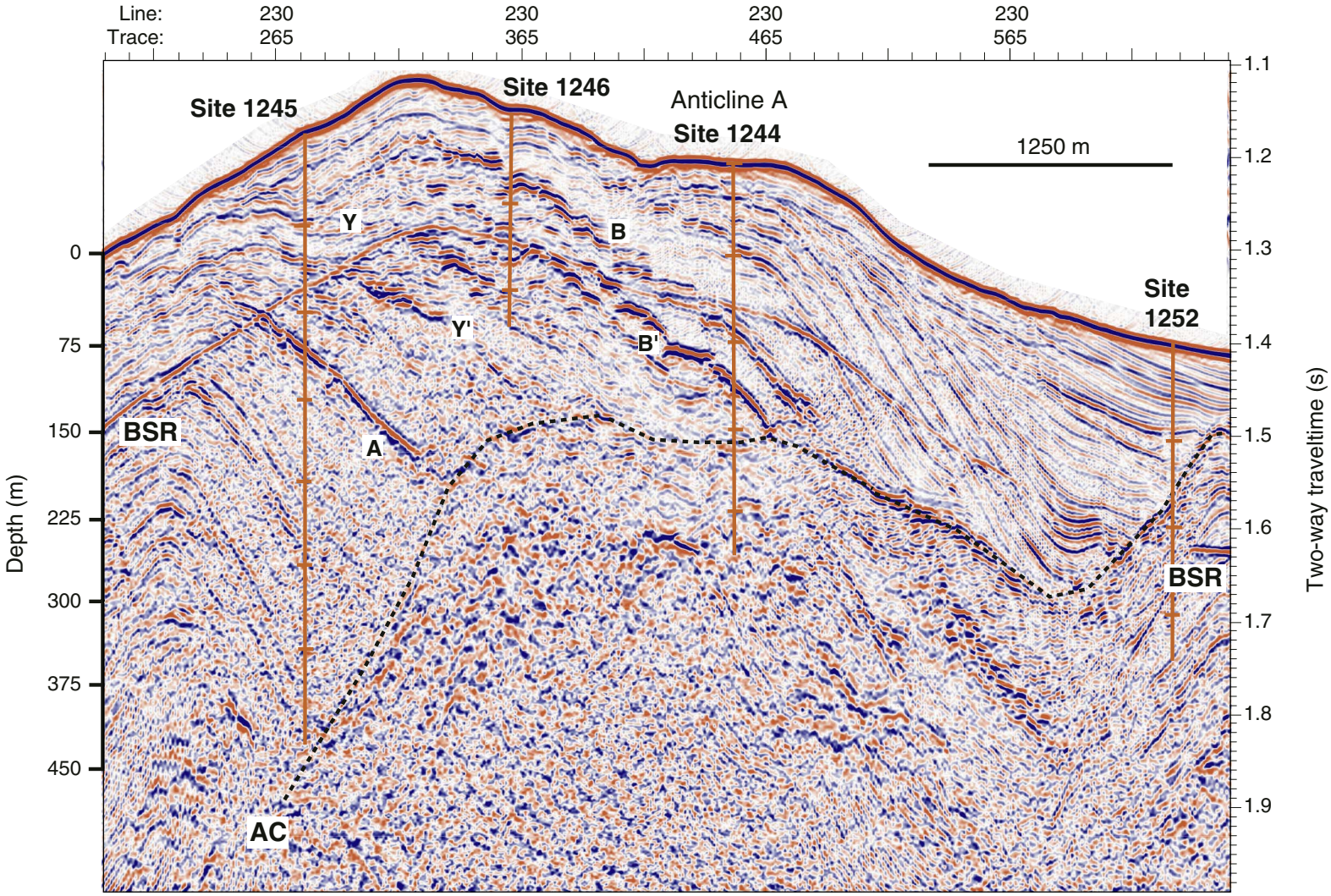

Figure F6. Panels above, center, and right show north-south–trending vertical slices from the 3-D seismic data volume (Tréhu and Bangs, 2001) that extend from the western flank to the summit (see map above, left). Sites drilled during Leg 204 are shown. From left, lower panels are maps of the depth of Horizon A beneath the bottom-simulating reflector (BSR) and the seafloor and of the amplitude of Horizon A. These maps show that changes in the amplitude of Horizon A are correlated with the depth of Horizon A beneath the sea surface (pressure) rather than depth beneath the seafloor (primarily temperature), suggesting that the onset of very strong reflectivity may indicate the onset of gas exsolution within Horizon A. Other labels as in Figure F5, p. 55. The length of the lines representing sites indicates maximum depth of penetration at that site, and horizontal ticks are located 75 m apart.

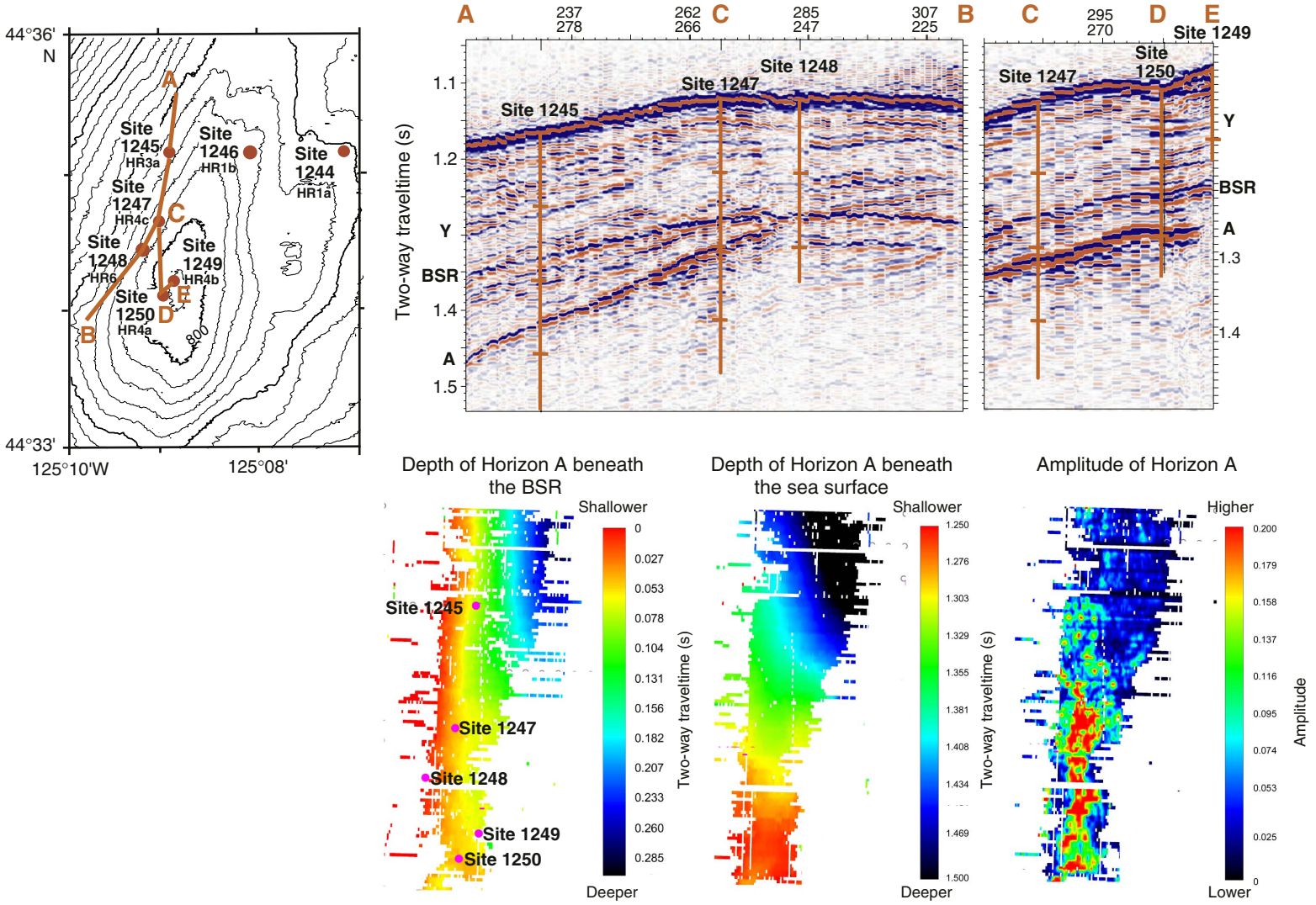

Figure F7. Seismic details near the summit of southern Hydrate Ridge in the vicinity of Sites 1248–1250. Seafloor reflectivity is also shown in the center at the same distance scale (from Johnson et al., in press). BSR = bottom-simulating reflector.

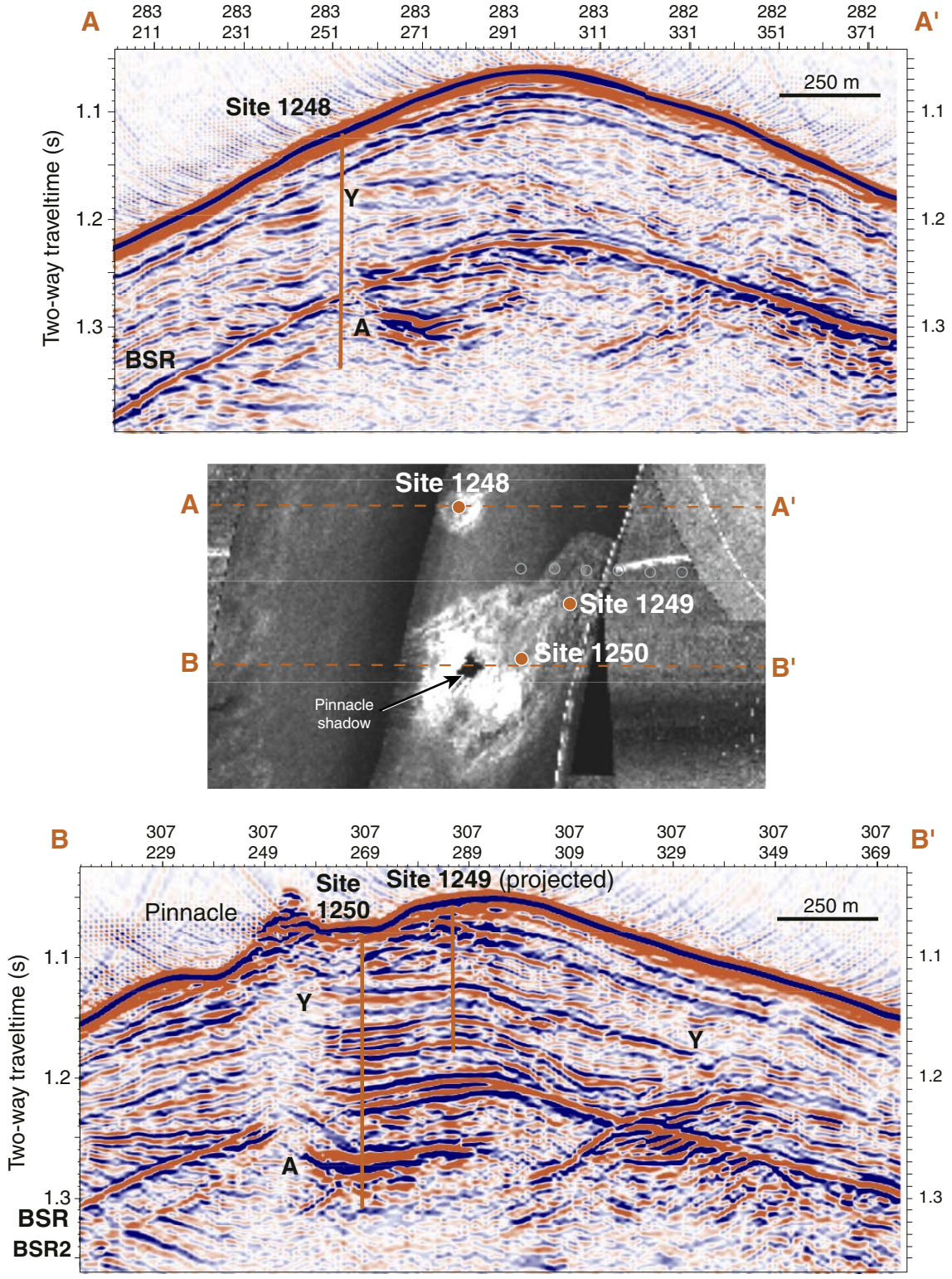

Figure F8. East-west–trending vertical slices through the seismic data around Sites 1251 and 1252. The slice for Site 1252 overlaps and extends through the slice shown in Figure F5. The slice for Site 1251 is offset to the south. Sites 1251 and 1252 are on the east and west flanks of anticline B, respectively. This anticline appears to have been active throughout the depositional history of the slope basin on the east flank of Hydrate Ridge, which included an unconformity (U) and two apparent massive debris flows (DF1 and DF2), which can be traced throughout the slope basin. Reflection AC is an unconformity that marks the top of older (>1.6 Ma) indurated and fractured sediments of the accretionary complex. BSR = bottom-simulating reflector.

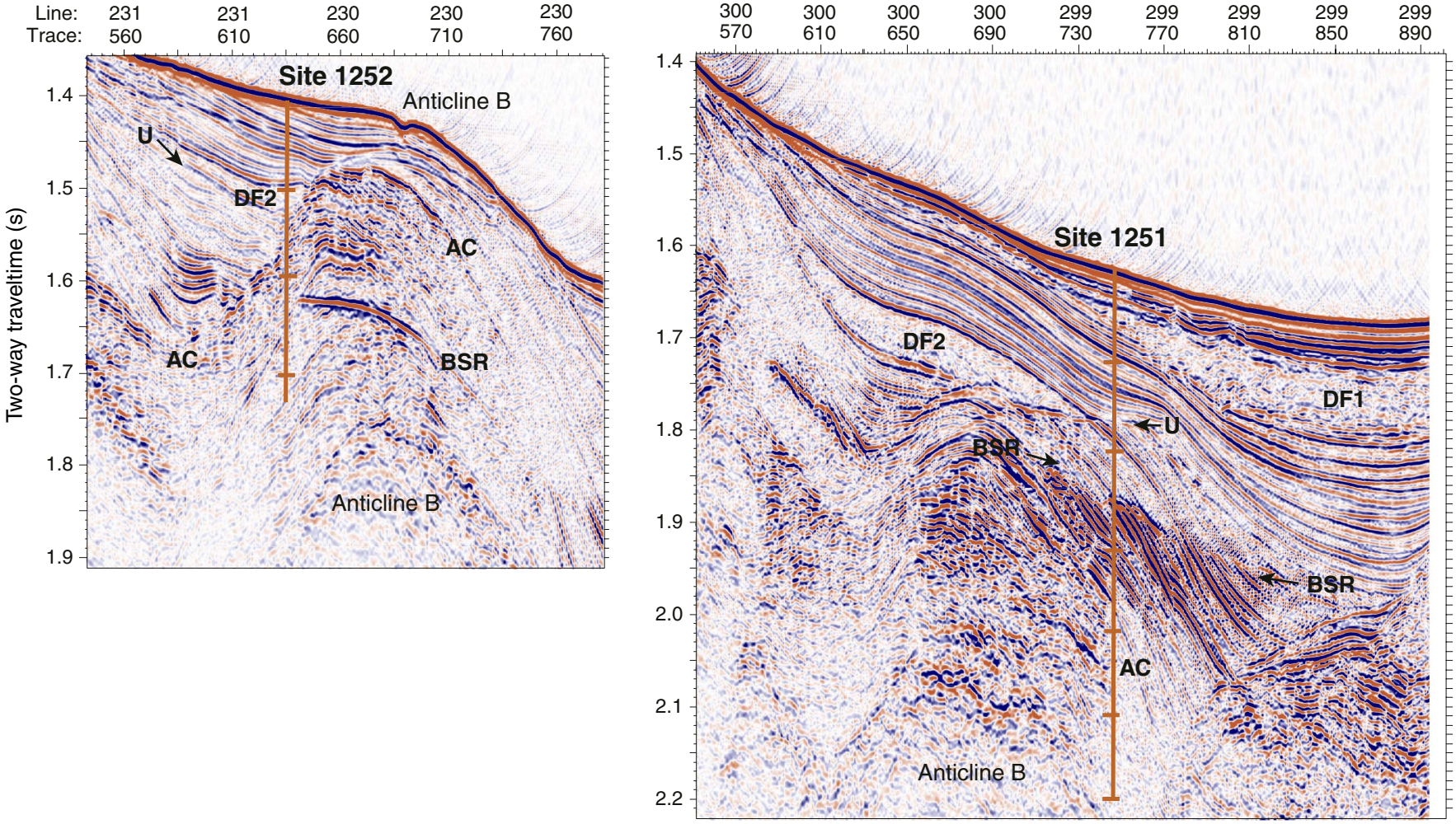

Figure F9. Examples of some of the characteristic lithologic features observed in cores from Leg 204. **A.** Glauconite sands and turbidites. **B.** Debris flows. **C.** Volcanic ash and glass–rich horizons.

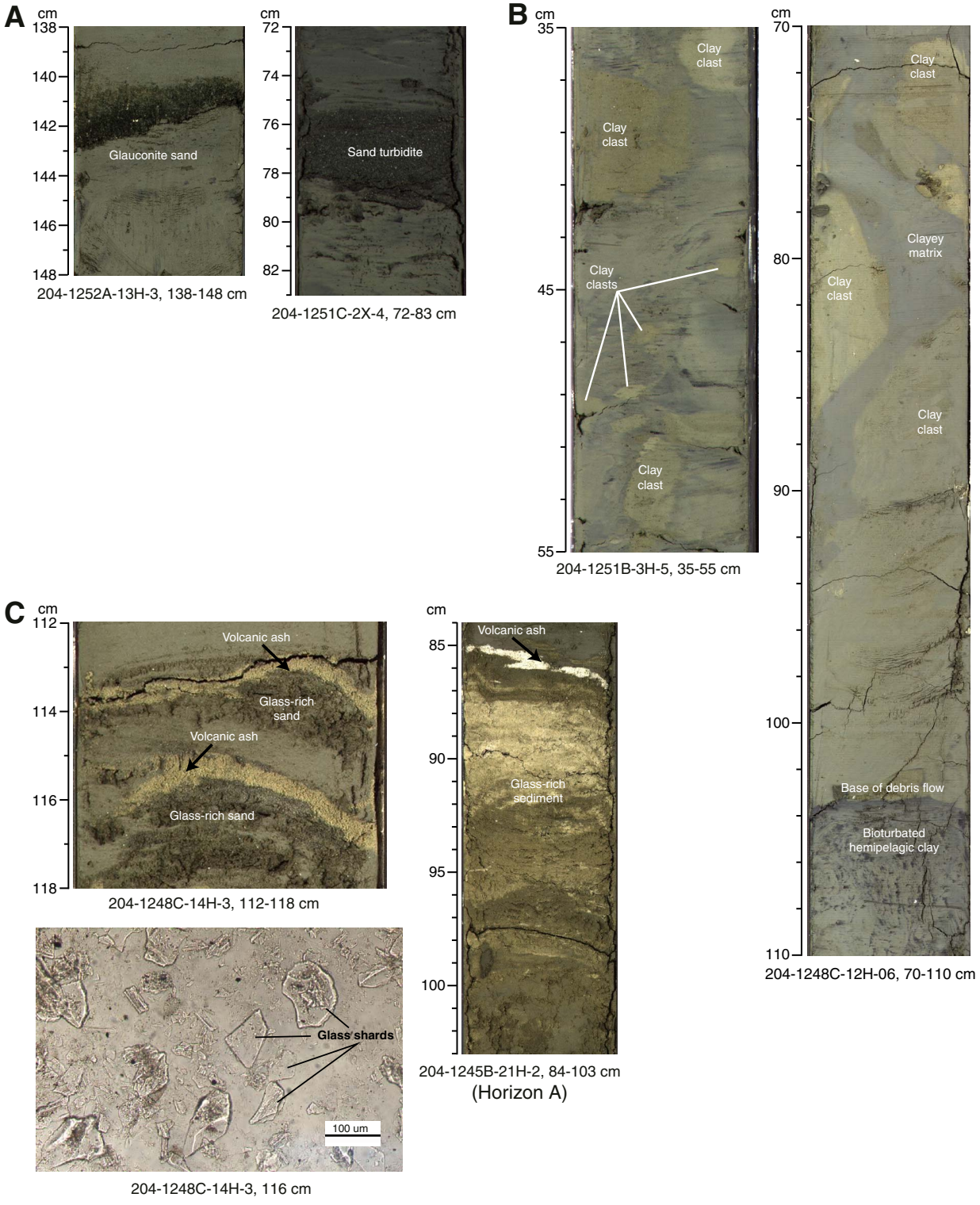

Figure F10. Summary of biostratigraphic and lithologic observations. Seismic correlation of Horizons A, B, B′, and Y and of unconformities (U) and the accretionary complex are also shown (see Figs. F5, p. 55, F6, p. 56, F8, p. 58). See text for more detailed descriptions of the characteristics of each lithostratigraphic unit. Note that Unit III along the north-south transect is not correlative with Unit III on the east-west transect. Correlation between these two transects is tentative. A comparison between the age constraints shown here and the geometric relationships shown in Figure F5, p. 55, suggests that Unit III at Site 1245 was deposited very rapidly at the base of the continental slope (i.e., in the trench) and, thus, represents a recent addition to the accretionary complex. Unit II was deposited in a very active tectonic environment on the lower slope and varies laterally in both thickness and lithology. Thorough integration of the seismic, biostratigraphic, and lithologic data is an ongoing postcruise project.

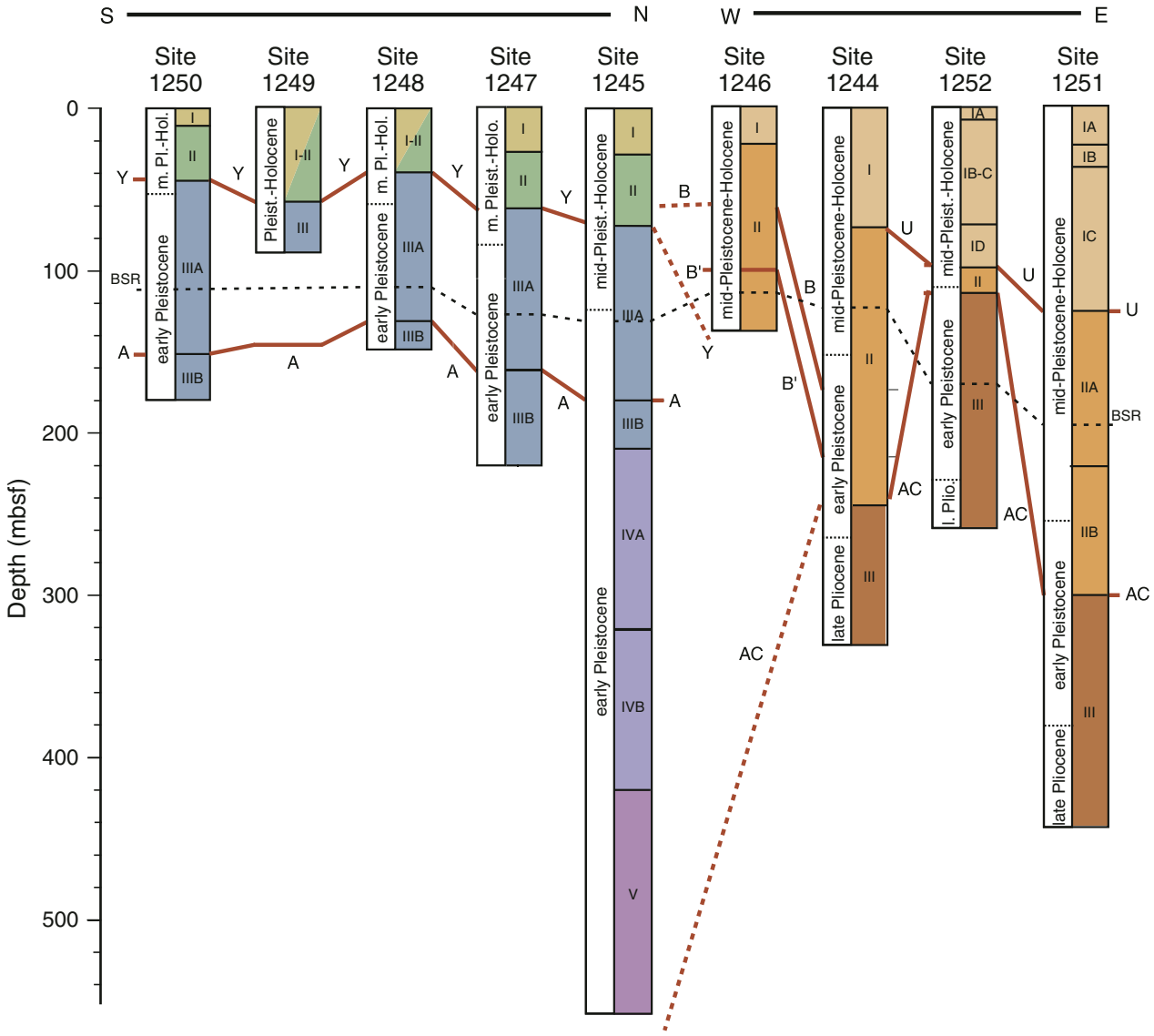

Figure F11. Correlation between 3-D seismic data, density, and resistivity measured downhole by logging while drilling (LWD), gamma density and magnetic susceptibility measured by MST on cores, and lithology at Sites 1244 and 1246. Seismic data were converted to depth assuming a velocity of 1550 m/s above the BSR and 1700 m/s below the BSR, as suggested by 3-D velocity tomography (Arsenault et al., 2001). VSPs confirmed that the velocities from the tomography study are quite close to in situ velocities (Fig. F19, p. 69). Seismic Horizon B corresponds to a double-peaked, high-density, high-magnetic susceptibility zone and seismic Horizon B′ corresponds to a thick glass-rich turbidite. Lithologic observations indicate that these anomalies result from ash-rich layers that contain a relatively high concentration of gas hydrate.

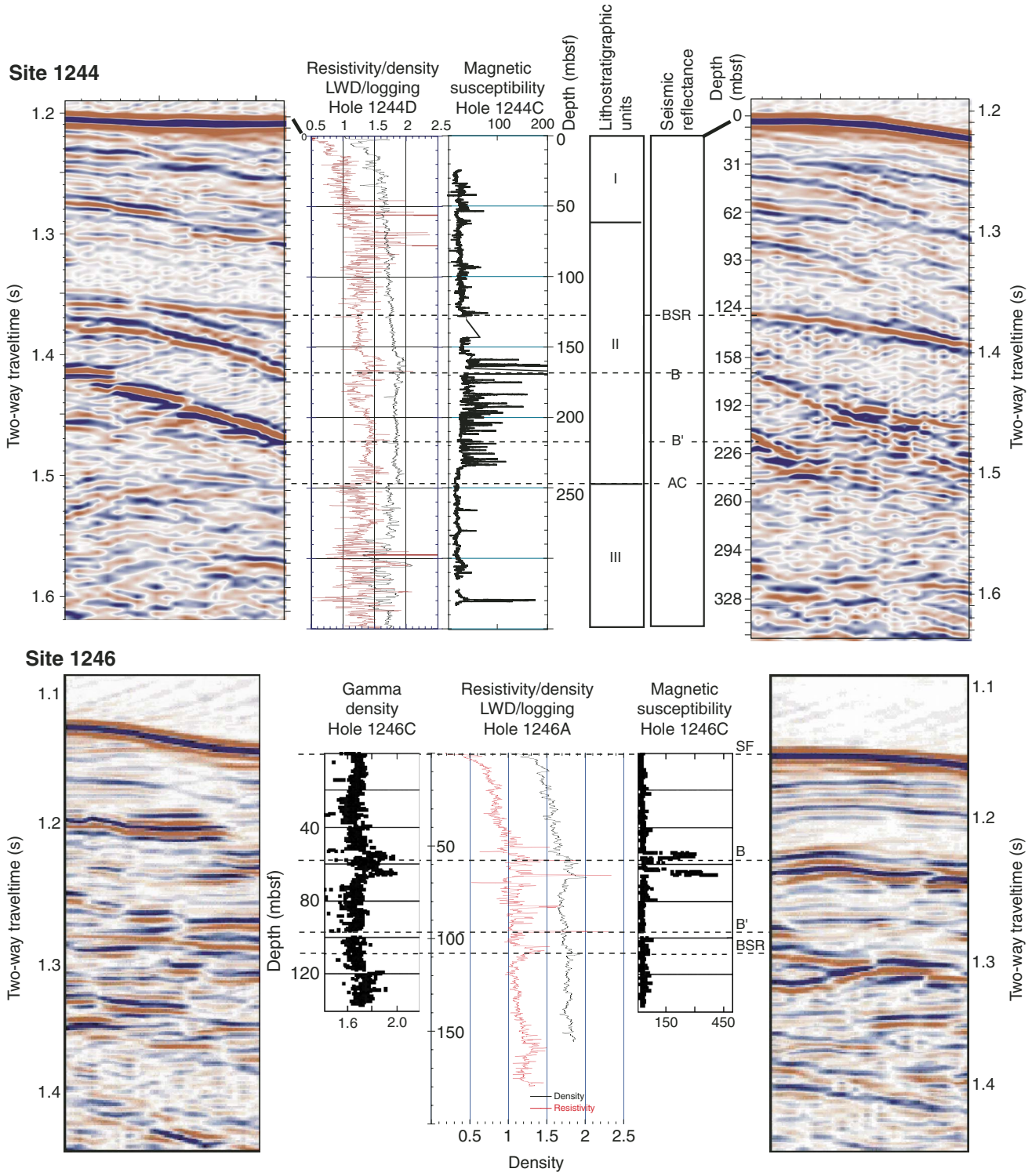

Figure F12. Comparison of IR images and hydrate samples extracted from the core liner. Outer core liner diameter in the IR images is 71.5 mm. Inner core diameter in the photographs is 66 mm. Mismatch between IR anomaly depth and sample depth is because IR scans were taken prior to compressing and cutting core sections.

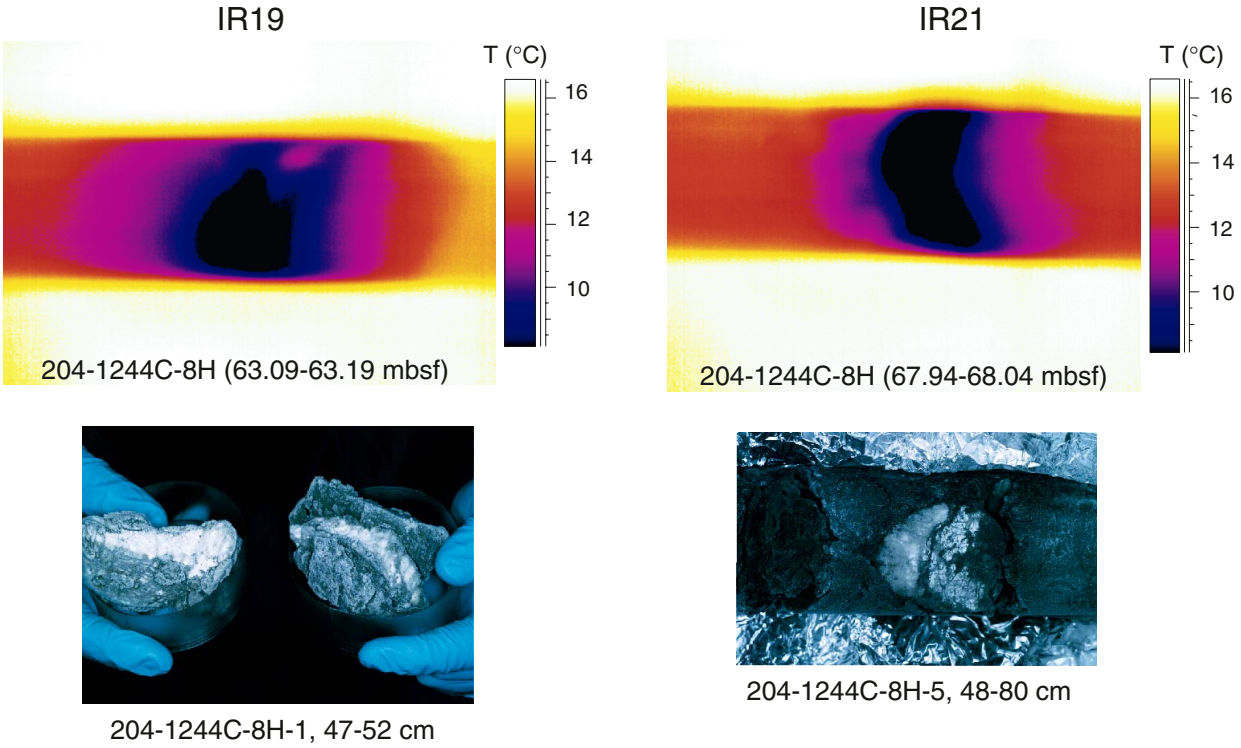

Figure F13. Relative borehole resistivity as imaged by LWD (golden/brown columns) compared to the presence of low-temperature anomalies in recovered cores as imaged by IR camera scans (blue spikes). The resistivity data show a clockwise scan from of the borehole wall north. Light shades represent higher resistivity. Horizontal bands are parallel to the strata, whereas S-shaped bands represent steeply dipping structures. IR anomalies represent the difference between local and background temperature. Background temperature was determined by eye and can be affected by many factors, including air temperature on the catwalk and coring method. Horizon A and the top of accretionary complex as defined by increased fracturing and variable density in the LWD data are shown. BSR = bottom-simulating reflector, RAB = resistivity at the bit.

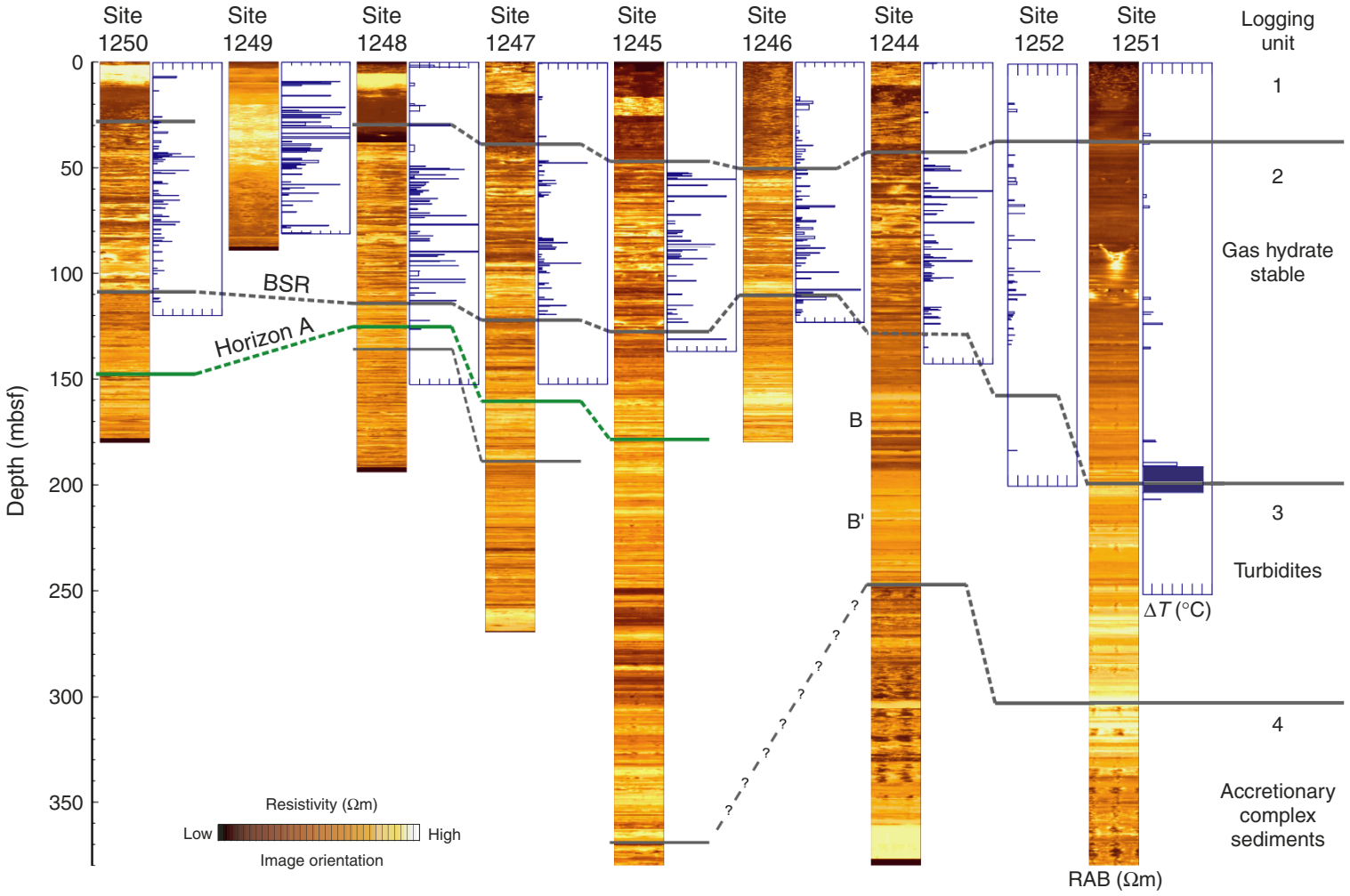

Figure F14. Comparison of the resistivity structure between Sites 1244 and 1248, showing the difference between a site where hydrate primarily fills steeply dipping fractures and a site where hydrate is primarily found along bedding planes. RAB = resistivity at the bit, 3-D = three-dimensional.

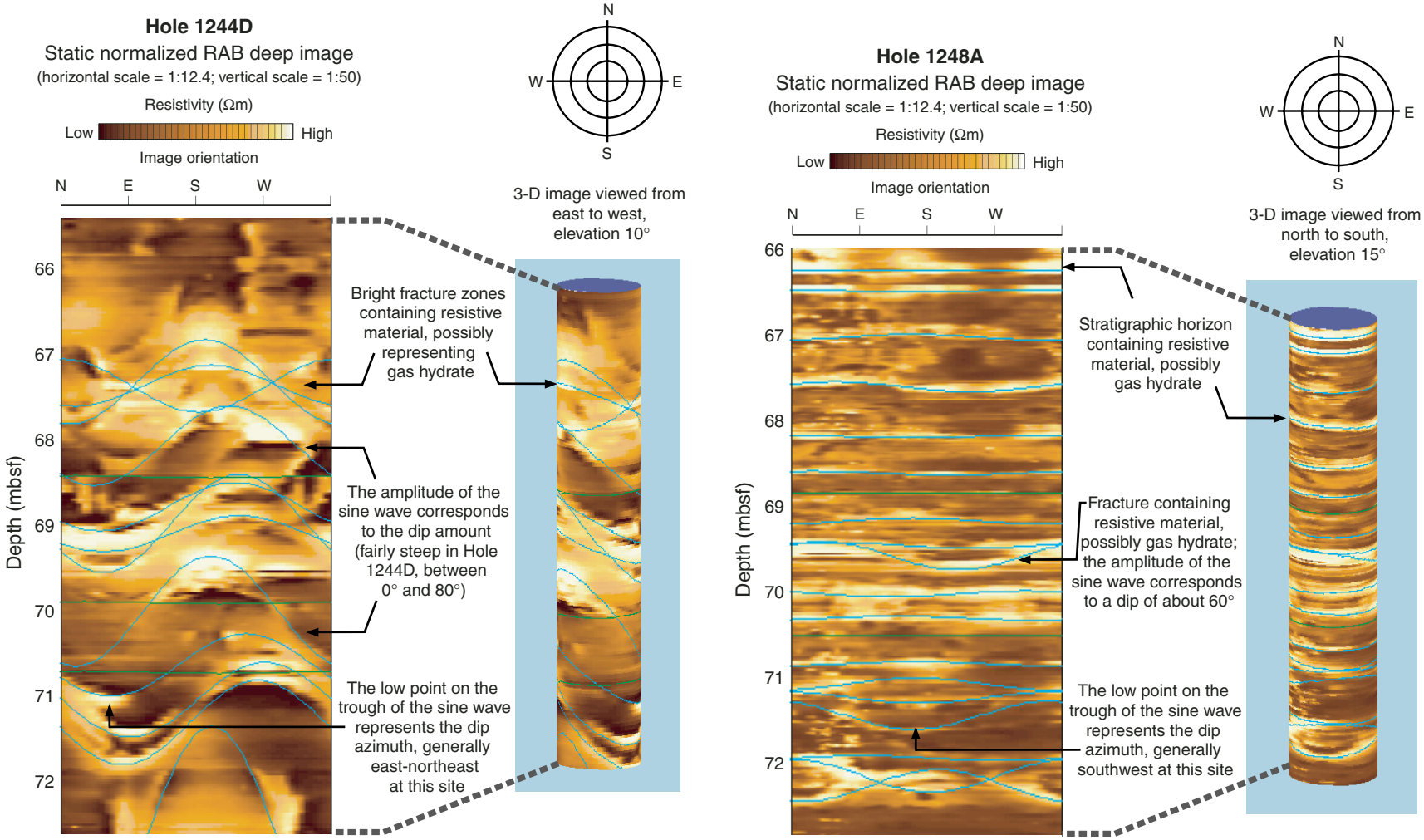

Figure F15. Chloride concentration values measured at all sites. In most cases, samples are spaced at ~5-m intervals (two per core). **A.** Sites on the western flank of Hydrate Ridge. **B.** Sites on the eastern flank of Hydrate Ridge. **C.** Sites near the summit of Hydrate Ridge. Bottom-simulating reflector (BSR) depth at each site is shown as a color-coded dashed line.

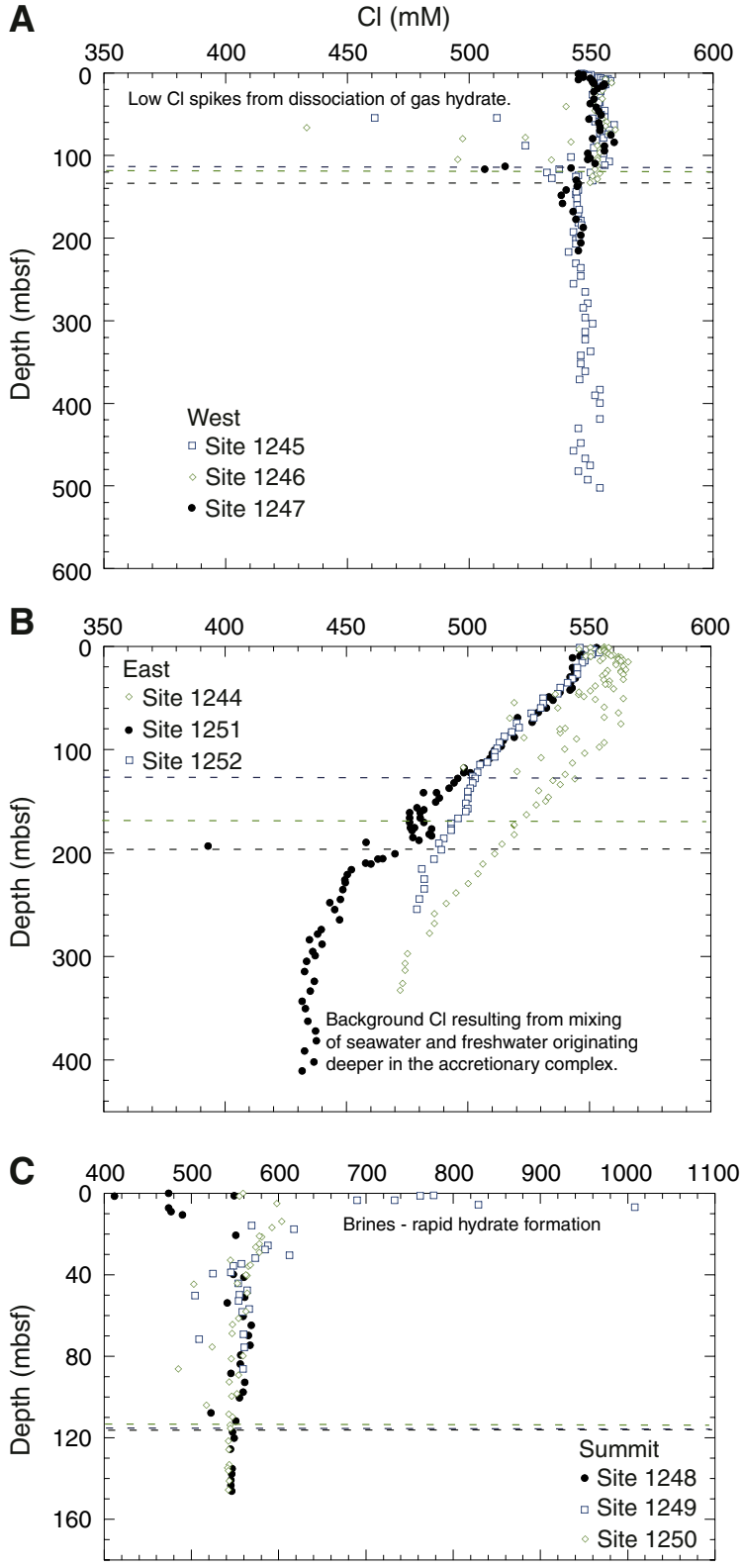

Figure F16. C_1/C_2 values measured at all sites from vacutainer samples. The same patterns are shown in headspace samples, although absolute values of C_1/C_2 are somewhat smaller. Samples are spaced at ~5-m intervals (two per core). **A.** Sites on the western flank of Hydrate Ridge. **B.** Sites on the eastern flank of Hydrate Ridge. **C.** Sites near the summit of Hydrate Ridge. Bottom-simulating reflector (BSR) and Horizon A depth at each site is shown as a color-coded dashed line.

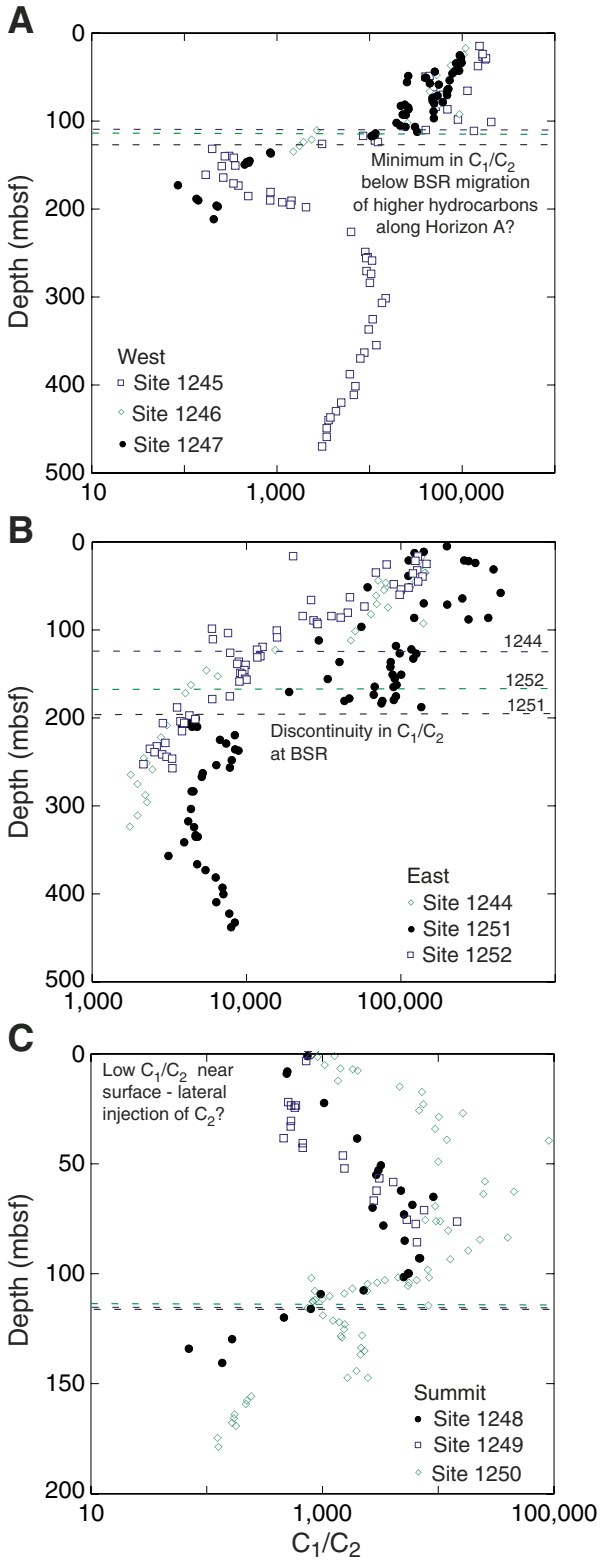

Figure F17. Methane concentrations determined from pressure core sampler (PCS) measurements. Approximate phase boundaries are shown between fields where dissolved gas, gas hydrate, and free gas are predicted to be present in the subsurface. Uncertainties (~30%) in the position of these boundaries are a result of a number of factors, including variations in the subsurface thermal gradient, gas composition, and pore fluid salinity. Although these boundaries give a first order view of where gas hydrate should be present, data points that fall near boundaries should be interpreted with caution. More detailed analysis of the predicted stability fields for conditions measured during Leg 204 is the subject of postcruise research. Near the summit, all PCS measurements from within the GHSZ indicate the presence of gas hydrate, with the highest concentration near the seafloor. On the flanks and in the basin, hydrate presence within the stability zone is intermittent and the highest concentration is just above the BSR.

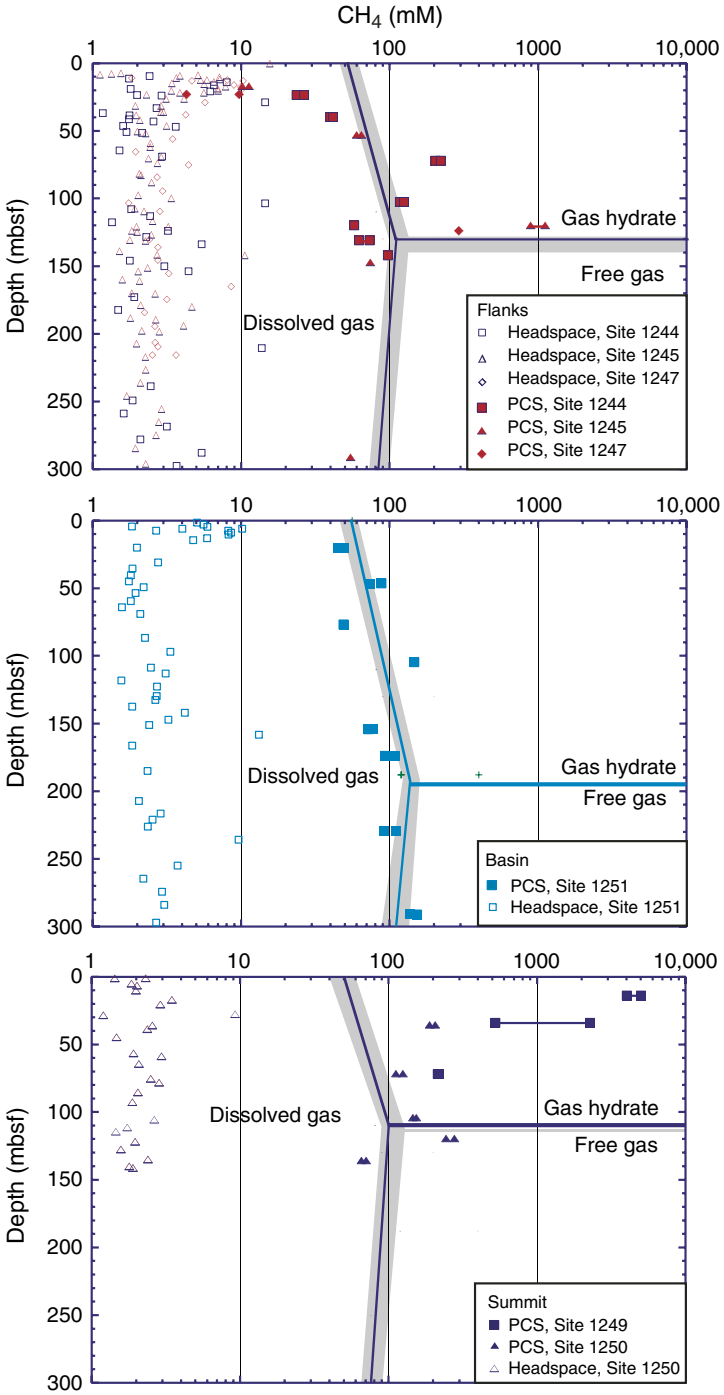

Figure F18. Density and resistivity at the bit (RAB) recorded through seismic Horizon A at Sites 1245 and 1247. These examples show the remarkable consistency in the signature of this horizon over distances of several kilometers. RAB images are static normalized.

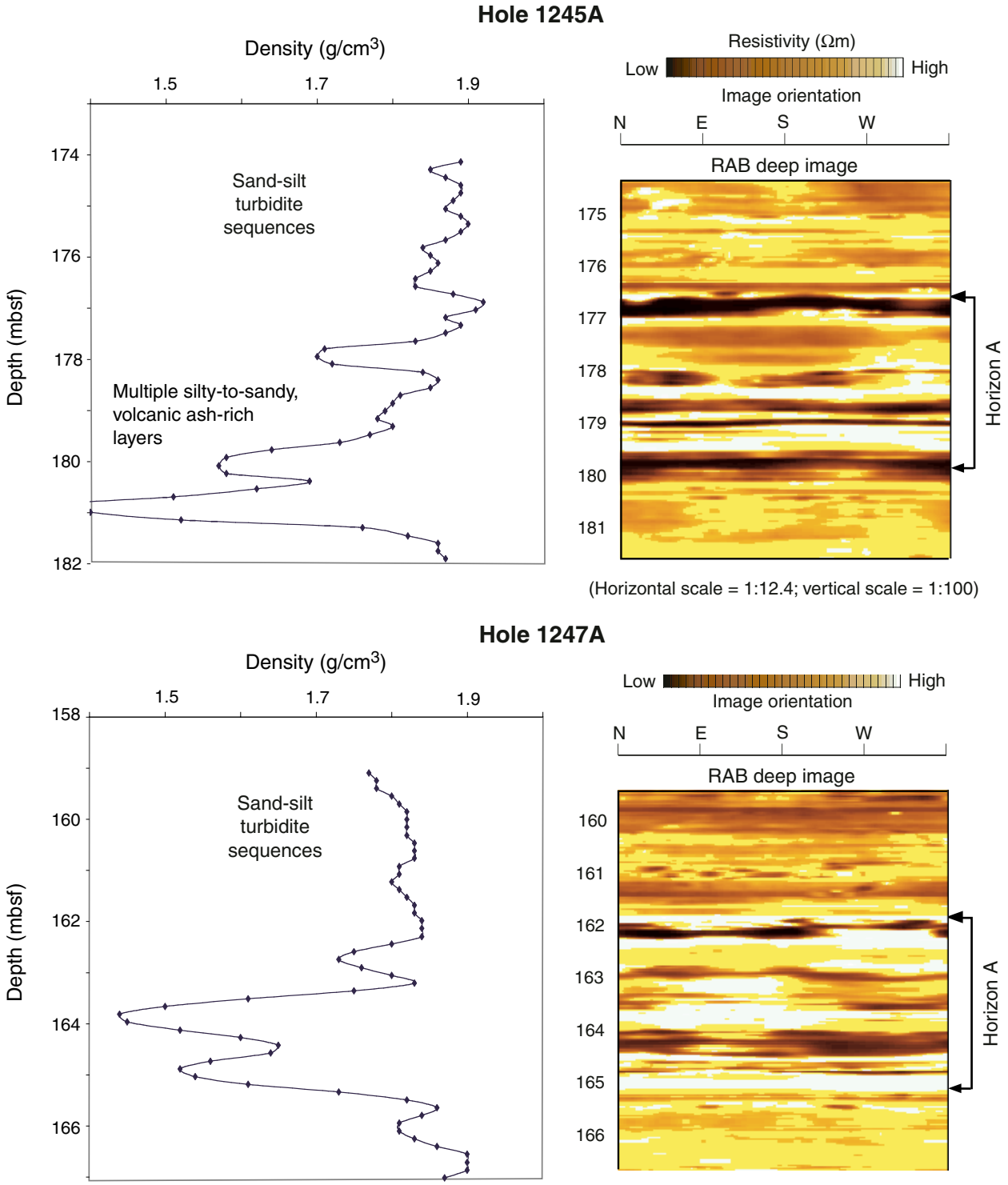

Figure F19. A. Sulfate and methane concentration at Site 1245 showing the sulfate/methane interface (SMI). **B.** Summary of sulfate measurements showing the SMI at all sites except for Sites 1248–1250, where no sulfate was detected.

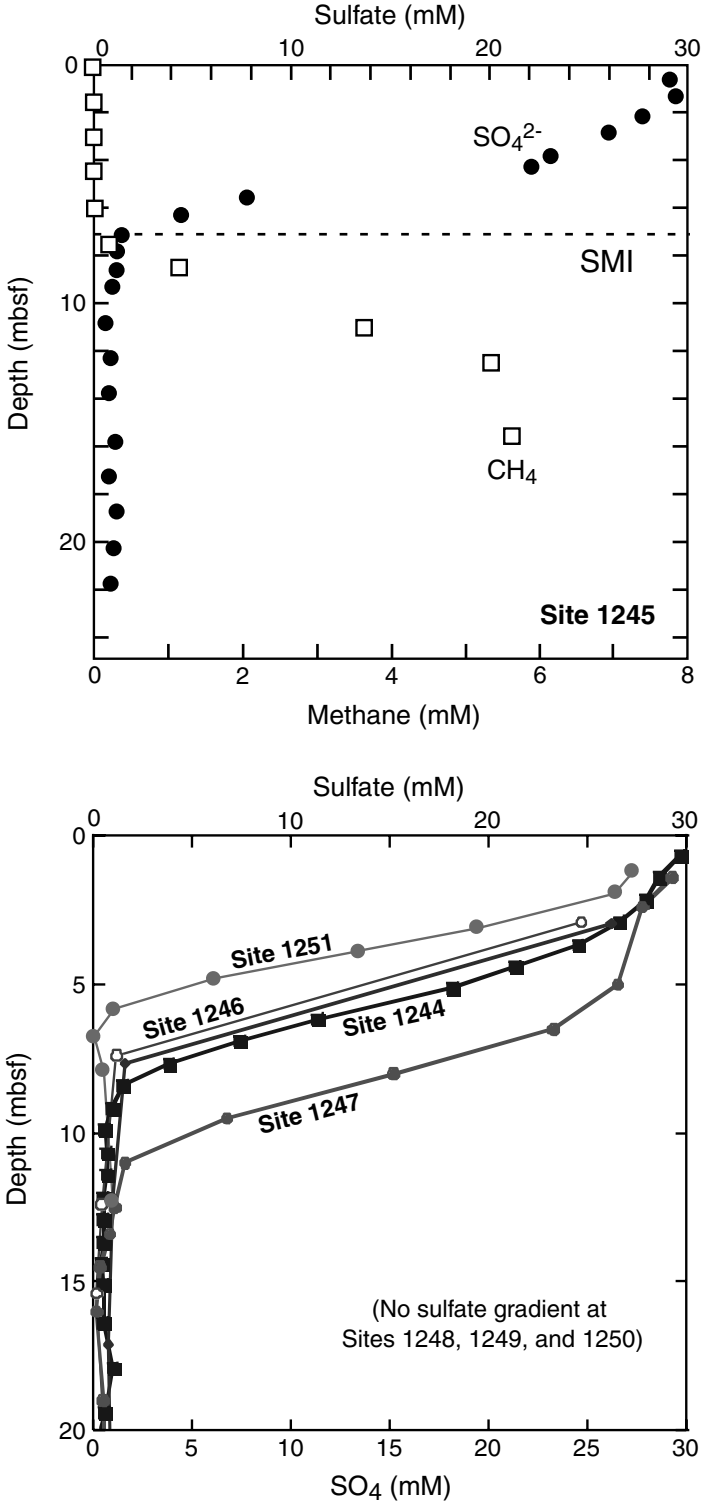

Figure F20. A. Infrared (IR) thermal anomalies measured in two different holes at Site 1251. Note that a major thermal anomaly in the 12 m above the bottom-simulating reflector (BSR) observed in Hole 1251D was not observed in Hole 1251B because that interval was not recovered from Hole 1251B (perhaps because of high hydrate concentration in situ). At this site, IR thermal anomalies are generally small and rare compared to most other sites drilled during Leg 204. **B.** Comparison between chloride anomalies measured from whole rounds and thermal anomalies for Hole 1251D. The IR data suggest two layers of high hydrate concentration immediately above the BSR but do not provide a good constraint on the concentration of hydrate within these layers. Chloride anomalies suggest a hydrate concentration of ~20% of pore space cannot constrain the thickness of hydrate-bearing layers because of the small number of samples. Moreover, at this site probable thin hydrate-bearing layers (based on IR and resistivity anomalies) were missed completely in the geochemical sampling. By calibrating the densely spaced geophysical data using the sparser geochemical data, improved estimates of hydrate distribution and concentration will be obtained.

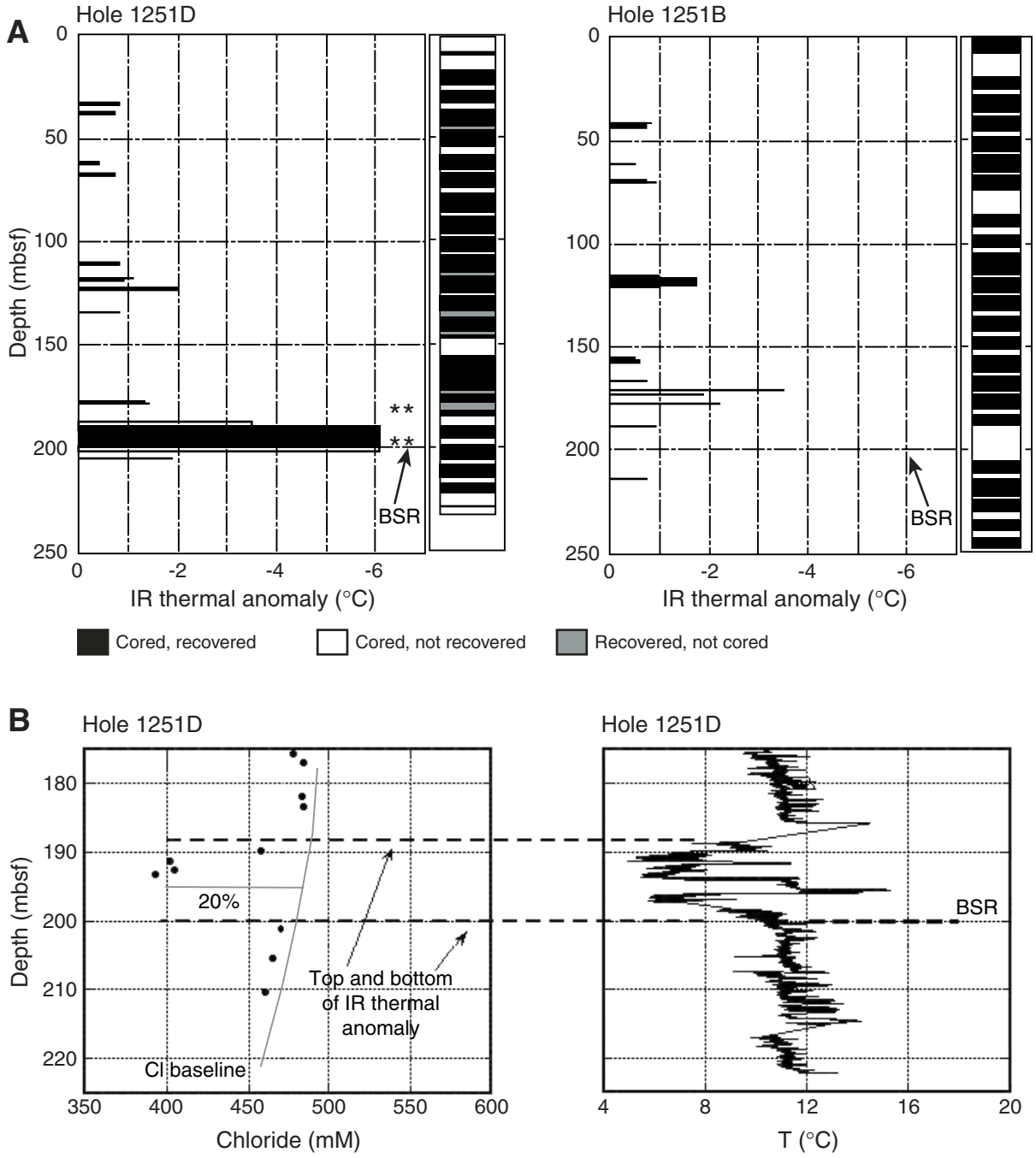

Table T1. Depth to major seismic horizons.

Site, hole	Seismic horizon	Estimated depth prior to Leg 204 (mbsf)	Confirmed or revised depth (mbsf)	Basis for revision
204-				
1244	BSR	124	127–129	VSP, WSL
	B	162	160	VSP
	B′	205	216–218	LWD, VSP
1245	Y	73		
	BSR	134		
	A	180		
1246	B	59		
	B′	97	96	LWD
	BSR	114		
1247A	Y	60		
	BSR	121		
	A	162	162–165	LWD
1247B	Y	62	65	VSP
	BSR	124	129–134	LVD, VSP, WSL
	A	158	150–160	VSP
1248	Y	46		
	BSR	115		
	A	128	127–129	LWD
1249	Y	53		
	BSR	115		
1250	Y	42		
	BSR	112	114	LWD, VSP, WSL
	A	150	148–152	LWD, VSP, WSL
1251	U	130		
	BSR	193		
1252	U	95		
	BSR	(170)		

Notes: VSP = vertical seismic profile, LWD = electrical resistivity from logging while drilling, WSL = wireline sonic log. The depth to major seismic horizons is estimated from 3-D seismic reflection data (Tréhu and Bangs, 2001; Tréhu et al., 2002) using velocities from 3-D OBS tomography (Arsenault et al., 2001). Updates of these estimates based on data acquired during Leg 204 are given when available from shipboard results. The bottom-simulating reflector (BSR) depth at Site 1252 is projected from nearby BSR observations.

Table T2. Leg 204 site summary.

Drilling order	Site	Hole	Latitude	Longitude	Seafloor (mbrf)	Number of cores	Cored (m)	Recovered (m)	Recovery (%)	Drilled (m)	Penetration (m)	Time on hole (hr)	Time on hole (days)
		204-											
1	HR1a	1244A	44°35.1701′N	125°7.1906′W	Missed	1	9.5	9.99	105.2	0.0	9.5	10.75	0.45
2		1244B	44°35.1702′N	125°7.1917′W	906.9	6	54.1	56.85	105.1	0.0	54.1	11.75	0.49
3		1244C	44°35.1784′N	125°7.1902′W	906.0	39	332.0	315.87	95.1	1.5	333.5	64.75	2.70
4		1244D	44°35.1865′N	125°7.1900′W	906.0	0	0.0	0.00	NA	380.0	380.0	37.50	1.56
35		1244E	44°35.1709′N	125°7.1719′W	904.8	19	135.8	137.73	101.4	114.2	250.0	74.75	3.11
36		1244F	44°35.1691′N	125°7.1705′W	907.4	4	24.1	24.90	103.3	0.0	0.0	5.00	0.21
					Site 1244 totals:	69	555.5	545.34	98.2	495.7	1027.1	204.50	8.52
5	HR3a	1245A	44°35.1697′N	125°8.9462′W	886.5	0	0.0	0.00	NA	380.0	380.0	28.75	1.20
29		1245B	44°35.1587′N	125°8.9455′W	881.0	53	471.7	418.27	88.7	2.0	473.7	80.50	3.35
30		1245C	44°35.1702′N	125°8.9316′W	880.0	29	198.7	185.31	93.3	3.0	201.7	32.75	1.36
31		1245D	44°35.1690′N	125°8.9312′W	881.5	3	24.0	24.82	103.4	0.0	24.0	3.50	0.15
33		1245E	44°35.1702′N	125°8.9605′W	881.0	8	66.6	18.5	27.7	473.7	540.3	104.50	4.35
					Site 1245 totals:	93	761.0	646.88	85.0	858.7	1619.7	250.00	10.42
6	HR1b	1246A	44°35.1642′N	125°8.1400′W	861.5	0	0.0	0.00	NA	180.0	180.0	18.25	0.76
32		1246B	44°35.1644′N	125°8.1235′W	860.8	16	136.7	135.34	99.0	0.0	136.7	18.75	0.78
					Site 1246 totals:	16	136.7	135.34	99.0	180.0	316.7	37.00	1.54
7	HR4c	1247A	44°34.6591′N	125°9.0096′W	845.0	0	0.0	0.00	NA	270.0	270.0	21.25	0.89
37		1247B	44°34.6589′N	125°9.0766′W	845.9	27.0	217.0	212.0	97.7	3.0	220.0	60.5	2.52
					Site 1247 totals:	27	217.0	212.00	NA	273.0	490.0	81.75	3.41
8	HR6	1248A	44°34.4515′N	125°9.1548′W	843.0	0	0.0	0.00	NA	194.0	194.0	15.50	0.65
21		1248B	44°34.4568′N	125°9.1482′W	841.0	3	17.0	7.45	43.8	0.0	17.0	10.75	0.45
22		1248C	44°34.45′N	125°9.1499′W	841.0	17	149.0	101.56	68.2	0.0	149.0	22.75	0.95
					Site 1248 totals:	20	166.0	109.01	65.7	194.0	360.0	49.00	2.04
9	HR4b	1249A	44°34.2246′N	125°8.8423′W	788.5	0	0.0	0.00	NA	90.0	90.0	9.75	0.41
13		1249B	44°34.2106′N	125°8.8412′W	788.5	8	45.0	14.01	31.1	29.9	74.9	28.00	1.17
14		1249C	44°34.2368′N	125°8.8410′W	788.5	14	88.5	58.84	66.5	1.5	90.0	22.25	0.93
26		1249D	44°34.2222′N	125°8.8366′W	788.5	3	16.5	4.78	29.0	2.0	18.5	5.25	0.22
27		1249E	44°34.2270′N	125°8.8369′W	788.5	3	9.0	4.38	48.7	2.0	11.0	4.75	0.20
28		1249F	44°34.2317′N	125°8.8377′W	788.5	16	82.5	57.37	69.5	7.5	90.0	22.75	0.95
39		1249G	44°34.2073′N	125°8.8416′W	788.5	5	43.0	11.24	26.1	0.0	43.0	9.00	0.38
40		1249H	44°34.2108′N	125°8.8365′W	788.5	6	52.5	27.52	52.4	0.0	52.5	8.50	0.35
41		1249I	44°34.2111′N	125°8.8437′W	788.5	4	33.6	8.69	25.9	0.0	33.6	6.00	0.25
42		1249J	44°34.2114′N	125°8.8422′W	788.5	3	32.5	7.69	23.7	0.0	32.5	5.50	0.23
43		1249K	44°34.2137′N	125°8.8392′W	788.5	5	43.2	16.87	39.1	1.0	44.2	8.25	0.34
44		1249L	44°34.2119′N	125°8.8439′W	788.5	5	38.5	14.15	36.8	0.0	38.5	10.25	0.43
					Site 1249 totals:	72	484.8	225.54	46.5	133.9	618.7	140.25	5.84
10	HR4a	1250A	44°34.1176′N	125°9.0179′W	807.0	0	0.0	0.00	NA	210.0	210.0	20.25	0.84
12		1250B	44°34.1174′N	125°8.9921′W	807.0	0	0.0	0.00	NA	180.0	180.0	19.50	0.81
23		1250C	44°34.1273′N	125°9.0178′W	807.0	19	143.0	117.29	82.0	2.0	145.0	28.50	1.19
24		1250D	44°34.1063′N	125°9.0182′W	807.0	19	142.0	133.56	94.1	3.0	145.0	26.00	1.08
25		1250E	44°34.1124′N	125°9.0171′W	807.0	2	16.0	11.93	74.6	0.0	16.0	3.50	0.15
35		1250F	44°34.1166′N	125°9.0025′W	807.0	13	77.0	70.10	91.0	103.0	180.0	74.25	3.09
					Site 1250 totals:	53	378.0	332.88	88.1	498.0	876.0	172.00	7.17
11	HR2alt	1251A	44°34.2197′N	125°4.4521′W	1228.0	0	0.0	0.00	NA	380.0	380.0	25.25	1.05
15		1251B	44°34.2191′N	125°4.4375′W	1224.4	53	442.1	368.56	83.4	3.0	445.1	86.25	3.59
16		1251C	44°34.2058′N	125°4.4366′W	1221.4	2	17.6	13.63	77.4	0.0	17.6	4.50	0.19
17		1251D	44°34.2060′N	125°4.4365′W	1221.4	30	226.5	194.40	85.8	4.0	230.5	38.25	1.59
18		1251E	44°34.2126′N	125°4.4358′W	1220.0	1	9.5	9.89	104.1	0.0	9.5	1.75	0.07
19		1251F	44°34.2159′N	125°4.4369′W	1220.0	1	9.5	9.92	104.4	0.0	9.5	0.25	0.01
20		1251G	44°34.2145′N	125°4.4364′W	1220.0	2	10.5	11.11	105.8	10.5	21.0	4.25	0.18
34		1251H	44°34.2089′N	125°4.4514′W	1220.0	0	0.0	0.00	NA	445.0	445.0	63.8	2.66
					Site 1251 totals:	89	715.7	607.51	84.9	842.5	1558.2	224.25	9.34
45	HR5	1252A	44°35.1671′N	125°5.5691′W	1051.0	28	259.8	253.79	97.7	0.0	259.8	51.00	2.13
					Site 1252 totals:	28	259.8	253.79	97.7	0.0	259.8	51.00	2.13
					Totals:	467	3674.5	3068.29	83.5	3475.8	7126.2	1209.75	50.41

Note: NA = not applicable.

Table T3. Leg 204 coring summary. (See table note. Continued on next page.)

Drilling order	Hole	Advanced piston corer			Extended core barrel			Pressure core sampler			Rotary core barrel		
		Number of cores	Cored (m)	Recovered (m)	Number of cores	Cored (m)	Recovered (m)	Number of cores	Cored (m)	Recovered (m)	Number of cores	Cored (m)	Recovered (m)
	204-												
1	1244A	1	9.5	9.99	0	0.0	0.00	0	0.0	0.00	0	0.0	0.00
2	1244B	6	54.1	56.85	0	0.0	0.00	0	0.0	0.00	0	0.0	0.00
3	1244C	15	138.5	138.76	21	190.5	173.85	3	3.0	3.26	0	0.0	0.00
4	1244D	0	0.0	0.00	0	0.0	0.00	0	0.0	0.00	0	0.0	0.00
35	1244E	14	130.8	133.81	0	0.0	0.00	4	4.0	3.00	0	0.0	0.00
36	1244F	3	23.1	23.90	0	0.0	0.00	1	1.0	1.00	0	0.0	0.00
Site 1244 totals:		39	356.0	363.31	21	190.5	173.85	8	8.0	7.26	0	0.0	0.00
5	1245A	0	0.0	0.00	0	0.0	0.00	0	0.0	0.00	0	0.0	0.00
29	1245B	14	127.8	122.14	36	340.9	293.75	2	2.0	2.00	0	0.0	0.00
30	1245C	16	134.6	127.54	7	58.1	53.52	3	3.0	3.00	0	0.0	0.00
31	1245D	3	24.0	24.82	0	0.0	0.00	0	0.0	0.00	0	0.0	0.00
33	1245E	0	0.0	0.00	0	0.0	0.00	0	0.0	0.00	8	66.6	18.48
Site 1245 totals:		33	286.4	274.50	43	399.0	347.27	5	5.0	5.00	8	66.6	18.48
6	1246A	0	0.0	0.00	0	0.0	0.00	0	0.0	0.00	0	0.0	0.00
32	1246B	16	136.7	135.34	0	0.0	0.00	0	0.0	0.00	0	0.0	0.00
Site 1246 totals:		16	136.7	135.34	0	0.0	0.00	0	0.0	0.00	0	0.0	0.00
7	1247A	0	0.0	0.00	0	0.0	0.00	0	0.0	0.00	0	0.0	0.00
37	1247B	13	111.6	114.99	11	102.4	94.01	3	3.0	3.00	0	0.0	0.00
Site 1246 totals:		13	111.6	114.99	11	102.4	94.01	3	3.0	3.00	0	0.0	0.00
8	1248A	0	0.0	0.00	0	0.0	0.00	0	0.0	0.00	0	0.0	0.00
21	1248B	3	17.0	7.45	0	0.0	0.00	0	0.0	0.00	0	0.0	0.00
22	1248C	11	94.0	84.00	6	55.0	17.56	0	0.0	0.00	0	0.0	0.00
Site 1248 totals:		14	111.0	91.45	6	55.0	17.56	0	0.0	0.00	0	0.0	0.00
9	1249A	0	0.0	0.00	0	0.0	0.00	0	0.0	0.00	0	0.0	0.00
13	1249B	0	0.0	0.00	0	0.0	0.00	0	0.0	0.00	0	0.0	0.00
14	1249C	11	85.5	55.84	0	0.0	0.00	3	3.0	3.00	0	0.0	0.00
26	1249D	2	15.5	3.98	0	0.0	0.00	0	0.0	0.00	0	0.0	0.00
27	1249E	2	8.0	3.38	0	0.0	0.00	1	1.0	1.00	0	0.0	0.00
28	1249F	10	73.1	51.38	1	4.4	1.28	3	3.0	3.00	0	0.0	0.00
39	1249G	3	28.5	7.13	1	13.5	3.36	0	0.0	0.00	0	0.0	0.00
40	1249H	4	38.0	25.07	1	13.5	1.70	0	0.0	0.00	0	0.0	0.00
41	1249I	3	20.1	8.29	1	13.5	0.40	0	0.0	0.00	0	0.0	0.00
42	1249J	2	19.0	7.69	1	13.5	0.00	0	0.0	0.00	0	0.0	0.00
43	1249K	4	29.7	16.05	1	13.5	0.82	0	0.0	0.00	0	0.0	0.00
44	1249L	2	19.0	7.15	2	18.5	6.65	0	0.0	0.00	0	0.0	0.00
Site 1249 totals:		43	336.4	185.96	8	90.4	14.21	7	7	7	0	0	0
10	1250A	0	0.0	0.00	0	0.0	0.00	0	0.0	0.00	0	0.0	0.00
12	1250B	0	0.0	0.00	0	0.0	0.00	0	0.0	0.00	0	0.0	0.00
23	1250C	15	133.5	104.80	1	6.5	9.60	2	2.0	2.00	0	0.0	0.00
24	1250D	12	111.0	103.95	3	27.0	26.33	3	3.0	3.00	0	0.0	0.00
25	1250E	2	16.0	11.93	0	0.0	0.00	0	0.0	0.00	0	0.0	0.00
38	1250F	3	19.8	17.47	7	54.2	49.63	3	3.0	3.00	0	0.0	0.00
Site 1250 totals:		32	280.3	238.15	11	87.7	85.56	8	8.0	8.00	0	0.0	0.00
11	1251A	0	0.0	0.00	0	0.0	0.00	0	0.0	0.00	0	0.0	0.00
15	1251B	21	189.6	152.86	26	246.5	210.90	3	3.0	3.00	0	0.0	0.00
16	1251C	1	8.1	8.18	1	9.5	5.45	0	0.0	0.00	0	0.0	0.00
17	1251D	15	142.5	132.49	9	78.0	56.82	4	4.0	4.00	0	0.0	0.00
18	1251E	1	9.5	9.89	0	0.0	0.00	0	0.0	0.00	0	0.0	0.00
19	1251F	1	9.5	9.92	0	0.0	0.00	0	0.0	0.00	0	0.0	0.00
20	1251G	1	9.5	10.11	0	0.0	0.00	1	1.0	1.00	0	0.0	0.00
34	1251H	0	0.0	0.00	0	0.0	0.00	0	0.0	0.00	0	0.0	0.00
Site 1251 totals:		40	368.7	323.45	36	334	273.17	8	8	8	0	0	0
45	1252A	14	125.0	134.10	14	134.8	119.69	0	0.0	0.00	0	0.0	0.00
Site 1252 totals:		14	125.0	134.10	14	134.8	119.69	0	0.0	0.00	0	0.0	0.00
	Totals:	244	2112.1	1861.25	150	1393.8	1125.32	39	39.0	38.26	8	66.6	18.48

Table T3 (continued).

Drilling order	Hole	Fugro Pressure Corer: Number of cores	Fugro Pressure Corer: Cored (m)	Fugro Pressure Corer: Recovered (m)	Hyacinth Rotary Corer: Number of cores	Hyacinth Rotary Corer: Cored (m)	Hyacinth Rotary Corer: Recovered (m)	Logging while coring: Number of cores	Logging while coring: Cored (m)	Logging while coring: Recovered (m)	Leg 204 coring statistics: Number of cores	Leg 204 coring statistics: Cored (m)	Leg 204 coring statistics: Recovered (m)	Leg 204 coring statistics: Recovered (%)
	204-													
1	1244A	0	0.0	0.00	0	0.0	0.00	0	0.0	0.00	1	9.5	9.99	105.2
2	1244B	0	0.0	0.00	0	0.0	0.00	0	0.0	0.00	6	54.1	56.85	105.1
3	1244C	0	0.0	0.00	0	0.0	0.00	0	0.0	0.00	39	332.0	315.87	95.1
4	1244D	0	0.0	0.00	0	0.0	0.00	0	0.0	0.00	0	0.0	0.00	NA
35	1244E	1	1.0	0.92	0	0.0	0.00	0	0.0	0.00	19	135.8	137.73	101.4
36	1244F	0	0.0	0.00	0	0.0	0.00	0	0.0	0.00	4	24.1	24.90	103.3
1244 totals:		1	1.0	0.92	0	0.0	0.00	0	0.0	0.00	69	555.5	545.34	98.2
5	1245A	0	0.0	0.00	0	0.0	0.00	0	0.0	0.00	0	0.0	0.00	NA
29	1245B	0	0.0	0.00	1	1.0	0.38	0	0.0	0.00	53	471.7	418.27	88.7
30	1245C	2	2.0	1.05	1	1.0	0.20	0	0.0	0.00	29	198.7	185.31	93.3
31	1245D	0	0.0	0.00	0	0.0	0.00	0	0.0	0.00	3	24.0	24.82	103.4
33	1245E	0	0.0	0.00	0	0.0	0.00	0	0.0	0.00	8	66.6	18.48	27.7
1245 totals:		2	2.0	1.05	2	2.0	0.58	0	0.0	0.00	93	761.0	646.88	85.0
6	1246A	0	0.0	0.00	0	0.0	0.00	0	0.0	0.00	0	0.0	0.00	NA
32	1246B	0	0.0	0.00	0	0.0	0.00	0	0.0	0.00	16	136.7	135.34	99.0
1246 totals:		0	0.0	0.00	0	0.0	0.00	0	0.0	0.00	16	136.7	135.34	99.0
7	1247A	0	0.0	0.00	0	0.0	0.00	0	0.0	0.00	0	0.0	0.00	NA
37	1247B	0	0.0	0.00	0	0.0	0.00	0	0.0	0.00	27	217.0	212.00	97.7
1246 totals:		0	0.0	0.00	0	0.0	0.00	0	0.0	0.00	27	217.0	212.00	97.7
8	1248A	0	0.0	0.00	0	0.0	0.00	0	0.0	0.00	0	0.0	0.00	NA
21	1248B	0	0.0	0.00	0	0.0	0.00	0	0.0	0.00	3	17.0	7.45	43.8
22	1248C	0	0.0	0.00	0	0.0	0.00	0	0.0	0.00	17	149.0	101.56	68.2
1248 totals:		0	0.0	0.00	0	0.0	0.00	0	0.0	0.00	20	166.0	109.01	65.7
9	1249A	0	0.0	0.00	0	0.0	0.00	0	0.0	0.00	0	0.0	0.00	NA
13	1249B	0	0.0	0.00	0	0.0	0.00	8	45.0	14.01	8	45.0	14.01	31.1
14	1249C	0	0.0	0.00	0	0.0	0.00	0	0.0	0.00	14	88.5	58.84	66.5
26	1249D	1	1.0	0.80	0	0.0	0.00	0	0.0	0.00	3	16.5	4.78	29.0
27	1249E	0	0.0	0.00	0	0.0	0.00	0	0.0	0.00	3	9.0	4.38	48.7
28	1249F	1	1.0	0.91	1	1.0	0.80	0	0.0	0.00	16	82.5	57.37	69.5
39	1249G	0	0.0	0.00	1	1.0	0.75	0	0.0	0.00	5	43	11.24	26.1
40	1249H	1	1.0	0.75	0	0.0	0.00	0	0.0	0.00	6	52.5	27.52	52.4
41	1249I	0	0.0	0.00	0	0.0	0.00	0	0.0	0.00	4	33.6	8.69	25.9
42	1249J	0	0.0	0.00	0	0.0	0.00	0	0.0	0.00	3	32.5	7.69	23.7
43	1249K	0	0.0	0.00	0	0.0	0.00	0	0.0	0.00	5	43.2	16.87	39.1
44	1249L	0	0.0	0.00	1	1.0	0.35	0	0.0	0.00	5	38.5	14.15	36.8
1249 totals:		3	3	2.46	3	3	1.9	8	45	14.01	72	484.8	225.54	46.5
10	1250A	0	0.0	0.00	0	0.0	0.00	0	0.0	0.00	0	0.0	0.00	NA
12	1250B	0	0.0	0.00	0	0.0	0.00	0	0.0	0.00	0	0.0	0.00	NA
23	1250C	1	1.0	0.89	0	0.0	0.00	0	0.0	0.00	19	143	117.29	82.0
24	1250D	0	0.0	0.00	1	1.0	0.28	0	0.0	0.00	19	142.0	133.56	94.1
25	1250E	0	0.0	0.00	0	0.0	0.00	0	0.0	0.00	2	16.0	11.93	74.6
38	1250F	0	0.0	0.00	0	0.0	0.00	0	0.0	0.00	13	77.0	70.10	91.0
1250 totals:		1	1.0	0.89	1	1.0	0.28	0	0.0	0.00	53	378.0	332.88	88.1
11	1251A	0	0.0	0.00	0	0.0	0.00	0	0.0	0.00	0	0.0	0.00	NA
15	1251B	2	2.0	1.80	1	1.0	0.00	0	0.0	0.00	53	442.1	368.56	83.4
16	1251C	0	0.0	0.00	0	0.0	0.00	0	0.0	0.00	2	17.6	13.63	77.4
17	1251D	1	1.0	0.87	1	1.0	0.22	0	0.0	0.00	30	226.5	194.4	85.8
18	1251E	0	0.0	0.00	0	0.0	0.00	0	0.0	0.00	1	9.5	9.89	104.1
19	1251F	0	0.0	0.00	0	0.0	0.00	0	0.0	0.00	1	9.5	9.92	104.4
20	1251G	0	0.0	0.00	0	0.0	0.00	0	0.0	0.00	2	10.5	11.11	105.8
34	1251H	0	0.0	0.00	0	0.0	0.00	0	0.0	0.00	0	0.0	0.00	NA
1251 totals:		3	3	2.67	2	2	0.22	0	0	0	89	715.7	607.51	84.9
45	1252A	0	0.0	0.00	0	0.0	0.00	0	0.0	0.00	28	259.8	253.79	97.7
1252 totals:		0	0.0	0.00	0	0.0	0.00	0	0.0	0.00	28	259.8	253.79	97.7
Totals:		10	10.0	7.99	8	8.0	2.98	8	45.0	14.01	467	3674.5	3068.29	83.5

Note: NA = not applicable.

Table T4. Leg 204 operations summary.

Proposed site	Hole	Drill order	Cored or LWD	Depth		PFT	Number of times deployed						HYACINTH tools	
				Seafloor (mbrf)	Hole (mbsf)	Wpaks F/MBIO	DSA	TAMU PCS	DVTP	DVTPP	APCT	APCM/ PCS	Number of FPC	Number of HRC
	204-													
HR1a	1244A	1	APC	None	10.0	0	0	0	0	0	0	0	0	0
HR1a	1244B	2	APC	906.9	54.1	0	1	0	0	0	1	0	0	0
HR1a	1244C	3	APC/XCB	906.0	333.5	3	3	3	0	2	3	0	0	0
HR1a	1244D	4	LWD	906.0	380.0	0	0	0	0	0	0	0	0	0
HR3a	1245A	5	LWD	886.5	380.0	0	0	0	0	0	0	0	0	0
HR1b	1246A	6	LWD	861.5	180.0	0	0	0	0	0	0	0	0	0
HR4c	1247A	7	LWD	845.0	270.0	0	0	0	0	0	0	0	0	0
HR6	1248A	8	LWD	843.0	194.0	0	0	0	0	0	0	0	0	0
HR4b	1249A	9	LWD	788.5	90.0	0	0	0	0	0	0	0	0	0
HR4a	1250A	10	LWD-1	807.0	210.0	0	0	0	0	0	0	0	0	0
HR2alt	1251A	11	LWD	1228.0	380.0	0	0	0	0	0	0	0	0	0
HR4a	1250B	12	LWD-2	807.0	180.0	0	0	0	0	0	0	0	0	0
HR4b	1249B	13	RAB-8	788.5	74.9	0	0	0	0	0	0	0	0	0
HR4b	1249C	14	APC	788.5	90.0	0	0	3	0	1	0	4	0	0
HR2alt	1251B	15	APC/XCB	1224.4	445.1	6	3	3	0	2	4	3	2	1
HR2alt	1251C	16	APC/XCB	1221.4	17.6	0	0	0	0	0	0	0	0	0
HR2alt	1251D	17	APC/XCB	1221.4	230.5	13	2	4	0	2	1	14	1	1
HR2alt	1251E	18	APC only	1220.0	8.1	1	0	0	0	0	0	0	0	0
HR2alt	1251F	19	APC only	1220.0	8.1	0	0	0	0	0	0	0	0	0
HR2alt	1251G	20	APC	1220.0	21.0	0	0	1	0	0	0	1	0	0
HR6	1248B	21	APC/XCB	841.0	16.0	0	0	0	0	0	1	0	0	0
HR7	1248C	22	APC/XCB	841.0	149.0	0	0	0	1	2	2	0	0	0
HR4a	1250C	23	APC/XCB	807.0	145.0	0	1	2	0	2	5	2	1	0
HR4a	1250D	24	APC/XCB	807.0	145.0	10	1	3	0	2	4	15	0	1
HR4a	1250E	25	APC	807.0	16.0	2	0	0	0	0	0	0	0	0
HR4b	1249D	26	APC	788.5	18.5	1	1	0	0	0	0	0	1	0
HR4b	1249E	27	APC	0.0	18.5	1	0	1	0	0	0	1	0	0
HR4b	1249F	28	APC	788.5	90.0	11	2	2	0	1	5	3	1	1
HR3a	1245B	29	APC/XCB	881.0	473.6	7	1	3	3	0	5	2	0	1
HR3a	1245C	30	APC/XCB	880.0	201.7	12	3	3	0	0	5	15	2	1
HR3a	1245D	31	APC	881.5	24.0	3	0	0	0	0	0	0	0	0
HR1b	1246B	32	APC	860.8	136.7	0	0	0	0	0	5	0	0	0
HR3a	1245E	33	RCB	881.0	540.3	0	0	0	0	0	0	0	0	0
HR2alt	1251H	34	Tricone	1220.0	445.0	0	0	0	0	0	0	0	0	0
HR1a	1244E	35	APC/XCB	904.8	250.0	12	1	4	0	2	6	16	1	0
HR1a	1244F	36	APC/PCS	907.4	24.1	3	0	1	0	0	0	1	0	0
HR4c	1247B	37	APC/XCB	845.9	220.0	0	0	3	2	0	6	16	0	0
HR4a	1250F	38	XCB ctr bit	807.0	180.0	0	0	3	2	0	0	3	0	0
HR4b	1249G	39	APC/XCB	788.5	43.0	0	1	0	0	0	1	0	0	1
HR4b	1249H	40	APC/XCB	788.5	52.5	0	3	0	0	0	0	0	1	0
HR4b	1249I	41	APC/XCB	788.5	33.6	0	0	0	0	0	0	0	0	0
HR4b	1249J	42	APC/XCB	788.5	32.5	0	0	0	0	0	0	0	0	0
HR4b	1249K	43	APC/XCB	788.5	44.2	0	3	0	0	0	0	0	0	0
HR4b	1249L	44	APC/XCB	788.5	38.5	0	2	0	0	0	1	0	0	1
HR5a	1252A	45	APC/XCB	1051.0	259.8	0	0	0	0	0	6	14	0	0
Total number of special tool deployments:						85	28	39	8	16	61	110	10	8
Total number of "successful" deployments:						85	17?	30	8	16	61	107	2	4

Notes: LWD = logging while drilling, PFT = perfluorocarbon tracer, Wpaks = Whirl Paks, MBIO = microbiology, PCS = pressure core sampler, DVTP = Davis-Villinger Temperature Probe, DVTPP = Davis-Villinger Temperature-Pressure Probe, APCT = advanced piston corer temperature tool, APCM = advanced piston corer methane tool, FPC = Fugro Pressure Corer, HRC = HYACE Rotary Corer. APC = advanced piston corer, XCB = extended core barrel, RAB = resistivity at the bit, ctr bit = center bit.